



CERTIFICATO DI FIRMA DIGITALE

Si certifica che questo documento informatico

TESI-Giulia_Rosini-PhD-XXXIV-ciclo-Medicina-Molecolare-UNISI-PDF-A.pdf

composto da n°181 pagine

È stato firmato digitalmente in data odierna con Firma Elettronica Qualificata (FEQ), avente l'efficacia e gli effetti giuridici equivalenti a quelli di una firma autografa, ai sensi dell'art. 2702 del Codice Civile e dell'art. 25 del Regolamento UE n. 910/2014 eIDAS (electronic IDentification Authentication and Signature).

PROCESSI INFORMATICI COMPLETATI

- **Apposizione di Firma Elettronica Qualificata Remota** emessa da Intesi Group S.p.A. in qualità di prestatore di servizi fiduciari qualificati autorizzato da AgID, per garantire con certezza l'autenticità, l'integrità, il non ripudio e l'immodificabilità del documento informatico e la sua riconducibilità in maniera manifesta e inequivoca all'autore, ai sensi dell'art. 20 comma 2 del CAD - D.lgs 82/2005.
- **Apposizione di Marca Temporale Qualificata** emessa da Intesi Group S.p.A. in qualità di prestatore di servizi fiduciari qualificati autorizzato da AgID, per attribuire una data e un orario opponibile a terzi, ai sensi dell'art. 20 comma 3 del CAD - D.lgs 82/2005 e per far sì che la Firma Elettronica Qualificata apposta su questo documento informatico, risulti comunque valida per i prossimi 20 anni a partire dalla data odierna, anche nel caso in cui il relativo certificato risultasse scaduto, sospeso o revocato.
- **Apposizione di Contrassegno Elettronico**, l'unica soluzione tecnologica che permette di prorogare la validità giuridica di un documento informatico sottoscritto con firma digitale e/o marcato temporalmente, rendendolo inalterabile, certo e non falsificabile, una volta stampato su supporto cartaceo, ai sensi dell'art. 23 del CAD - D.lgs 82/2005.



Per risalire all'originale informatico è necessario scansionare il Contrassegno Elettronico, utilizzando l'applicazione HONOS, disponibile per dispositivi Android e iOS.



UNIVERSITA' DI SIENA

DIPARTIMENTO di Medicina Molecolare e dello sviluppo

DOTTORATO DI RICERCA IN
Medicina Molecolare

CICLO XXXIV

COORDINATORE: Professor Vincenzo Sorrentino

TITOLO DELLA TESI: New insights and tools to study innovative delivery strategies of therapeutic peptides: Apolipoprotein A-I_{Milano}, administered orally via genetically modified rice plants, exerts anti-inflammatory effects *in vivo*.

SETTORE SCIENTIFICO-DISCIPLINARE: BIO/18

DOTTORANDO
Giulia Rosini

TUTOR
Prof. Stefano Landi

CO-TUTOR
Prof. Roberto Giovannoni

ANNO ACCADEMICO: 2021/2022

"Andate avanti, perché il mondo ha bisogno di scienza e ragione."

-Umberto Veronesi-

Summary

1 Introduction	10
1.1 Oral peptide delivery	10
1.1.1 Oral peptides assessed in humans	12
1.2 Apolipoprotein A-I: a crucial role in cardiovascular diseases (CVDs)	14
1.2.1 APOA-I natural variants	15
1.2.1.1 APOA-I variants with therapeutic potential against CVD	16
1.2.1.2 APOA-I clinical variants	18
1.3 APOA-I role in HDL metabolism and formation	19
1.3.1 HDL: Structure and metabolism	21
1.3.2 HDL molecular components	24
1.3.2.1 HDL proteome: Not only APOA-I, other major proteins key roles	24
1.3.2.2 HDL Lipidome	25
1.3.3 Another lipoprotein's crucial role in CVD: VLDL and LDL	26
1.3.4 Cholesterol levels and atherosclerosis disease	28
1.3.5 HDL anti-atherosclerotic biological functions	30
1.3.5.1 Reverse cholesterol transport	31
1.3.5.1.1 Proteomics of RCT	34
1.3.5.1.1.1 ABCA1/ABCG1	34
1.3.5.1.1.2 LXR Receptor	35
1.3.5.1.1.3 LCAT	36
1.3.5.1.1.4 Endothelial lipase and hepatic lipase	36
1.3.5.1.1.5 CETP	36
1.3.5.1.1.6 PLTP	37
1.3.6 HDL Antioxidant activity	37
1.3.7 HDL Anti-inflammatory activity	38
1.3.8 The quality not so much the quantity for protective role of the HDL.	39
1.3.9 Recombinant HDL/APO drugs	40
1.3.9.1 Preliminary stage studies in course	41
1.3.9.2 A Promising class of therapeutic agents: APOA-I mimetic peptides	43
1.3.9.2.1 Plants as bioreactor for therapeutics agents	44
1.4 APO- Rice project strategy	46
1.5 Rationale and aim of the work	50
2 Materials and methods	50
2.1 APO biodistribution of proof-of-concept iAPO rice	50
2.1.1 Protein extraction from rice flour	50
2.1.1.1 Extraction of the rice salt-soluble and salt-insoluble proteins	51
2.1.1.2 Extraction of the rice total proteins	52
2.1.2 Determination of rice extracts protein concentration	52
2.1.2.1 2 D Quant kit assay	52
2.1.2.2 Quick Start Bradford Protein Assay	53
2.2 In vivo study protocol and tissue biopsies availability	54
2.2.1 Extraction of total protein from tissue biopsies	54
2.2.1.1 Preparation lysates	55
2.2.1.2 Determination of tissue lysates protein concentration	56
2.2.1.2.1 Assay preparation	56
2.2.1.2.2 Measurement of the samples and standards	57
2.2.1.2.3 Data analysis	57
2.2.2 Western Blot	57
2.2.2.1 Polyacrylamide gel electrophoresis (PAGE)	58
2.2.2.2 Transfer step	59
2.2.2.3 Detection step	60
2.2.2.4 Normalization	61
2.2.3 ELISA assay	62
2.2.3.1 Reagent preparation	63

2.2.3.2	<i>Standard preparation</i>	63
2.2.3.3	<i>Sample preparation</i>	63
2.2.3.4	<i>Assay procedure</i>	63
2.2.3.5	<i>Data analysis</i>	64
2.2.4	<i>Ex vivo analyses, immunohistochemistry and histology on liver tissues</i>	65
2.3	<i>APOA1 sequence mutagenesis and molecular cloning plasmids</i>	66
2.3.1	<i>F2A peptide details</i>	67
2.3.2	<i>Gibson cloning assembly</i>	69
2.3.2.1	<i>PCR protocol</i>	71
2.3.2.2	<i>Gel electrophoresis</i>	72
2.3.2.3	<i>Purification inserts by gel extraction</i>	72
2.3.2.4	<i>Restriction enzyme digestion</i>	74
2.3.2.5	<i>Gibson Assembly protocol</i>	75
2.3.2.6	<i>Ligase Ligation Protocol</i>	76
2.3.2.7	<i>Transformation</i>	77
2.3.2.7.1	<i>Selection plates preparation</i>	77
2.3.2.7.2	<i>NEB 5-alpha Competent E. coli cells transformation</i>	78
2.3.2.8	<i>Plasmid purification from bacterial cells</i>	78
2.3.2.9	<i>Samples analysis and sequencing</i>	80
2.3.3	<i>APOA1 mutagenesis: the Milano variant</i>	80
2.3.3.1	<i>pGEM-T Easy Vector System</i>	80
2.3.3.1.1	<i>PCR for APOA1 sequence mutagenesis</i>	81
2.3.3.1.2	<i>pGEM ligation reaction protocol</i>	82
2.3.3.1.3	<i>NZ5-α competent cells transformation protocol</i>	83
2.3.4	<i>Functional in vitro validation of plasmids built</i>	84
2.3.4.1	<i>Cell line</i>	84
2.3.4.1.1	<i>Handling procedure</i>	84
2.3.4.1.2	<i>Subculturing procedure</i>	84
2.3.4.2	<i>Electroporation</i>	85
2.3.4.2.1	<i>Cell preparation</i>	85
2.3.4.2.2	<i>Neon electroporation system</i>	86
2.3.4.2.3	<i>Cell sorting and Immunocytochemistry</i>	86
3	Results	88
3.1	<i>Analysis of AIM distribution</i>	88
3.1.1	<i>Rice flour's protein fractions analysis</i>	88
3.1.2	<i>Analysis of AIM protein biodistribution</i>	90
3.1.2.1	<i>Immunohistochemistry preliminary results</i>	91
3.1.3	<i>Mouse ApoA-I protein analyses</i>	94
3.1.3.1	<i>Preliminary results on liver samples</i>	94
3.1.3.2	<i>Preliminary results on intestine samples</i>	96
3.2	<i>Set plasmids production for cell transfection experiments</i>	99
3.2.1	<i>APOA1 sequence mutagenesis</i>	100
3.2.2	<i>Multicistronic expression plasmids construction strategy</i>	104
3.2.2.1	<i>Control plasmids</i>	107
3.2.2.1.1.	<i>pCX-F2A plasmid</i>	107
3.2.2.1.2.	<i>pCX-APO plasmid</i>	108
3.2.2.1.3.	<i>pCX-AIM plasmid</i>	111
3.2.2.1.4.	<i>pCX-EGFP plasmid</i>	115
3.2.2.1.5.	<i>pCX-APO-F2A-EGFP plasmid</i>	117
3.2.2.1.6.	<i>pCX-EGFP-F2A-APO plasmid</i>	122
3.2.2.1.6.1	<i>pCX-EGFP-F2A plasmid: first step</i>	122
3.2.2.1.6.2	<i>pCX-EGFP-F2A-APO plasmid: final step</i>	123
3.2.2.1.7.	<i>pCX-EGFP-F2A₁-APO₁-F2A₂-APO₂</i>	126
3.2.2.2	<i>AIM-expressing multicistronic plasmids</i>	129
3.2.2.2.6	<i>pCX-AIM-F2A-EGFP plasmid</i>	129
3.2.2.2.7	<i>pCX-EGFP-F2A-AIM plasmid</i>	133
3.2.2.2.8	<i>pCX-EGFP-F2A₁-AIM₁-F2A₂-AIM₂ plasmid</i>	136
3.2.2.2.9	<i>pCX-EGFP-F2A₁-AIM₁-F2A₂-AIM₂-F2A₃-AIM₃ plasmid</i>	139
3.3.	<i>Preliminary results of in vitro functional validation of plasmids set</i>	143

3.3.1.	<i>Transfection efficiency evaluation</i>	143
3.3.2.	<i>Evaluation AIM protein expression: ICC results</i>	151
4	<i>Discussion</i>	153
5	<i>Future perspectives</i>	163
6	<i>Conclusions</i>	164
7	<i>Bibliography</i>	165
8	<i>Thanks</i>	180

Abstract

In the proof-of-concept study published by Romano and others in *Int.Cardiology* 2018, was shown a new approach for treatment of cardiovascular disease (CVDs) because, despite the high therapeutic potential of Apolipoprotein A-I protein, the practical application is hampered by the low efficiency of purification and delivery. A genetically modified rice plants expressing Apolipoprotein A-I variant Milano (AIM) were created. The product was tested *in vitro*, and *in vivo* mouse atherosclerotic model treated with genetically modified rice-milk (in the form of protein extract of rice seed proteins) or wild type rice-milk and it was found to be safe and effective. For subsequent aims, initially, in this context, the APO rice flour (RF) product was better characterized to further understand the potential of transgenic rice seeds as an efficient oral production and delivery system for recombinant AIM protein. WT and APO RF were analysed by ELISA and Western Blot (WB) and APO protein was detected in APO rice as expected. To better understand the biodistribution of the AIM protein administered orally in APO3 pre-clinical study and the molecular mechanisms underlying the athero-protective and anti-inflammatory effects, ELISA, WB and immunohistochemistry (IHC) assays were performed on mice liver and/or other organs. AIM in liver and intestine lysates was not detected by ELISA and WB. By increasing the spatial resolution by IHC, positive spots were detected in the liver sections of the treated mice. These investigations were fundamental to lay the foundations for the main purpose, namely the development of a new system of functional AIM product to improve both in quality and quantity of delivered protein to be able to extend the product for future use in humans. In this order, a set of vectors carrying the coding sequence of the AIM and the respective control vectors was constructed, to be tested at a functional level *in vitro* and subsequently to be used as source of the AIM sequence to engineer the new rice product.

1 Introduction

1.1 Oral peptide delivery

A wide variety of peptide-based drugs are now being produced on a commercial scale as a result of advances in biotechnology. Most of these therapeutic peptides are still administered parenterally due to insufficient absorption from the gastrointestinal (GI) tract which impairs the systemic absorption of intact peptide molecules and proteins. The use of daily injections for long treatments, as for use in chronic conditions, represents a limitation and an invasive method for the patients. Consequently, many studies have explored the feasibility of delivering proteins via alternative routes, including formulations suitable for oral, nasal, ophthalmic, pulmonary, buccal and transdermal administration ¹. The oral route offers the advantage of self-administration with a high degree of patient acceptability and compliance. The main reasons for the low oral bioavailability of peptide drugs are the pre-systemic enzymatic degradation and poor penetration of the intestinal mucosa. Research therefore focused on overcoming the challenges presented by these barriers to provide effective oral administration of peptide and protein drugs. Attempts to improve the oral bioavailability of peptide drugs have ranged from changing the physicochemical properties of peptide molecules to the inclusion of functional excipients in specially adapted drug delivery systems. However, progress in the development of an effective peptide delivery system has been hampered by factors such as the inherent toxicities of the excipients that enhance absorption, variability in absorption between individuals, and potentially high manufacturing costs ².

The first problem to be faced is the functional and structural barriers that the non-degraded therapeutic agent encounters during transit through the intestinal epithelium and subsequent secretion into the lymphatic system or blood flow. Ingested peptide formulations first

encounter salivary enzymes including amylase and lipase and then in the stomach a highly acidic environment containing highly efficient proteolysis enzymes such as pepsin and cathepsin ³. Additional proteolytic enzymes are present in the lumen of the small intestine whose epithelium acts as a barrier to the absorption of proteins and peptides ⁴.

In particular, the mucous layer protects a monolayer of epithelial cells, connected by tight junctions, which act as an effective barrier against the permeation of proteins and peptides ⁵. Mucus is also needed as a reservoir for antibacterial defences and physically traps microorganisms on the outside superficial layers of mucus, preventing the direct access of most bacterial species, as well as large molecules ⁶. Therefore, penetration through the intestinal epithelium represents a significant challenge for hydrophilic high molecular weight proteins and peptides ⁷. However, the extent to which studies on the peptide drug permeation through the experimental mucus *ex vivo* modelled systems recapitulated the complexity of the mucous layer *in vivo* remains uncertain. Another important consideration for the development of an oral peptide is the enormous inter-individual variability in the physiology of the GI tract, including the extent of mucus and enzyme production and the control of gastric emptying and intestinal motility ⁸.

The gastrointestinal transit rate is a key factor determining epithelial exposure to an ingested peptide and can be affected by the size, composition and time of the ingested meal, as well as by aging. Variability in intestinal motility and differential absorption rates are particularly relevant for the development of therapies such as insulin for diabetes as individuals with mild dysglycemia or diabetes may have intestinal motility dysregulation. Furthermore, inter-individual differences in the luminal epithelial environment, including the relative expression of digestive enzymes, peptidases and related transporters, potentially contribute to the timing and degree of transmucosal absorption of the drug ⁹.

1.1.1 Oral peptides assessed in humans

Numerous studies have suggested the use of various strategies to improve bioavailability and to overcome the stability and permeability barriers in the oral cavity. Among them, there are several such as, for example: (i) the absorption enhancers to increase absorption such as modification by lipidation or conjugation to target ligands, (ii) the physicochemical modification of macromolecular drugs, such as formulations with protease inhibitors and pH-lowering excipients and muco-adhesive delivery systems such as the use of excipients capable of opening paracellular channels, disrupting the intestinal membrane and increasing muco-adhesion ¹⁰.

Unfortunately, many strategies have shown promising results only in preclinical or early-stage clinical trials, so very few have achieved human clinical trials ¹¹. Most of the research on oral delivery has been carried out with calcitonin and insulin, probably due to the frequency of their administration and clinical importance ^{12 13}. Some research has also focused on improving the oral delivery, in particular for cyclosporin A, desmopressin, pancreatin and peptide hormones such as leuprolide, oxytocin and octreotide, as illustrated in table 1 ¹⁴.

The oral delivery of larger molecules was poorly attempted due to the intrinsic difficulties of maintaining their complex structure during transit in the GI tract and the greater difficulty of absorption of such large molecules. Despite the arrest of many projects, some have completed successful clinical trials and are pursuing filings in the near future.

Biocon Limited, India continued development of an oral insulin formulation, named IN-105, originally invented by Nobex Corporation. Phase III clinical trials did not meet desired expectations ¹⁵. Despite this, the effectiveness of the formulation was not questioned, and the project is still under development. Another oral peptide / protein delivery systems that has completed Phase III

clinical trials is Tarsa Therapeutics' (USA) OSTORA, for Salmon Calcitonin Tablets. It has successfully met all clinical endpoints and represents the most promising oral peptide strategy for future availability. However, an FDA Advisory Committee decided in 2013 that salmon calcitonin should no longer be broadly marketed, as the risk of it causing cancer outweighs its benefits by putting an end to its development. Chiasma's oral octreotide is currently undergoing in phase III clinical trials and may submit a new drug application in the near future for its commercialization.

The programs involve all peptides/proteins <6 kDa, with the exception of the interferon- α which is targeted at receptors in the throat and therefore it should overcome the problems of stability and permeability of oral systemic administration. Many studies and research are still needed, especially for oral administration of larger proteins to systemic circulation. However, the success of Tarsa Therapeutics' Phase III clinical trial with calcitonin could constitute a starting point for the administration of relatively large hydrophilic peptides.

The formulations developed by Tarsa Therapeutics (USA), Chiasma, Inc. (USA) and Oramed Pharmaceuticals, Inc. (USA) include protective and enhancing elements of enteric permeation such as coatings that contain protease inhibitors and permeation enhancers¹⁶. These strategies have the best potential for future success and indicate that formulations must provide protection against acids and enzymes of the GI tract and the enhancement of permeation. Many emerging strategies for oral administration of peptides/proteins in preclinical or ongoing clinical trials rely on modified nanoparticles such as Access Pharmaceuticals formulations, NOD Pharmaceuticals and Nanomega Corp. that are currently developing oral administration methods for insulin.

In addition, the FDA has recently approved the oral administration of Desmopressin and Cyclosporine peptides and vaccines against *Vibrio cholerae* (Vaxchora, PaxVax, Inc.), *Salmonella enterica* subsp.

enterica serovar *typhi* Ty21a (Vivotif, PaxVax, Inc.) and rotavirus (Rotarix, GlaxoSmithKline) (RotaTeq, Merck). Other studies are currently in progress (over 100 vaccines and over 80 trials on Desmopressin) ¹⁷.

Current trials and approved products for the oral delivery of biologics				
Delivery approach	Oral formulation	Biologic	Application / Indication	ClinicalTrials.gov identifier
Ovarest (Enteris BioPharma)	Peptelligence: improved solubility and absorption of peptides for oral delivery.	Leuprolide for Endometriosis.	Pharmacokinetic and pharmacodynamic profiles in healthy female volunteers.	NCT02807363 (phase II)
ORMD-0801 (Oramed Pharmaceuticals, Inc., USA)	Oral insulin capsule that prevents enzyme degradation and enhances intestinal absorption.	Insulin.	Type 1 and type 2 diabetes.	phase II clin. Trials: NCT02094534 NCT02954601 NCT02653300 NCT01889667 NCT02535715 NCT02496000 NCT00867594
Tregopil; formerly IN-105 (Biocon Limited, India)	Tablet.	Novel oral insulin molecule.	Type 1 diabetes.	NCT01035801 (phase I)
Oral HDV Insulin (Diasome) ¹⁸	Capsule containing insulin targeted to the liver.	Insulin.	Type 2 diabetes.	Phase II/III clin. trials NCT00814294() NCT00521378
Neoral (Novartis), Sandimmune (Novartis)	Capsule with surfactants (FDA approved).	Cyclosporin A.	Organ rejection prophylaxis.	>250 trials, including: NCT02706470 NCT00977977 (phase II)
DDAVP (Ferring Pharmaceuticals)	Tablet (FDA approved).	Desmopressin.	Antidiuretic replacement therapy for diabetes insipidus.	>85 trials, including: NCT03051009 NCT02636387 (phase III)
Neoral (Novartis), Sandimmune (Novartis)	Capsule with surfactants (FDA approved).	Cyclosporin A.	Organ rejection prophylaxis.	>250 trials, including: NCT02706470 NCT00977977 (phase II)
DDAVP (Ferring Pharmaceuticals)	Tablet (FDA approved).	Desmopressin.	Antidiuretic replacement therapy for diabetes insipidus.	>85 trials, including: NCT03051009 NCT02636387 (phase III)

Table 1 the table summarizes the main formulations and strategies for the delivery of therapeutic peptides. Some have already been approved by the FDA and others are being tested.

1.2 Apolipoprotein A-I: a crucial role in cardiovascular diseases (CVDs)

This thesis project focuses on Apolipoprotein A-I (APOA-I), the main protein component of High-Density Lipoprotein (HDL) (70% of the

protein mass of HDL) and the most abundant apolipoprotein in humans (plasma concentration of approximately 130 mg / dL).

The major functions of APOA-I involve interaction with cellular receptors, activation of lecithin/cholesterol acyltransferase (LCAT) and endowing HDL with multiple anti-atherogenic activities including antioxidant and anti-inflammatory properties ¹⁹.

Synthesized in both the liver and the intestine as a preproprotein, this is co-translationally cleaved to the proprotein, which is secreted into plasma. Within the vascular compartment, pro-APOA-I is converted to the mature form, a 243-amino acid long polypeptide, by the action of a calcium-dependent protease. In its mature form (in humans has a size of 28 kDa), is composed of 10 conserved α -amphipathic helices, eight 22-meres and two 11-meres ²⁰. The strong interaction between APOA-I and phospholipids is promoted by amphipathic α -helix structures in APOA-I, which possess a hydrophilic face and a hydrophobic face. These helices are stabilized by contact with themselves and / or with lipids, and the structure of lipid associated APOA-I in the discoidal or spherical HDL particles reflects such stabilizing interactions ²¹.

The plasma half-life of APOA-I is around 4 days, with the main sites of catabolism and elimination being the liver and kidney. Lipid-rich APOA-I can be removed from plasma, along with mature HDL or LDL particles, by hepatic HDL holoparticle receptors or LDL receptors, respectively, whereas lipid-poor APOA-I can be removed via glomerular filtration in the kidneys.

The APOA-I serves on a structural level and functional roles, especially in mediating the formation of HDL species for lipid transport, as part of the RCT pathway ²¹.

1.2.1 APOA-I natural variants

Several variants of the APOA-I protein have been discovered that are caused by point mutations, deletions, or rearrangements in the

corresponding gene. A number of these mutations can cause peptides with impaired functions and an abnormal metabolism of lipoproteins ²².

1.2.1.1 APOA-I variants with therapeutic potential against CVD

ApolipoproteinA-I Milano (AIM), the first mutant form of APOA-I described, was discovered by Cesare Sirtori in the late 1980s, and is characterized by an arginine to cysteine substitution in the amino acid position 173 as shown in figure 1. Individuals carrying this mutation, detected in a population of Limone sul Garda, are heterozygous for the mutant allele and have low to extremely low HDL levels associated with an increased incidence of hypertriglyceridemia. Interestingly, no increased incidence of cardiovascular disease has been reported for individuals with the AIM mutation despite their hypoalphalipoproteinemia ²³. Evaluations revealed that due to the presence of a cysteine residue, AIM can form disulfide-bound dimers and is present in the plasma lipoproteins as a monomer, a heterodimer with APOA-II and a homodimer with itself ²⁴.

Some studies on the interaction of AIM with lipids and HDLs isolated from patients carrying the mutation, have shown that the substitution of arginine with cysteine in AIM resulted in an accelerated rate of association of AIM with lipids and a reduced stability of the lipid-apolipoprotein complexes. A preferential distribution of AIM monomers and dimers with HDL₃ was also observed in HDL separated by gel filtration chromatography ²⁵.

Furthermore, *in vitro*, and *in vivo* studies demonstrated significantly faster catabolism of AIM compared to APOA-I WT in study subjects. The analysis of the catabolic rates of the monomeric and dimeric forms of AIM has shown that the monomeric form, in addition to being catabolized more rapidly than the wild type (WT) APOA-I, is catabolized much more rapidly than the dimeric forms. Conversely, the dimeric forms are catabolized somewhat more slowly than WT APOA-I in these

individuals. These results were important in understanding why AIM is present in plasma at a higher concentration than the normal form of APOA-I and why subjects with the lowest levels of APOA-I and HDL cholesterol have the quantities higher than AIM, relative to wild-type APOA-I ²⁶.

Thus, in individuals carrying AIM variant, the decrease in APOA-I levels is caused by the rapid catabolism of APOA-I and not a reduced production rate, and the abnormal AIM leads to both rapid catabolism of the normal and mutant forms of APOA-I in affected individuals ²⁷.

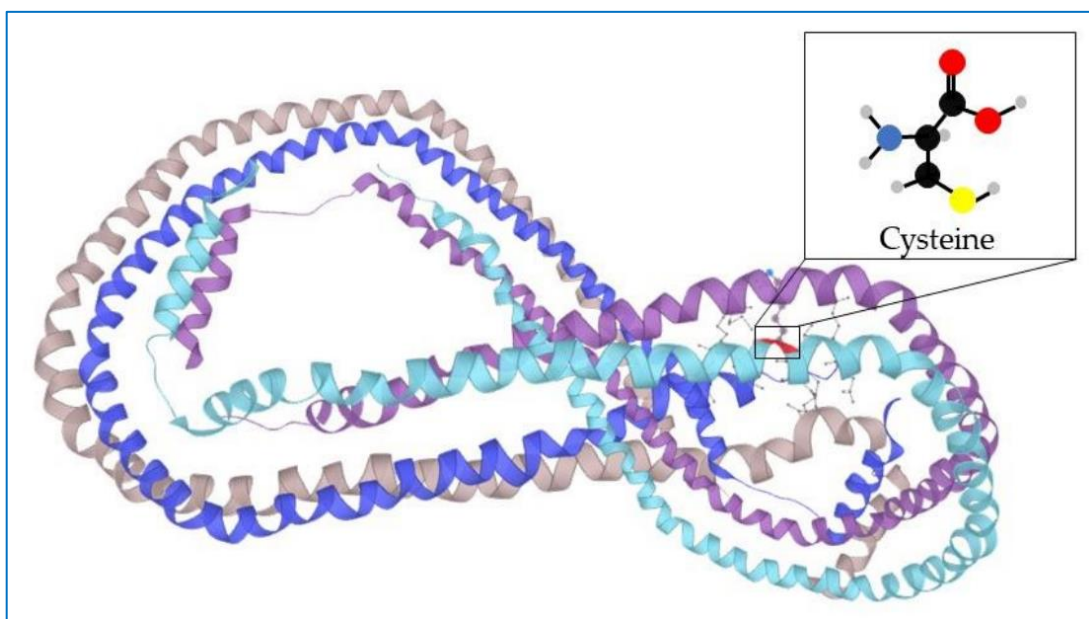


Figure 1 ApolipoproteinA-I _{Milano}. Representative X-ray structure of an AIM tetramer. Highlighted in red the aminoacidic substitution from arginine to cysteine in position 173, characterizing of the Milano variant. Image by UniProt database (with modifications).

Recently, another mutation of APOA-I, called APOA-I _{Paris} (AIP), has been described in a French family where the subjects had severe hypoalphalipoproteinemia and no signs to suggest a premature onset of atherosclerosis or coronary heart disease (CHD) were found either in the proband or in the family over three generations. The mutant form of AIP is characterized by the arg-to-cys missense substitution in position 151 (R151C). It is believed that, due to the anomalous presence of a cysteine residue, AIP can form disulphide-bound dimers, and is present

in the plasma lipoproteins as a monomer, as a heterodimer with APOA-II and as a homodimer with itself.

Therefore, HDL particles exhibit complex characteristics with monomers, homo and heterodimers ²⁸.

Concerning the Paris variant, the studies are still in the initial phase but a similarity with the Milano variant is still hypothesized as regards the catabolism and the beneficial effect downstream ²⁹.

1.2.1.2 APOA-I clinical variants

Defects in the APOA1 gene (HGNC:600) are found in patients with Hypoalphalipoproteinemia, primary, 2 (FHA2) attributed to natural variant VAR_083307 and natural variant VAR_083309. The disease is a rare disorder of lipoprotein metabolism, biochemically characterized by complete or partial APOA-I deficiency and mild to severe reduction of serum HDL-C.

Severe hypoalphalipoproteinemia characterized by undetectable levels of APOA-I is an autosomal recessive condition, generally associated with markedly increased atherosclerotic cardiovascular disease, xanthomas and corneal opacities. Mild hypoalphalipoproteinemia characterized by half the normal plasma APOA-I and HDL-C levels is inherited as an autosomal dominant trait, may be associated with xanthomas and corneal opacities, but most patients do not have increased cardiovascular risk ^{30 31 32}. Many naturally occurring mutations in human APOA1 gene are associated with reduced plasma HDL levels and hereditary systemic amyloidosis.

The hereditary APOA-I amyloidosis is characterized by the deposition of the N-terminal 80–100-residue fragments of the variant protein as amyloid fibrils in peripheral organs such as heart, liver, kidneys, or GI tract resulting in nephrotic syndrome, arterial hypertension, hepatosplenomegaly, cholestasis, petechial skin rash without involvement of the nervous system.

To date, over 20 naturally occurring mutations in human APOA1 gene associated with familial amyloid polyneuropathy have been reported. For some APOA-I amyloidosis, it is known that a preferential fibril deposition in certain tissues and organs occurs such that the amyloidogenic APOA-I variants with mutations clustered in residues 1–75 deposit predominantly in kidneys and liver. However, the molecular basis for the preferential accumulation of APOA-I amyloid fibrils is largely unknown.

Studies showed that a G26R mutation, the first and most common amyloidogenic mutation found in APOA1 destabilizes the alpha-helix structure in the highly amyloidogenic regions upon membrane binding, facilitating fibril formation of the N-terminal 83 fragment of APOA-I^{33 34 35 36 37 38}.

1.3 APOA-I role in HDL metabolism and formation

Cardiovascular diseases (CVDs), including atherosclerosis, hypertension, heart failure, atrial fibrillation and myocardial fibrosis, are associated with high morbidity and mortality. Over 80% of all mortality from CVDs occurs in developing countries and not only mortality, but also disability caused by CVDs remains extremely high (fig.1)^{39 40}.

The World Health Organization (WHO) has underlined the importance of lifestyle in the explosion of cardiovascular disease in the Western world. Many risk factors are widely known, such as smoking, poor dietary habits, dyslipidaemia, obesity, diabetes mellitus and high cholesterol levels, but these cannot fully explain the incidence of CVDs worldwide⁴¹.

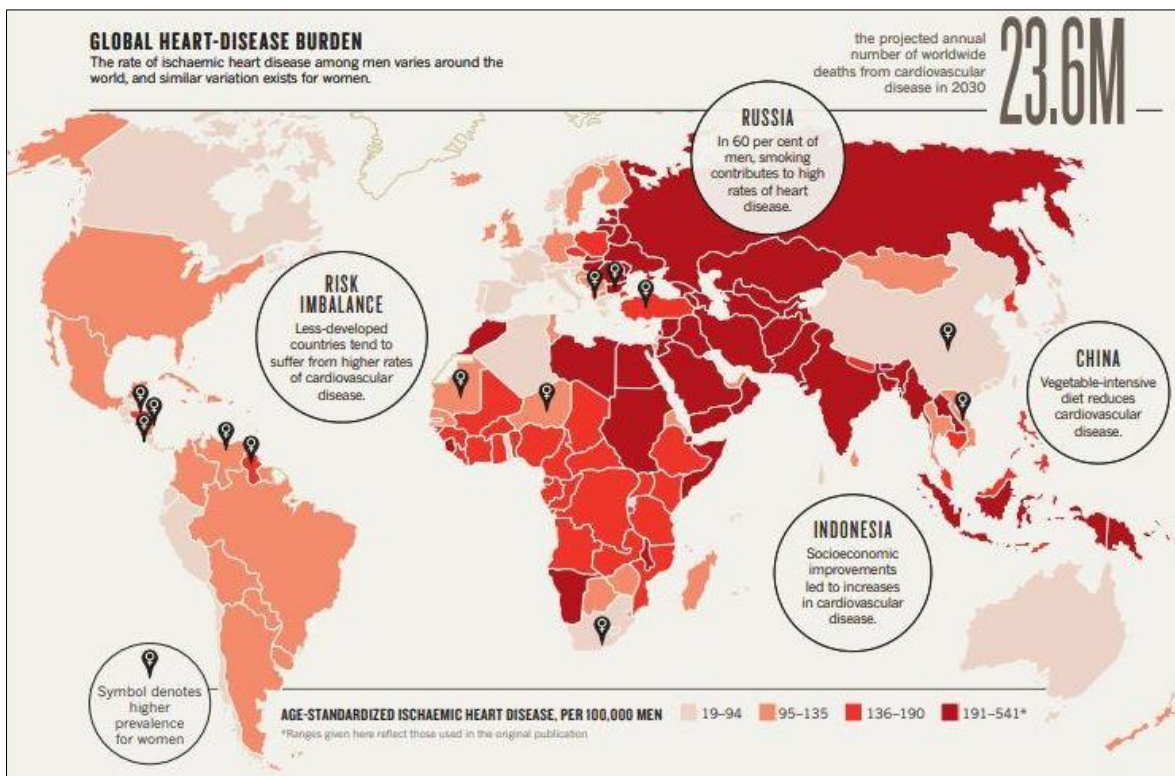


Figure 2 CVDs are widespread worldwide with an estimated number of deaths caused of about 23.6 million in 2030. Among the most important risk factors for the onset of CVDs are smoking, diets poor in vegetables but rich in fat. These diseases are prevalent in women in the populations of South America and Eastern Europe. (Cannon B., Nature 2013) ⁴².

A crucial role for the onset and progression of CVDs is represented by plasma lipoproteins that are complex spherical structures. They have the function of carrying endogenous triglycerides and cholesterol in esterified form to peripheral tissues and are then eliminated by the liver because hydrophobic nature of these molecules makes their solubilization difficult in the blood stream ⁴³. Lipoproteins are generally composed by an apolar core containing cholesterol esters and triacylglycerols surrounded by a hydrophilic surface containing amphipathic molecules ⁴⁴. Lipoproteins are classified according to size and density into HDL, low-density lipoproteins (LDL), very low-density lipoprotein (VLDL) and are synthesized by the liver ⁴⁵. APOA-I is the major component of HDL. HDL are macromolecular complexes composed of proteins, free and esterified cholesterol, phospholipids, and triglycerides, complement components and protease inhibitors as well as microRNAs ⁴⁶.

In the late 1950s, Eder and colleagues isolated HDL from human serum as a chemical entity by ultracentrifugation, but it was only in the 1960s that the biological roles of serum lipoproteins and their impact on the cardiovascular system were established ⁴⁷.

HDLs are well known as "good cholesterol" because they not only remove excess cholesterol from atherosclerotic plaques, but also exhibit anti-inflammatory and anti-oxidative properties. These capabilities coupled with the antithrombotic and vasodilatory capabilities give rise to the overall cardioprotective behaviour of HDL. Of considerable importance, epidemiological studies have shown that plasma HDL concentrations are inversely related to the risk of premature atherosclerotic heart disease, but it is important to underline that these anti-atherogenic effects of HDL do not depend only on its concentration in the circulating blood but also on its biological quality ⁴⁸. Today, it is well known that HDL plays critical roles in the transport and metabolism of lipids, such as cholesterol and triglycerides, while a combination of high LDL and low HDL levels is major risk factor for atherosclerotic heart disease ⁴⁹.

1.3.1 HDL: Structure and metabolism

HDL constitutes a heterogeneous group of particles differing in density, size, electrophoretic mobility, lipid composition and apolipoprotein content. Therefore, the different HDL subpopulation can be distinguished based on different parameters and on different techniques according to their physicochemical properties. Human HDL can be separated by ultracentrifugation into two major subfractions on the basis of density, HDL2 (1.063–1.125 g/ml) and HDL3 (1.125–1.21 g/ml), which is relatively protein-rich. HDL2 and HDL3 can be further divided on gradient gel electrophoresis into HDL2b (10.6 nm), HDL2a (9.2 nm), HDL3a (8.4 nm), HDL3b (8.0 nm) and HDL3c (7.6 nm) in decreasing order of particle diameter. In addition, HDL can be separated into two main subpopulations on the basis of electrophoretic mobility:

the major subfraction has a relatively high negative surface charge density and is called α -HDL, whereas the other fraction is called pre β -HDL⁵⁰. Most of the HDL particles in plasma are α -HDL and pre β -HDL represents only approximately 5%.

In normal plasma, most of HDL are spherical, and consist of a hydrophobic core (mainly cholesteryl esters with a small amount of triglycerides) surrounded by a surface monolayer consisting of phospholipids, unesterified cholesterol and apolipoproteins. A small HDL population has a discoidal shape delipidated, characterized by only a bilayer of phospholipids with some unesterified cholesterol and apolipoproteins, without hydrophobic core. Plasma HDL contains two main apolipoproteins, being APOA-I (70% of total HDL content) and APOA-II (20%). Other proteins such as APOA-IV, APOA-V, APOC, APOD, APOE, APOJ and APOL can be present in minor amounts and especially enzymes can be incorporated in HDL particles and play an important role in their metabolism^{51 52}.

The biosynthesis of endogenous HDL starts with the production and secretion of APOA-I, the main protein of HDL, by the liver (80%) or intestine (20%) in a lipid-free form. Nascent, discoidal HDL in the plasma, is then formed through lipidation of APOA-I, which is achieved through the efflux of free phospholipid and cholesterol mediated by the ATP-binding cassette transporter A1 (ABCA1)⁵³.

Subsequently, the low amount of cholesterol presents in these discoidal HDLs is esterified by LCAT enzyme forming converting free cholesterol into cholesterol ester (CE), highly hydrophobic, which can then be internalized into the core of the HDL particle, initiating its transformation from discoidal pre- β HDL into spherical alpha HDL that predominates in the plasma. Initially, these newly formed spherical HDLs contain only two molecules of APOA-I per particle. However, they are subject to extensive remodelling by various factors, changing their composition and size⁵⁴.

The free cholesterol esterification is thought to form a cholesterol gradient that enables more cholesterol to bind onto the HDL surface in

the subsequent steps of reverse cholesterol transport (RCT). Spherical HDL can further internalize cholesterol effluxed by ATP-binding cassette transporter G1 (ABCG1), and scavenger receptor type B-I (SR-BI) to become more mature, larger spherical HDL. Mature HDL can also exchange CE for triglycerides from LDL, a process that is mediated by cholesteryl ester transfer protein (CETP). Mature HDL is typically composed of a hydrophobic core containing 8 cholesterol esters and triglycerides and a hydrophilic surface containing lipids, proteins such as APOA-I, unesterified cholesterol as shown in figure 3. Mature HDL delivers its cargo molecules to hepatocytes where they are metabolized through an SR-BI-mediated process ⁵⁵.

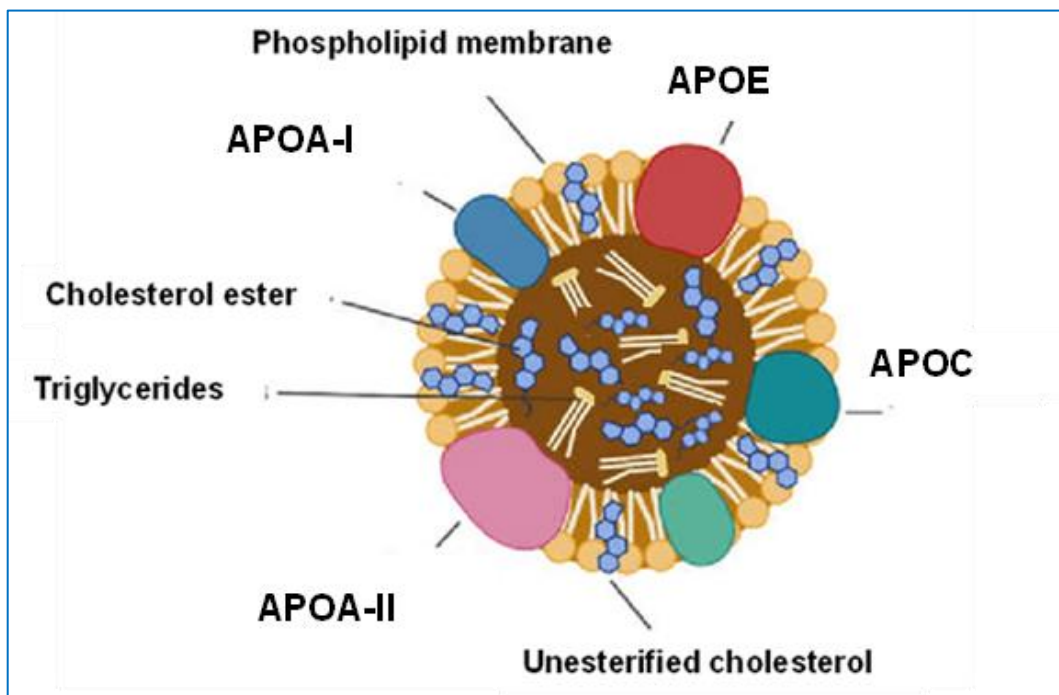


Figure 3 Mature HDL cross section. The mature HDL particle is composed by a hydrophobic core containing 8 cholesterol esters and triglycerides and an hydrophilic surface containing proteins such as APOA-I, the main one, APOE, APOC, APOA-II, membrane phospholipids and unesterified cholesterol. (Image by Biorender.com with modifications).

1.3.2 HDL molecular components

1.3.2.1 HDL proteome: Not only APOA-I, other major proteins key roles

Proteins form the major structural and functional component of HDL particles.

HDL carries a large number of different proteins as compared to other lipoprotein classes.

APOA-I is the main component of HDL (about 70% of the total protein mass) while another 15-20% is made up of APOA-I; but the key biological functions in which HDL are involved in lipid metabolism and redox reactions are also assisted by the associated enzymatic component.

The main enzymes include LCAT, paraoxonase 1 (PON1), paraoxonase 3 (PON3), platelet activation factor-acetyl hydrolase (PAF-AH) and glutathione seleno peroxidase 3 (GSPx-3) ⁵⁶.

Plasma activity of LCAT is mainly associated with HDL (75%), but is also present in other lipoproteins, where it catalyses the esterification of cholesterol to cholesterol esters ⁵⁷.

Human paraoxonases (PONs) are a family of calcium-dependent lactonases. A member of this family, PON1, is present in serum predominantly anchored to the HDLs surface and has hydrolytic activity for various substrates including oxidized phospholipids, cholesterol hydroxides contained in oxidized LDL (ox-LDL). Therefore, PON1 is able to limit the accumulation of ox-LDL and the formation of foam cells, which constitute a fundamental step in the development of atherosclerosis ⁵⁸. In plasma, PAF-AH primarily circulates associated to LDL lipoproteins, but around a 30% can be found on HDL particles. PAF-AH has calcium-independent hydrolytic activity and is responsible for platelet-activating factor (PAF) inactivation as well as pro-inflammatory oxidized short-chain phospholipids degradation. Studies have shown that levels of HDL-associated PAF-AH increase when APOA-I is

overexpressed, suggesting a possible participation of this enzyme to HDL anti-inflammatory and anti-oxidative properties ⁵⁹.

Gspx-3, present in the serum exclusively associated with HDL particles, has the ability to catalyse the reduction of hydrogen peroxide, lipid peroxides and organic hydroperoxides, thus preserving the biological components from oxidative damage thus contributing to the anti-oxidative function of HDL ⁶⁰.

Under inflammatory conditions, proteins involved in the acute-phase response can become predominant among HDL-associated proteins. Major acute phase reactants are serum amyloid A (SAA) proteins. During acute inflammatory response, SAA circulating levels can transiently increase by more than 1000-fold and SAA is found primarily associated to HDL where it can become the most abundant apolipoprotein ³⁴.

1.3.2.2 HDL Lipidome

The lipid elements represent a very heterogeneous component of the HDL constituting about the half of the total weight ⁵⁰.

The main lipid class are the phospholipids (PLs), arranged in a surface lipid monolayer where we can identify mainly phosphatidylcholine. This latter is the more abundant and equitably distributed among the various subpopulations of HDL given its structural role. Others important PLs are lysophosphatidylcholine, phosphatidylcholine and plasmalogens ⁶¹.

Negatively charged PL, including phosphatidylinositol (PI), phosphatidylserine (PS), phosphatidylglycerol (PG), phosphatidic acid (PA) and cardiolipin, although present at very low concentrations, may have a significant effect on the HDL-load dependent interactions involving various protein components (e.g. lipase, lipid transfer proteins, membrane proteins) modifying the net surface charge of HDL. Sphingolipids are the second most abundant class of lipids (5-10% of the weight of total lipids in HDL) and perform other major structural

functions, since their amount can modulate the surface pressure of lipoproteins, the stiffness, thereby affecting the HDL-activity of the associated proteins ⁶¹.

Sphingolipids ceramides (signalling molecule of crucial importance in cell survival, growth and differentiation) and sphingosine 1-phosphate (S1P, playing a role in vascular biology) represent two other minor bioactive molecules. S1P plasmatic bioavailability primarily depends on HDL transport and its binding to receptors on endothelial and smooth muscle cells is essential for regulating signalling pathways involving cell proliferation, motility, angiogenesis and immune response.

In the HDL surface lipid monolayer, along with PLs, unesterified (free) sterols are also found, essentially constituted by cholesterol which contributes to regulate the monolayer fluidity ⁶². Finally, HDL lipid core contains two large classes of highly hydrophobic lipids: cholesteryl esters and triglycerides, roughly accounting for 35 and 10 % of HDL lipid mass respectively.

1.3.3 Another lipoprotein's crucial role in CVD: VLDL and LDL

An important role in the transport of triglycerides and cholesterol is also played by VLDLs and LDLs. The VLDLs, synthesized in the liver, carry triglycerides and cholesterol from the liver to peripheral tissues are composed mainly of APOB-100 and APOC-II and their synthesis increases with the increase of free intrahepatic fatty acids, as in high-fat diets and in cases of release of free fatty acids from excess fat tissue directly circulating, for example in obesity and uncontrolled diabetes mellitus. APOC-II on the VLDL surface activates endothelial lipoprotein lipase to break down triglycerides into free fatty acids and glycerol, which are then absorbed by cells. Intermediate-density lipoproteins (IDLs) are the product of VLDL and chylomicron processing by LPL. The IDLs and the remnants of the chylomicrons, both of which are rich in

cholesterol, are eliminated by the liver or metabolized by hepatic lipase into LDL.

The products of VLDL and IDL metabolism are LDL, shown in figure 4, the richest in cholesterol lipoproteins. About 40-60% of all LDL is cleared by the liver in a process mediated by APOB and liver LDL receptors. The remainder is taken up by hepatic receptors for LDL or by non-hepatic receptors not specific for LDL (scavenger). The liver LDL receptors are down-regulated by the arrival of cholesterol to the liver through chylomicrons and by a diet rich in saturated fat; instead they are over-regulated by a diet low in fat and cholesterol. Non-hepatic scavenger receptors, particularly those of macrophages, capture excess oxidized LDL circulating, not processed by hepatic receptors. Oxidized LDL-rich monocytes migrate into the subendothelial space and become macrophages; these macrophages capture more oxidized LDL and form foam cells within atherosclerotic plaques.

The LDL particle size varies from large and buoyant to small and dense. The small and dense LDL are particularly rich in cholesterol esters and are associated with metabolic disorders such as hypertriglyceridemia and insulin resistance ⁶³.

It is well known that high levels of LDL in the circulatory stream are directly related to the onset of CVDs such as atherosclerosis.

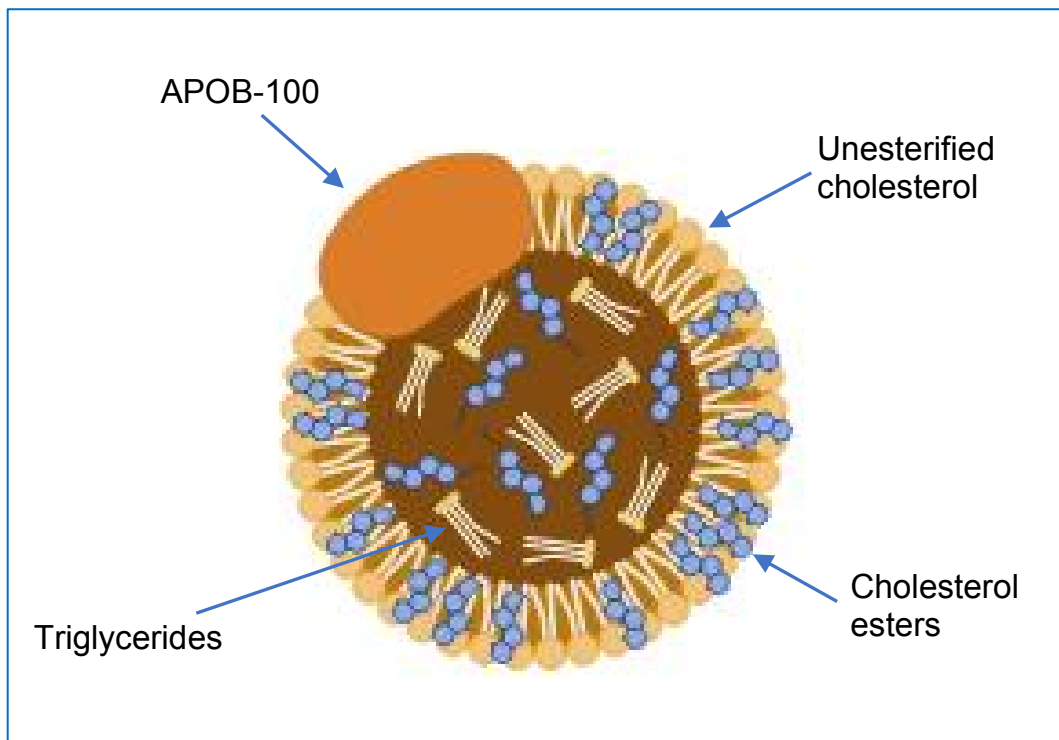


Figure 4 LDL cross-section. LDL particles have a structure consisting of a core containing triglycerides and rich in cholesterol esters and a hydrophilic surface containing apoproteins, phospholipids, unesterified cholesterol. The main differences between VLDL, IDL, and LDL are the size, the amount of esterified cholesterol and triglycerides in the core and the lipid and apoprotein classes on the surface. These characteristics are peculiar for the different functions that each lipoprotein covers in the body. Image by Biorender.com (with modifications).

1.3.4 Cholesterol levels and atherosclerosis disease

The onset and progress of atherosclerotic lesions are regulated by multiple interrelated factors that contribute to endothelium damage (Fig. 5). Of crucial importance in the establishment of endothelial dysfunction are the accumulation of lipids, biomechanical stress and chronic inflammation⁶³.

Atherosclerosis is a chronic multifactorial disease characterized by the accumulation of lipid inflammatory cells and fibrous tissue within the arteries' tunica intima. This process leads to an asymmetrical and focal thickening of the underwear. In the process of plaque development, complex interactions between the vascular wall cells and immune system lead to a progressive reduction of the fibrous cap and a simultaneous increase in the thickness of the so-called lipid nucleus, together with an increase in inflammatory activity ⁶⁵. This process

underlies the formation of the so-called 'Vulnerable plaque', that is an atherosclerotic plaque with a high-risk rupture resulting in the exposure of highly thrombogenic intra-plaque material in the bloodstream and the formation of thrombi or emboli which often lead to the occlusion of the injured artery. These events are preferred by high levels of LDL, resulting in oxidation of LDL and accumulation of oxidized LDL (Ox-LDL) in the subendothelial space.

Ox-LDLs are highly atherogenic molecules with the ability to promote a strong inflammatory response at the site of the nascent lesion. IL-1 and TNF- α are two main cytokines involved in this process promoting greater expression of the adhesion molecules VCAM1 and ICAM1, both on the surface of arterial endothelial cells and in their soluble form. Ox-LDLs also stimulate endothelial secretion of MCP-1. This accumulation in the arterial wall contribute significantly to the recruitment of circulating monocytes, their adhesion to the endothelium and their maturation into tissue macrophages ⁶⁶. The early lesion, or lipid streak, is predominantly composed of lipid-embedded macrophages (foam cells) and some T lymphocytes. Furthermore, ox-LDL-induced activation of nuclear factor-kappa B (NF- κ B) is associated with vasoconstriction, platelet aggregation, thrombosis and a potent mitogenic effect on vascular smooth muscle cells (VSMC). Compared to the latter process, the increased expression of platelet-derived growth factor (PDGF) plays an important role in inducing phenotypic switching in VSMCs which from the contractile state become proliferative and show migratory and synthetic activity. VSMCs then migrate from the media to the intima at the site of the vascular lesion where they proliferate and produce components of the extracellular matrix that contribute to the formation of a fibrous cap on the necrotic lipid-rich nucleus. This results in the progression of the primary fatty streak into a mature fibrofatty atheroma.

Advanced atherosclerotic lesion, or atherosclerotic plaque, therefore, is a complex structure: at the centre of the plaque there are mainly foamy cells and extracellular lipids, surrounded by a cap of VSMC and

extracellular matrix rich in collagen ⁶⁷. The activation of macrophages and other inflammatory cells that infiltrate the lesion induces the release of proinflammatory cytokines, amplifying and inducing a chronic inflammatory response that, far from resolving the disease state, feeds it and contributes to progressively aggravate it. Hypercholesterolemia is one of the main risk factors for atherosclerosis.

The total concentration of cholesterol in the human body is affected by its absorption through the GI tract, its synthesis starting from the components of the diet, its removal from tissues and blood by apolipoproteins and its consequent degradation to bile acids.

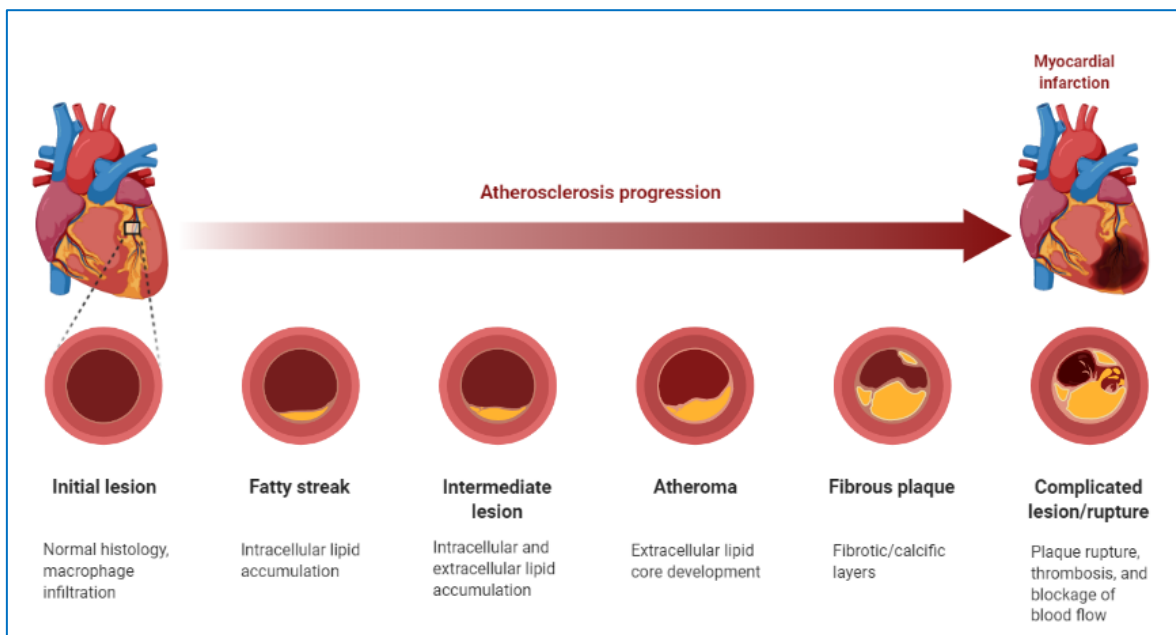


Figure 5 Atherosclerosis disease progression steps until myocardial infraction. A crucial role is covered by plasmatic lipoprotein contains cholesterol that under dyslipidaemia conditions or in response to harmful stimuli are deemed and accumulated at the sub-endothelial level in the arterial walls. This triggers the recruitment of innate immunity cells that eventually lead to intraplaque inflammation and a pro-thrombotic state. Increased total cholesterol (CT) in the blood and LDL-C, as well as the so-called atherogenic lipid triad (increased VLDL; increased small and dense LDL and reduction of HDL) appear to be relevant to the onset of cardiovascular disease. (Imagine from BioRender.com)

1.3.5 HDL anti-atherosclerotic biological functions

HDLs perform very important functions not only concerning cholesterol homeostasis (RCT from peripheral tissues to liver) but also antioxidant, anti-inflammatory and endothelial protection properties that contribute

to its cardioprotective potential. These functions have been functionally linked to the well-known ability of HDL to induce the activation of the efflux pathways of cellular cholesterol ⁶⁷.

1.3.5.1 Reverse cholesterol transport

RCT is the process by which excess cholesterol from peripheral tissues leaves cells (including foam cells in atherosclerotic plaques), enters blood circulation and is excreted into the stool. In this process HDL acts as a specific cholesterol acceptor that carries excess cholesterol reserves within peripheral plasma tissues, and then delivers it to the liver, where it can be excreted directly into bile or metabolized into bile acids/bile salts before excretion ⁶⁹ (fig.6).

Dietary cholesterol is absorbed by intestinal cells and becomes esterified by acyl-coenzyme A: cholesterol acyltransferase (ACAT). This esterified cholesterol is subsequently packaged into chylomicrons and via the lymph ducts transported to the blood plasma. In the plasma, the triglycerides which are also present in the chylomicrons are broken down by lipoprotein lipase (LPL), releasing free fatty acids as a source of energy or to be stored in adipose tissues. The remaining residual chylomicrons containing dietary cholesterol are finally absorbed by the liver which also produces endogenous cholesterol. Additionally, the liver itself also produces endogenous cholesterol. From the liver, cholesterol (together with triglycerides) is incorporated into VLDLs which are secreted into the plasma, where the triglycerides are again broken down by LPL. By the loss of triglycerides, VLDL particles are in a complex series of reactions converted in LDL particles which are triglyceride-poor but cholesterol-rich.

Via LDL, the cholesterol will be delivered and deposited in peripheral tissues making use of the LDL receptor.

In contrast, HDL, and in particular APOA-I, can accept cholesterol from macrophages in the arterial wall in a process that depends on ABCA1.

Cholesterol efflux, along with phospholipids, from macrophages to APOA-I is the first step in the transport path of potentially cardioprotective RCT, so excess cholesterol from peripheral tissues leaves cells (including foam cells in atherosclerotic plaques), enters the bloodstream and is excreted in the stool. The efflux of cholesterol and phospholipids in APOA-I generates nascent and discoidal HDL particles that are quickly converted from LCAT to spherical HDL that are found in plasma 63.

The HDL then acts effectively as a specific cholesterol acceptor that carries excess cholesterol reserves within peripheral plasma tissues, and then delivers it to the liver, where it can be excreted directly into bile or metabolized into bile acids/bile salts before excretion 42.

Cholesterol efflux from a variety of cell types, including macrophages, to HDL in the extracellular space is mediated by two distinct processes: cholesterol outflow induced by a specific cell carrier and the aqueous diffusion of passive cholesterol from cell membranes.

Macrophage extracellular cholesterol is primarily derived from the internalization of plasma lipoproteins or from the efferocytosis of apoptotic cells, which enter the cellular pool together with newly synthesized cholesterol. To prevent toxicity, surplus cholesterol is effluxed from the cells to extracellular acceptors or converted to cholesteryl ester (CE) and stored in cytosolic lipid droplets (LDs) 71.

Lipid-free or low-lipid APOA-I secreted in the liver can mediate cellular efflux of both cholesterol and phospholipid levels from macrophages via the ABCA1 and collect them on the surface of the pre- β HDL, resulting in rapid lipidation of APOA-I to generate a mature HDL.

ABCA1 and ABCG1 are critical receptors for the initial phase of RCT in atherosclerosis plaques, i.e. outflow of cholesterol from foam cells. Foam cells are traditionally cholesterol-loaded macrophages from monocytes, but they may also be macrophage-like cells from vascular smooth cells loaded with cholesterol muscle cells. Prior to efflux, cholesterol must be in its "free" (non-esterified) form to be pumped out of the cells.

LD cholesterol undergoes constitutive cycles of hydrolysis and re-esterification. Free cholesterol released by LD via CE hydrolysis can be transported to the plasma membrane and effluxed to a cholesterol acceptor, or, in a "futile cycle", re-esterified by the ER-resident acyl-CoA protein: cholesterol acyl transferase (ACAT) ⁷².

After the transfer of cholesterol to the HDL particles, the next step is the esterification of cholesterol acquired by LCAT enzyme to form CE, giving rise to mature HDLs. HDL remodelling particles can occur through HDL triglyceride mediated hydrolysis of phospholipids hepatic lipase (PLP) and endothelial lipase (EL) respectively. In humans the HDL core can be transferred to triglyceride lipoproteins, VLDL and LDL, by cholesterol ester transfer protein (CETP) via hepatic elimination in the liver via the LDLR, or selectively absorbed via SR-B1 which acts as a hepatic receptor for CE on HDL.

Therefore, RCT to liver cell-derived cholesterol in humans provides two routes: direct (HDL-SR-B1) and indirect (HDL-LDL / VLDL-liver LDLR).

In the final step of RCT, CE is hydrolysed back to free cholesterol and converted in bile acid or transported by ABCG5 and ABCG8 into the bile for its excretion into the faeces.

It is now established that the great bulk of RCT is driven by APOA-I, and *in vivo* evidence have demonstrated that its overexpression is able to enhance specific RCT from macrophages, which privilege ABCA1-mediated efflux. This mechanism largely accounts for APOA-I protective properties against atherosclerosis ⁷³.

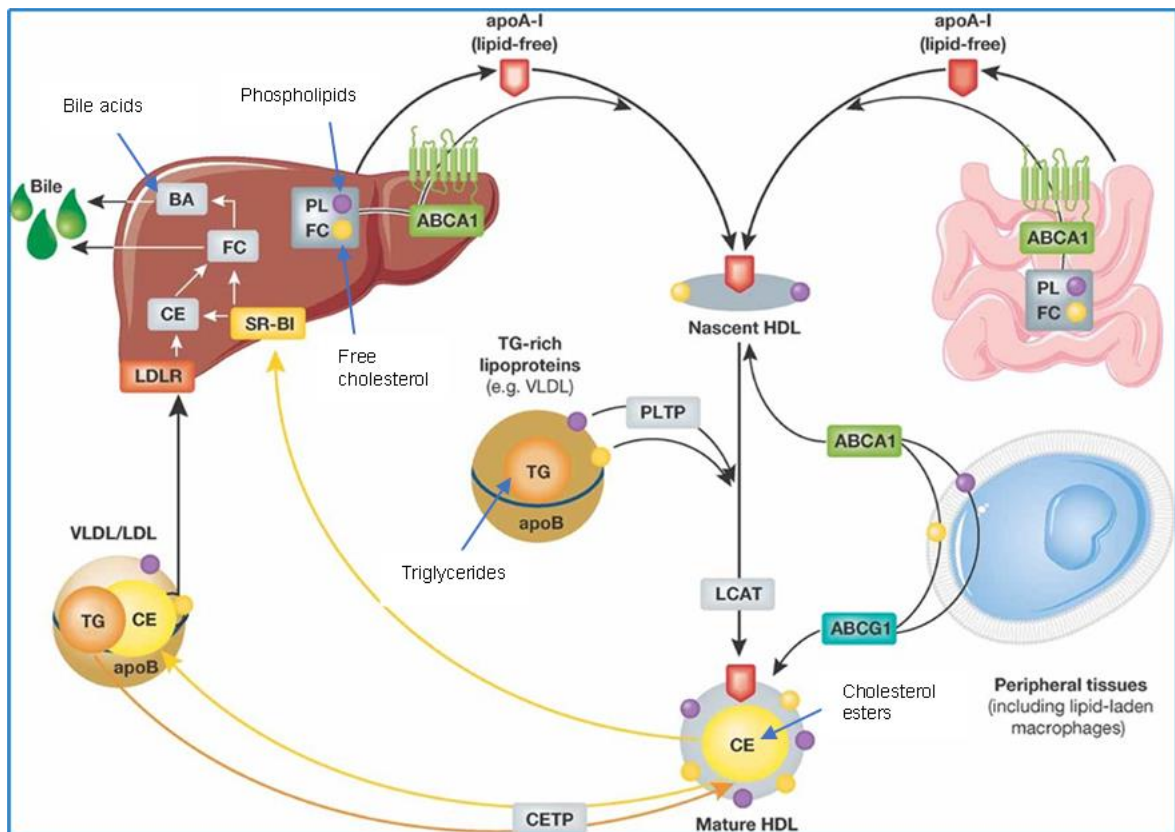


Figure 6 Overview of HDL role in RCT. A crucial role in cholesterol catabolism is covered by HDL. The nascent lipid-poor HDL particle composed mainly of APOA-I, in the circulatory torrent acts as an effluxed cholesterol acceptor from peripheral tissue cells through ABCA1 and ABCG1 transporters. The esterified cholesterol from the enzyme LCAT is transported to the liver for its catabolism contributing also to the maturation of the HDL particle itself. (Imagine by Besler C et al. EMBO Mol Med. 2012;4:251-268).

1.3.5.1.1 Proteomics of RCT

1.3.5.1.1.1 ABCA1/ABCG1

ABCA1 and ABCG1 are members of the ATP-binding cassette transporter family. ABCA1 and ABCG1 are responsible for the majority of macrophage cholesterol efflux to serum or HDL into macrophage foam cells, but other less efficient pathways such as passive efflux are also involved.

ABCA1 is expressed in peripheral cells and facilitates the export of cellular cholesterol to its extracellular acceptor protein, APOA-I. In macrophages, ABCA1 preferentially interacts with APOA-I catalysing its rapid lipidation, thus generating a mature HDL, called nascent HDL. It subsequently interacts with ABCG1 and (SRB-1) receptor to form

mature HDL particles. Studies have shown that abnormally low levels of serum HDL-C and an acceleration of cholesterol accumulation in peripheral tissues occur when loss of function of one of the two ABCA1 genes occurs, as in the case of Tangier disease ⁷⁴.

ABCG1 is a transmembrane half transporter that exports cellular lipids to extracellular acceptors and mediates cholesterol efflux, by playing a critical role in the efflux of cellular PL and FC for HDL maturation, with major affinity for spherical HDL than lipid-poor APOA-I particles.

The primary function of ABCG1 is stimulate net cholesterol efflux to spherical HDL. ABCG1 also effluxes cholesterol to LDLs, liposomes and cyclodextrin and it exports sphingomyelin, phosphatidylcholine and oxysterols to HDL and albumin.

ABCA1 and ABCG1 are activated directly by liver X receptors (LXR) to promote RCT ⁷⁵.

1.3.5.1.1.2 LXR Receptor

Liver X-receptors (LXRs), members of the nuclear steroid receptor superfamily and activated by oxysterol, are transcription factors which, after heterodimerization with the 9-cis-retinoic acid receptor (RXR), bind to specific LXR response elements (LXRE), thus regulating the expression of target genes involved in intra and extracellular lipid metabolism.

Oxidation of steroids by FC can activate LXR and regulate gene expression of ABCA1 and ABCG1 to enhance peripheral tissue cholesterol secretion. Meanwhile, LXRs are also readily oxidized by Peroxisome Proliferator Activated Receptor Alpha (*PPAR- α*) which is a protein that controls lipid and glucose metabolism in various tissues and cell types including liver, heart, kidney, adipose tissue and macrophages. *PPAR- α* activation suppresses chylomicrons and increases HDL production by enterocytes. Furthermore, its agonists promote macrophage cholesterol secretion by stimulating the expression of ABCA1 and LXR to increase the RCT ⁶⁹.

1.3.5.1.1.3 LCAT

LCAT, an enzyme associated with lipoproteins, has two different catalytic activities that explain its ability to esterify cholesterol in HDL: the activity of phospholipase A2, and the transesterification activity 69. It requires APOA-I and, to a lesser extent, other apolipoproteins, which most likely activate LCAT by modifying the presentation of its substrates, namely, phospholipids and cholesterol, on the lipoprotein surface. Cholesterol esters formed by the LCAT action, which are more hydrophobic than free cholesterol, are transferred from the surface of the lipoproteins to the hydrophobic core. This process converts pre- β HDL particles to HDL2 and HDL3, which are the main ones HDL species found in plasma representing larger spherical migratory HDL forms. This particle is capable of acquiring more cholesterol through other pathways, such as diffusion, SR-BI, and ABCG1 transporter. LCAT is important in the RCT process by generating a free cholesterol gradient from cells to HDL. This effect of LCAT prevents the back exchange of cholesterol by passive diffusion from HDL to peripheral cells and therefore is believed to promote the net removal of cholesterol from peripheral cells in HDL 77.

1.3.5.1.1.4 Endothelial lipase and hepatic lipase

HL and EL are members of the triglyceride lipase family, which also includes LPL. EL has a high phospholipase A1 activity and remodels HDL into small particles, while HL is more effective in hydrolysing triglycerides and also promotes the release of poor lipids APOA-I. The combined functions of HL and EL have a significant effect on HDL-C plasma levels 78 74.

1.3.5.1.1.5 CETP

CETP is a hydrophobic glycoprotein synthesized in different tissues but mainly in liver. It facilitates the exchange of cholesterol esters and

triglycerides between HDL and containing APOB particles (LDL, IDL, VLDL) and represents an important branching point for RCT. This results in cholesterol recycling and an increasing attenuation of blood circulation, with the potential to go back into the artery wall. Most CEs derived from LCAT do not return to the liver via the HDL SR-B1 pathway but, rather, via a more atherogenic pathway ⁷⁹. CETP mediates the transfer of most CEs from HDL to VLDL or other more atherogenic intermediate density lipoproteins and residues, and the transfer of triglycerides from VLDL-1 to HDL results in larger, relatively triglyceride-enriched LDL species. Transfer of CE from HDL directly to LDL from CETP could also be antiatherogenic if LDL is cleared from the liver LDL receptor ⁶⁹.

1.3.5.1.1.6 PLTP

Another transfer protein in this part of the RCT, PLTP, transfers phospholipids between VLDL and HDL. PLTP is a major modulator of plasma HDL size, composition and function and a major modulator of plasma HDL metabolism. The level of HDL or HDL production is dramatically reduced in *PLTP*^{-/-} mice and PLTP deficiency attenuates plaque accumulation in different atherosclerotic patterns ⁸⁰. This indicates that the PLTP plays an important role in atherogenesis, and its function goes far beyond that of transferring phospholipids between lipoproteins particles ⁷³.

1.3.6 HDL Antioxidant activity

Although RCT is the primarily recognized function of HDL, its athero-protective effects are also linked to antioxidant and anti-inflammatory properties ⁸¹.

The powerful antioxidant function is mainly expressed in the prevention of LDL pro-atherogenic oxidative modifications contributing to the removal and inactivation of lipid hydroperoxides, which are the main lipid peroxidation product accumulated in oxidized LDL (ox-LDLs) ⁸². The

HDL antioxidant properties critically involve enzymes associated with HDL, such as PON1, phospholipase A2 and LCAT, which have been reported to hydrolyse and thus neutralise oxidized phospholipids into lyso-phosphatidylcholine. In addition, HDL carries GSPx-3, which can reduce lipid peroxide (LOOH) to the corresponding hydroxides and thereby detoxify them ⁸³. Lipid transfer proteins also appear to contribute significantly to the antioxidant activity of HDL. In particular, CETP, by facilitating the absorption of HDL of lipid hydroperoxides from LDL particles, could increase their ability to inhibit the generation of ox-LDLs ⁸³. In addition, APOA-I shows great potential in the removal of lipids oxidized by LDL, suggesting that HDL can work as an acceptor of oxidized lipids. In particular, two residues of methionine in positions 112 and 148 allow APOA-I to directly reduce these species to form inactive lipid hydroxides making, therefore, LDL resistant to cell-mediated vascular oxidation and preventing LDL-induced oxidated monocyte adhesion and chemotaxis ⁸⁰.

Of considerable interest, some APOA-I variants carrying additional cysteine residues, such as the Milano variant, showed a stronger antioxidant activity *in vitro* than the WT APOA-I, suggesting a key role of the free thiol group.

1.3.7 HDL Anti-inflammatory activity

Also the inflammatory properties of HDL have an important impact on the development and progression of atherosclerosis as they result mainly with the inhibition of pro-inflammatory mechanisms.

The ability of HDLs to reduce the expression of adhesion molecules in endothelial cells is of central importance. Indeed, as described in more detail in section 1.3.4, the accumulation of macrophages in the arterial wall, a first step in the formation of atherosclerotic plaques, strongly depends on the adhesion of the hematic monocytes to the endothelial cells and their subsequent migration into the sub-endothelial space. The anti-inflammatory properties of HDL include suppression of the

production of inflammatory cytokines of macrophages and inhibition of the expression of endothelial cell adhesion molecules that promote the entry of monocytes and neutrophils into arteries as vascular cell adhesion molecule-1 (VCAM-1), intercellular adhesion molecule-1 (ICAM-1), e-selectin and monocyte chemoattractant protein-1 (MCP-1). One of the mechanisms behind this anti-inflammatory effect is the inhibition of sphingosine kinase of endothelial cells, which results in the suppression of the expression of adhesion molecules induced by TNF α and the inhibition of nuclear translocation NF- κ B, which is also involved in promoting the synthesis of adhesion proteins ⁸⁶.

In addition, the ability of HDL to induce nitric oxide (NO) synthesis is considered important to further prevent NF- κ B activation ⁸⁷.

1.3.8 The quality not so much the quantity for protective role of the HDL.

Although HDLs are known for their antiatherogenic and cardioprotective potential, in some studies it has been shown that, in particular conditions such as systemic inflammation, HDLs are subjected to several changes in structure and composition. This can cause not only the impairment of their physiological role but their transformation in inflammatory agents able to induce the production of reactive oxygen species (ROS) and to decrease the cholesterol efflux and the production of nitric oxide (NO) ⁸⁸.

Indeed, HDLs isolated from individuals affected from a condition of acute or chronic inflammation such as coronary artery disease (CAD) or coronary heart disease (CHD), appear to be dysfunctional because they show pro-inflammatory behaviour and do not exhibit the crucial protective effects at the endothelial level as in normal subjects. Precisely, the conversion into dysfunctional HDLs results from both the oxidative damage of essential lipid and protein components and the concurrent enrichment of these particles in pro-inflammatory proteins to the detriment of cardioprotective ones ⁸⁹.

Studies about this abnormal behaviour date back to the mid-nineties when it was observed that in the acute inflammatory phase, the positive acute phase reactant SAA is produced by the liver and other tissues and associates with HDLs. As the result, the HDLs exhibit a several changings in proteome. A significant enrichment in SAA resulting with a consequent depletion of APOA-I, is a condition that has been associated to an impairment of cholesterol efflux, stimulation of ROS production and decrement of NO. It has also been observed that during inflammation HDLs have also been reported to lose essential anti-inflammatory and antioxidant enzymes including PON and PAF-AH. A substantial contribution to HDL dysfunctionality has further been attributed to detrimental modifications of APOA-I, catalysed by the enzyme myeloperoxidase. This enzyme in an inflammatory environment such as in atherosclerotic tissues, leads to residue-specific oxidation and a consequent suppression of the capacity of APOA-I to promote macrophage-specific cholesterol efflux and LCAT activation. In line with these evidence, various doubts have been raised as to what benefits the rise in HDL-C levels (too high) could bring if there could be an inherent potential increase in atherosclerotic risk ⁹⁰.

At the same time, the lack of a causal relationship between HDL-C levels and cardiovascular risk has opened the way rather to functional improvement of HDL as a main therapeutic goal and not so much to the increase of their quantity.

1.3.9 Recombinant HDL/APO drugs

Epidemiological studies revealed that HDL/APOA-I levels are inversely associated to cardiovascular (CV) events and evidence in animal model studies have further shown that HDL mimetics have athero-protective properties ⁹¹. These observations led to the development of new therapies to reduce cardiovascular risk and the possible clinical efficacy of these mimetics was investigated *in vitro* and *in vivo* ⁹².

The first pre-clinical study on the therapeutic role of HDL in CVD has started in the late 1980s in animal models, particularly in rabbits fed with high cholesterol diet. They were subjected to intravenous infusion with 50 mg per week of purified HDL isolated from normal rabbits to test for possible reduction of aortic lesions. This led to a 60% reduction in the development of atherosclerotic-like lesions and a significant decrease in lipid deposits in the arterial wall compared to controls.

Other studies subsequently carried out using also the AIM led to promising results and since the 2000s clinical trials have been extended to primates and humans ⁹³. Unfortunately, most of the various formulations required venous administration and were both difficult and expensive to produce, primarily due the purification steps of the protein itself, leading to the interruption of the clinical trials.

In these formulations the APOA-I is usually produced in bacteria from which it must necessarily be highly purified in order not to carry with it residues of bacterial components that would be toxic or would trigger an immune response in the patient.

Together with the invasiveness towards the patient of some treatments / formulations, the one described above is the main limitation of the formulations tested to date, summarized in table 2.

1.3.9.1 Preliminary stage studies in course

HDL Therapeutics, Inc developed a new system, named PDS-2 to effectively delipidate plasma HDL and convert it to pre β -HDL, the only form of HDL that is effective in the initial phase of the RCT and present however at very low concentrations in the plasma. The autologous plasma was collected and delipidated and reinfused into the patient. In a preliminary study, 28 subjects with ACS underwent 7 weekly infusions of autologous delipidated plasma enriched in pre β -HDL. It was observed that treatment could lead to a decrease size in coronary plaque. The treatment was extended to a group of patients with familial hypercholesterolemia (HoFH) on stable lipid-lowering therapy. Patients,

studied at baseline and after 7 weekly of infusions, tolerated the treatment and a significant regression of the total cross-sectional area of the atheroma and of necrotic low-density central plaques (important marker of heart attack) were observed. Despite the small sample size of the study (as HoFH is a rare disease), these results provide the first clinical evidence for an improvement in RCT in humans ⁹⁴.

Another formulation that aims to improve the RCT acted on the increase of cholesterol efflux by activating LXR. T1317 was a synthetic HDL phospholipid encapsulated in nanoparticles and constituted of a APOA-I-derived 22-residues peptide designed to deliver LXR agonists to the atheroma. An atherosclerotic mouse model (ApoE-deficient) fed with high fat diet was administrated with injection of 30mg/kg or 1.5 mg/kg dose of T1317, or placebo, three times a week for six-weeks. No statistically significant reduction in the size of atherosclerotic plaques was observed at the lowest dose of 1.5 mg/kg. Instead, a significant reduction was observed at the dose of 30mg/kg compared with baseline. A similar result was observed for the aortic root plaque area. In addition, the upregulation of ABCA1 mRNA expression was measured in white blood cells. These preliminary results suggested that T1317 could constitute a promising therapeutic approach for the treatment of atherosclerosis ⁹⁵.

Other formulations are reported in table 2.

Drug	Composition	Treatment	Outcomes	Reference
ETC-216	Recombinant AIM and PL.	5 weekly intravenous infusions (15 or 45 mg/kg)	Significant regression of atherosclerotic disease burden (-1% and -4.2% of percent and total atheroma volume respectively). One serious adverse event resulted in the death of the patient.	⁹⁶
MDCO-216	Dimeric recombinant AIM and POPC	5 weekly intravenous infusions (20 mg/kg)	Increased cholesterol efflux capacity but no additional benefit on plaque burden in patients with ACS receiving statin therapy.	NCT02678923 ⁹⁷
CSL-111	APOA-I purified from human plasma and PC	5 weekly intravenous infusions (20 mg/kg)	No significant reduction of plaque and atheroma volume. Improvement of coronary score and plaque characterization index. Hepatotoxicity.	NCT00225719 ,
CSL-112	APOA-I purified from human plasma and PC	4 weekly infusions (2 or 6 g)	Considerable enhancement of cholesterol efflux capacity (>3-fold increase of ABCA-1-dependent efflux).	NCT03473223 ⁹⁸

Preβ-like HDL	Autologous selectively delipidated preβ-HDL enriched plasma	7 weekly infusions	Significant reduction in the total atheroma cross-sectional area associated to a decrement of low-density and necrotic core plaques volume in HoFH patients.	99
Peptide D-4F	18 all D-amino acids APOA-I mimetic peptide dissolved in 25% sucrose-water	13 daily oral doses (100, 300 or 500 mg)	Doses above 300 mg significantly dropped HII to an anti-inflammatory level in high-risk CHD subjects already under statin therapy	100
Peptide 6F	Transgenic tomato plants expressing an 18 amino acid APOA-I mimetic peptide	Added to WD at 2.2% by weight for 13 weeks	Significant reduction in the percent of the aorta with lesion and improvement of several plasma biomarkers including total cholesterol, triglycerides and PON activity in LDL receptor-null mice	101

Table 2 recombinant HDL/apo drugs. Clinical and pre-clinical stage studies.

1.3.9.2 A Promising class of therapeutic agents: APOA-I mimetic peptides

Another very promising class of therapeutic agents consists of APOA-I mimetic peptides. Despite having no sequence homology to human APOA-I protein, but just mimicking its main structural motif, these peptides can also reproduce many of its anti-inflammatory and lipid-binding properties ¹⁰². A great part of the interest for some APOA-I mimetic peptides definitely arises from their oral bioavailability.

In this regard, D-4F (Ac-D-W-F-K-A-F-Y-D-K-V-A-E-K-F-K-E-A-F-NH₂) is probably the most extensively studied peptide. It is synthesized from all D-amino acids, which makes it resistant to enzymatic degradation and allows an oral delivery of this therapeutic agent.

Both D-4F administrated through gastric gavage in LDL receptor-null mice on a Western Diet, and administration of D-4F added to the drinking water to *Apoe*^{-/-} mice are able to significantly reduce LDL-induced monocyte chemotactic activity and produce a substantial increase in the protective capacity of HDL. A pronounced regression (79%) of atherosclerotic lesions has also been observed, underlining its pharmacological potential for the treatment and prevention of atherosclerosis and chronic inflammatory disease ¹⁰³.

Studies investigating the mechanisms of action of D-4F have revealed that its oral administration in *Apoe*^{-/-} mice induces positive HDL remodelling forming preβ-HDL enriched in APOA-I and paraoxonase

activity. Also, D-4F rapidly promotes cholesterol efflux from macrophages both *in vitro* and *in vivo*. These effects could likely account for its strong athero-protective properties.

A first proof of concept assessed that single doses ranging from 0.43 to 7.14 mg/kg of oral D-4F administered to an atherosclerotic mouse model are safe and rapidly absorbed. Preliminary results have additionally pointed out a significant improvement of HDL inflammatory index (HII). This study further reinforced the enthusiasm for a promising oral therapy to prevent atherosclerosis ¹⁰⁴.

Unfortunately, efficiency of D-4F mimetic peptide strongly depends on the presence of end blocking groups: addition of an acetyl group at the alpha-amino terminus and an amide at the alpha-carboxyl terminus improves the class A amphipathic helix stability. This means that the production of D-4F especially depends on chemical synthesis which is also the main cause of excessive production costs.

Another mimetic peptide under study is RG33, a small peptide that was synthesized and chemically modified at the terms for increased stability which corresponds to the last two helices of the APOA-I structure which was observed to have stability and solubility in serum, to be able to control glucose *in vivo* in an insulin-resistant mouse model and promote the efflux of cholesterol from cultured macrophages. The impact of the peptide on cholesterol transport and glucose control in insulin-resistant mouse model (at single dose 12 mg/kg by intraperitoneal or subcutaneous injection) compared with controls, made it a good therapeutic candidate for the treatment of diabetes and evaluation for an use in atherosclerotic diseases is also under review ^{105 106}.

1.3.9.2.1 Plants as bioreactor for therapeutics agents

A new goal is to consider the plant itself as an oral vehicle of recombinant proteins using edible plant tissues (EPT). This means that an exhaustive purification is not necessary, since they can be

administered orally as partially purified formulations that are safe for consumption ¹⁰⁷.

The plant is thus no longer only the instrument of action of genome editing, but a delivery instrument for humans.

Recombinant proteins can be expressed in leaves, seeds, fruits and food tubers, depending on the plant species. Many different edible species have been studied, including carrot, lettuce, tomato, potato, corn, wheat, barley, strawberry, soy, banana, and rice.

The concept of edible pharmaceutical products of plant origin was initially conceived in the early 90s, when Charles J. Arntzenc emphasized the idea of making vaccines in edible fruits, initially using potato as a model. Although the feasibility of orally administered plant-derived vaccines has been demonstrated and numerous phase clinical trials have been completed, the raw potato is unsightly, and cooking has the potential to destroy most of the protein-based vaccine candidates ¹⁰⁸.

To stem some difficulties that may arise in the consumption of the whole plant such as the specific control of the dosage requirements and the fluctuation of the consistency that varies from fruit to fruit, from plant to plant and from generation to generation, the idea of consuming the fruit directly it has been replaced by the use of dried or partially purified formulations to standardize for each use ¹⁰⁹.

Cereal crops, therefore, become among the major candidates for the expression of pharmaceutical proteins since the seeds accumulate recombinant proteins at high levels in a stable, dried environment, thus allowing long-term conservation of antigens without the need for particular storage conditions ¹¹⁰.

Particular focus has been placed on 6F (DWLKAIFYDKFFEKFKEFF), which shows to have similar efficacy *in vitro* to D-4F and especially oral administration of such peptide is effective even in the absence of end blocking groups in model mice.

Unlike D-4F, 6F production could therefore be implemented exploiting living organisms to obtain large amount of peptide in a simpler and cheaper way.

To this end, tomato plants have been genetically engineered to express the 6F peptide in their fruit (6F tomatoes), providing a possible upgrade to APOA-I mimetic oral therapy. Studies conducted by the group of Fogelman and Navab have shown that feeding atherosclerotic mice with 6F tomatoes powder as dietary supplement to a fat diet for 13 weeks improves the level of atherosclerosis compared to the control group ¹¹¹. Precisely, they revealed that the peptide retains unaltered anti-inflammatory properties being able to significantly lower SAA, total cholesterol, triglycerides and lysophosphatidic acid (LPA) plasma levels, while improving plasma HDL cholesterol, PON activity and atherosclerotic lesions. This study also showed that 6F acts at the level of the small intestine (it has been detected intact) where its function has been further validated and therefore provides the basis for a new approach to oral mimetic therapy with APOA-I ¹⁰¹.

1.4 APO- Rice project strategy

Taking inspiration from the 6F tomatoes, our group has taken advantage of genetic engineering of edible plants in order to obtain at once an effective system of production and delivery for AIM protein.

To this extent, a study conducted by Romano and others in 2018, has shown a new approach for treatment of CVDs because, despite the high therapeutic potential of APOA-I proteins, the practical application is hampered by the low efficiency of purification and delivery ¹¹².

This involves the use of the mutein AIM, known to have athero-protective functions in carriers and anti-inflammatory properties ^{113 114 115}.

In this novel production and delivery system, genetic transformation of rice plants (*Oryza sativa ssp. Japonica* Rosa Marchetti) has been performed by means of *Agrobacterium tumefaciens* cells containing an

engineered plasmid expressing the AIM gene under the control of the tissue specific rice prolamin promoter. This results in the specific expression of the full-length AIM protein in the seeds of transgenic rice plants and AIM was supplied as a protein extract from transgenic rice seeds without need for purification¹¹². The mechanical grinding of the rice seeds thus obtained without any phase processing is called "rice flour" (RF). The safety, tolerability and efficacy of the product and delivery method were measured in an *in vitro* model of ox-LDL-loaded macrophages and in an *in vivo* atherosclerosis model such as *Apoe*^{-/-} mice fed with Western Diet (WD). Both experimental trials further confirmed the fundamental anti-inflammatory and antiatherogenic properties of the AIM muteins.

In vitro tests have shown that APO rice administration is able to inhibit MCP-1 expression and lipids accumulation in THP-1 macrophages stimulated with ox-LDLs, leading to a significant reduction of foam cells formation. Furthermore, the AIM proteins in this formulation were still found to be able to promote RCT thus also maintaining one of the key biological roles of human APOA-I.

In this pre-clinical study, called APO2 study, a daily oral dose of 0.83 mg / kg of APO rice for 5 days/week for three weeks was tested in treated group. The control mice were fed with WD supplied with WT rice of the same variety of rice engineered. More importantly, from a therapeutic point of view, oral administration of APO RF dissolved in water (APO-milk), was able to reduce early / intermediate atherosclerotic lesions in *Apoe*^{-/-} mice treated with WD and improvement of systemic inflammation were observed.

The treatment showed to be well tolerated and safe. For the treated group, a noticeable regression of plaque extension and a reduction in macrophage activation in the liver was observed, compared to the control group. The reduction of the atherosclerotic plaque in the aortic sinus and aortic arch in the treated group, was continued throughout the duration of the treatment, despite the administration of a high-fat diet.

These results suggested that AIM muteins, administered orally as a whole protein in rice milk, maintained the antiatherogenic properties that other groups observed by infusion of higher concentration of HDL-Milano. It has also been shown that HDL-Milano infusion also has systemic anti-inflammatory effects. A 7 weeks high-fat diet was associated with liver inflammation in *ApoE*^{-/-} mice. Then, it was investigated whether the anti-inflammatory properties of AIM could be preserved in the oral delivery of APO rice milk and inflammation in the liver of APO treated and control mice was evaluated. Treatment with AIM has been shown to slightly but significantly reduce CD68 positive liver cells (expressed by circulating macrophages and tissue macrophages such as Kupffer cells), supporting the hypothesis that AIM protein released orally retained anti-inflammatory properties at sites other than the vascular system. On the other hand, no reduction in liver fibrosis was observed and this result is consistent with the fact that fibrosis is a complex and multifactorial condition that requires a long-term therapeutic approach to be resolved.

This thesis focuses on a subsequent preclinical study, called APO3 study, where a daily oral dose of 0.63mg/kg of APO rice for 5 days/week for four weeks was tested in in the same atherosclerotic model of APO2 study. The control mice were fed with WD supplied with WT rice of the same variety of rice engineered. The treatment resulted safety and efficacy. Moreover an improvement of atherosclerotic conditions and systemic inflammation was observed.

The effect of AIM milk administered by gavage on atherosclerotic plaques and on the liver could be attributed to the fact that our approach is based on synthesis sources and a different AIM delivery route. The AIM protein is synthesized by the cells of the endosperm tissue of rice and then, delivered to the affected organism by oral administration. One of the functions, considered relevant for APOA-I anti-atherosclerotic and anti-inflammatory effects, and, to a greater extent of AIM, is the RCT, which is the ability to efflux the cholesterol from cells and transport it to the liver for catabolism. HDL/APOA-I(M)

complexes can be quite heterogeneous in size and shape, and this could impact their function. Unlike almost other HDL formulations, our method does not provide pre-assembled HDL/APO particles, but any assembly could be directly in the bioreactor and thus be more natural. We rely on the transformation of the AIM protein into rice cells and the ability of the AIM protein to assemble with lipids and other AIM proteins (by AIM dimerization). The biological properties of AIM synthesized in rice seeds are maintained in our formulation.

The rice seeds act both as bioreactors for the synthesis of recombinant AIM and as a safe delivery vehicle. This way of drug synthesis and delivery is safe and efficient, allowing reduced drug dosages with the same beneficial effects.

Formulations based on the variant Milano or recombinant HDL have not shown significant effects on patients with coronary artery disease in clinical trials and some were toxic to the patients. Instead, in the perspective of drug development, this specific biotechnological approach holds great advantages over bacterial systems and chemical synthesis, including cost-effectiveness, safety, unnecessary purification, along with a more practicable route of administration, all contributing to make the APOA-I rice milk a promising candidate among APOAI-based therapeutics.

Despite the interesting target that could be the AIM and effectiveness and safety of the delivery tool used shown in this study, the bioavailability for effective treatment of CVDs in human clinical trials may be low and the amount of AIM protein per gram of rf administered should therefore be increased. However, considering recent studies confirming the beneficial effects of APOA-I and APOA-I mimetic peptides in mouse models, this functional food could open new scenarios for CVDs or inflammatory bowel disease (IBD) treatment.

1.5 Rationale and aim of the work

This thesis project is part of a much larger collaborative project based on the study previously published by Romano et al. Int J Cardiol. 2018, in which our research group reported the proof of concept findings of this project ¹¹². The initial purpose of this thesis was to better characterize APO RF, in order to further understand the potential of transgenic rice seeds as an efficient oral production and delivery system for recombinant AIM protein.

It was also important to better understand in more detail the biodistribution of the AIM protein administered orally in the form of "RF" in APO3 study investigating what could be the molecular mechanisms induced in treated animals that could explain the athero-protective and anti-inflammatory effects of the treatment.

These investigations were fundamental to lay the foundations for the main purpose of this project, namely the development of a new system of functional APO products. To the innovative improved both qualitatively and quantitatively from the point of view of the genetic engineering of base and the processes of cultivation and lyophilization of the downstream foods, that can be extended to a future use in the humans. In this regard, a set of vectors carrying the coding sequence (CDS) of the AIM and the respective control vectors has been constructed, to be tested at a functional level *in vitro* and subsequently to be used as source of the AIM sequence to engineer the new rice product.

2 Materials and methods

2.1 APO biodistribution of proof-of-concept iAPO rice

2.1.1 Protein extraction from rice flour

The genetically modified APO-rice and the WT control rice seeds were provided by the GRG Gene Technology SA (Minusio, Switzerland) in form of flour (mechanically grinded rice seeds).

AIM genetically modified RF and WT RF, as control, were analysed in their protein component for human APOA-I protein detection. We based our approach on the work published by Lang and others in 2013 ¹¹⁶ for the extraction and subsequent quantification of the salt soluble, salt insoluble and total protein fractions.

2.1.1.1 Extraction of the rice salt-soluble and salt-insoluble proteins

The salt-soluble proteins fraction was extracted three times from each 100mg of transgenic or WT RF.

For the first extraction, 1mL of the extraction buffer (30mM Tris-HCl (pH 8.0), 1M NaCl and protease inhibitor cocktail tablets, Sigma Aldrich) was added to 100mg of RF in a 2-mL micro centrifuge tube and mixed by vortexing. The tube was stirred on a rotary mixer at room temperature (25°C) for 2h. After centrifuging at 15000xg for 10 min at 4°C, the supernatant was recovered in a new collection tube.

For the second extraction, a volume of extraction buffer equal to recovered volume of supernatant from the previous extraction, was added to the corresponding precipitate in tube. The precipitate was suspended and mixed by vortexing. The tube was mixed on a rotary mixer and subsequently centrifuged as described for the first extraction. The third protein extraction followed the same procedure as the second. To extract the salt insoluble proteins fraction, 1mL of extraction buffer (55-mM Tris-HCl (pH 6.8), 2% (w/v) SDS, 10% (v/v) glycerol and 11 mg/mL of DTT and protease inhibitor cocktail tablets) was added to the remaining precipitate after third salt soluble protein extraction. The tube was incubated on bath at 90°C for 3 minutes, then the precipitate has been suspended by vortexing, and centrifuged at 15000 x g for 10 min at 4°C. The supernatant was recovered in a new collection tube.

2.1.1.2 Extraction of the rice total proteins

For total protein fraction extraction, 1mL of extraction buffer (50mM Tris-HCl (pH 7.5), 2% (w/v) SDS, 0.6% (v/v) 2-mercaptoethanol and 4M urea and protease inhibitor cocktail tablets, Sigma Aldrich) was added to 25mg of RF in a 2-mL micro centrifuge tube and mixed by vortexing. The tube was rotated on a rotary mixer at room temperature (25°C) for 2 h. The resulting supernatant was collected to a new tube after centrifuging at 15000 x g for 10 min at 4°C.

Two independent extractions were made for each fraction. (Evaluation of Extraction Solutions for Biochemical Analyses of the Proteins in Rice Grains).

2.1.2 Determination of rice extracts protein concentration

Protein concentration of salt-insoluble and total fractions extracted was determined by 2-D Quant Kit (GE Healthcare). Quick Start Bradford Assay kit (Bio-Rad) was used to determine the concentration of salt-soluble proteins.

2.1.2.1 2 D Quant kit assay

The 2-D Quant Kit procedure involves the formation of a protein precipitate of the test sample, in this way solutions that could interfere in the final quantification does not affect the performance of the assay.

The assay is based on the specific binding of copper ions to protein. Precipitated proteins are resuspended in a copper-containing solution and unbound copper is measured with a colorimetric agent. The absorbance at size of 480 nm is inversely related to the protein concentration.

As described in the manufacturing protocol, prior to perform the assay an appropriate volume of working colour reagent was prepared by mixing 100 parts of colour reagent A with 1 part of colour reagent B. Each individual assay requires 1 ml of working colour reagent.

For the standard curve, a set of six standard samples was prepared by adding 0, 5, 10, 15, 20 and 25 μl of the Bovine serum albumin (BSA) standard solution provided by the kit (2 mg/ml) in six different tubes.

An appropriate number of tubes containing 25 μl of the samples to be assayed was prepared in triplicate.

Then, 500 μl of precipitant were added to each tube, including the standard curve tubes, and the solution was incubated for 3 minutes at room temperature after briefly mixing by vortexing. After the incubation, 500 μl of co-precipitant were added to each tube and mixed briefly through vortexing. The samples were centrifuged at maximum speed for 5 minutes to sediment the proteins.

After the centrifugation, the supernatants were decanted, and the tubes were further briefly centrifuged with the pellet facing outwards to bring any remaining liquid to the bottom of the tube. The remaining supernatant was removed using a micropipette.

Then, 100 μl of copper solution and 400 μl of deionized water were added to each tube. The samples were briefly mixed by vortexing to dissolve the precipitated proteins. Afterwards, 1 ml of working colour reagent was added to each tube as rapidly as possible to ensure instantaneous mixing. The samples were then mixed by inversion and incubated at room temperature for 20 minutes. The absorbance was read at size of 480 nm using water as reference.

2.1.2.2 Quick Start Bradford Protein Assay

The Bradford assay is a protein determination method that involves the binding of Coomassie Brilliant Blue G-250 dye to proteins ¹¹⁷. The dye exists in three forms: cationic (red), neutral (green), and anionic (blue) ¹¹⁸. Under acidic conditions, the dye is predominantly in the doubly protonated red cationic form ($A_{\text{max}} = 470 \text{ nm}$). However, when the dye binds to protein, it is converted to a stable unprotonated blue form ($A_{\text{max}} = 595 \text{ nm}$) ¹¹⁹. It is this blue protein-dye form that is detected at

595 nm in the assay using a spectrophotometer or microplate reader (iMark™ Microplate Absorbance Reader, Biorad).

The assay was performed as described below.

Before use, the 1X dye reagent was removed from 4°C storage to let warm to room temperature and was inverted a few times to mix. A set of 8 standard samples were prepared by diluting the 2 mg/ml standard in the same buffer present in the samples (salt-soluble proteins extraction solution), according to the manufacturer's indications.

Then, 5 µl of each standard and unknown sample were pipetted into the microplate wells. A volume of 250 µl of 1X dye reagent was added to each well before mixing the samples on a microplate shaker.

The samples were incubated at room temperature for 45 minutes before reading the absorbance at 595 nm using a microplate reader (iMark™ Microplate Absorbance Reader, Biorad).

2.2 *In vivo* study protocol and tissue biopsies availability

2.2.1 Extraction of total protein from tissue biopsies

Tissue lysis was performed on mouse liver, intestinal and brain samples, summarized in Table 3, from the "APO3 study", stored at -80 °C.

The animal experiments were performed at the Foundation for Cardiovascular Research and Education institute (Taverne, Switzerland) and were approved by Cantonal Department for Animal Experiments according to EU63/2010 directive. In this study, 8-10 weeks old *B6.129P-Apoe^{tm1Unc/J} (Apoe^{-/-})* male mice were fed with Western Diet for 56 days ad libitum. After 56 days, mice were randomized in two groups and administered with APO (0.63mg/kg, 5 days a week) or WT rice extract for 4 weeks by oral gavage. Western Diet (WD) was maintained for the whole period of the experiments. Intestine protein lysates used in this thesis were provided already processed from intestine biopsies by Prof. Barisani's group (School of Medicine, University of Milano Bicocca).

Samples were stored at -80°C until use.

	Animal	Liver biopsy	Intestine lysate	Cerebellum biopsy	Brain biopsy
Administrated with APO rice (Treated)	3.8	X	X	X	X
	3.9	X	X	X	X
	3.10	/	X	/	/
	3.11	X	X	X	X
	3.12	X	X	X	X
	3.13	X	X	X	X
	3.14	X	X	X	X
	3.15	X	X	X	X
Administrated with WT rice (Control)	3.22	X	X	X	X
	3.23	X	X	X	X
	3.24	X	X	X	/
	3.25	X	X	X	X

Table 3 Biopsies of treated animals and controls are summarised. The organs examined for each animal are the liver, intestine, cerebellum and brain.

2.2.1.1 Preparation lysates

Each tissue sample of interest was rapidly dissected with a scalpel on ice, weighed and placed in micro centrifuge tube. Lysis buffer (150 mM sodium chloride, 1.0% NP-40 or Triton X-100, 0.5% sodium deoxycholate, 0.1% SDS (sodium dodecyl sulphate), 50 mM Tris, pH 8.0 and protease inhibitor cocktail tablets) was prepared as Abcam protocol described.

The corresponding volume of ice-cold lysis buffer was quickly added to each tube in relation to the amount of tissue present.

For each ~ 5 mg, it was ~ 300 µl (or 250 µl for brain samples) of ice-cold lysis buffer. Each sample of liver and brain was homogenized with Dounce and Potter homogenizer on ice until was obtained a homogeneous solution with no debris instead the intestine samples were processed in collaboration with University of Milano, Bicocca following the same protocol. Each sample was kept under constant stirring on orbital shaker for 2 hours at 4°C.

At the end, each sample was centrifuged for 20 min at 12,000 rpm at 4 °C and the supernatant was collected in a fresh new tube kept on ice.

Amount of proteins in each tissue lysate was quantified with the Pierce BCA Protein Assay Kit (Thermo Fisher Scientific).

2.2.1.2 Determination of tissue lysates protein concentration

Before proceeding with subsequent analyses, the Pierce™ BCA Protein Assay Kit (Thermo Scientific™) was employed to assess total protein concentration in the samples. This method combines the reduction of Cu^{2+} to Cu^{1+} by protein in an alkaline medium (the biuret reaction) with the highly sensitive and selective colorimetric detection of the cuprous cation (Cu^{+1}) using a unique reagent containing bicinchoninic acid (BCA). The purple-coloured reaction product of this assay is formed by the chelation of two molecules of BCA with one cuprous ion. This water-soluble complex exhibits a strong absorbance at 562 nm that is nearly linear with increasing protein concentrations over a broad working range (20–2000 $\mu\text{g}/\text{mL}$). Protein concentrations can be determined and reported with reference to standards of a common protein such as bovine serum albumin (BSA).

2.2.1.2.1 Assay preparation

Tissue lysates were diluted 1:50 to allow better interpolation of each expected concentration with the standard curve.

Scalar dilutions of an Albumin Standard (BSA) stock (2mg/ml) (Thermo Scientific™) were carried out according to the manufacturer's instructions using the same diluent samples (1:50 diluted lysis buffer in sterile water) to cover linear work range of 20-2000 $\mu\text{g}/\text{ml}$. Working Reagent was prepared by mixing 50 parts of reagent BCA A (Thermo Scientific™) with 1 part reagent BCA B (Thermo Scientific™) (50:1, reagent A:B), the mixture was kept in the dark.

2.2.1.2.2 Measurement of the samples and standards

25 μ l of each standard or unknown sample were pipetted into a 96-well microplate in triplicate followed by the addition of 200 μ l WR to each well. The plate was shaken for 30 seconds on a plate shaker before incubation in the dark for 1h at 37°C. After that, the plate was cooled to RT and absorbance was measured at 565 nm using a microplate reader (iMark™ Microplate Absorbance Reader, Biorad).

2.2.1.2.3 Data analysis

The average absorbance value was calculated for each albumin standard concentration, including 0 μ g/mL (blank control). Then the average absorbance value of blank control was subtracted from all other average absorbance values and a standard curve was created by plotting the blank-corrected absorbance values (x-axis) against the BSA concentration in μ g/mL related to each standard (y-axis). A four parameter (4PL) algorithm was chosen to fit a curve to the data. The concentration of total proteins in each sample was determined by interpolating the absorbance value of the sample, after blank control subtraction, against the standard curve. The resulting value was then multiplied by sample dilution factor (i.e. by 50).

2.2.2 Western Blot

Western blot (WB) technique was used as a semi quantitative method to detect the protein of interest (APOA-I both variant Milano and wild endogenous murine protein) in protein lysates previously extracted.

In order to optimize the detection conditions for both human and mouse APOA-I, several combinations of parameters was needed, including sample concentration, blocking conditions and antibody dilutions were tested.

The experiment was conducted on liver, intestine and brain protein lysates derived from animals 3.15 and 3.22, along with salt-soluble,

salt-insoluble and total proteins extracted from transgenic and WT RF to investigate the presence of AIM protein as shown in Tab.4.

Furthermore, liver and intestine protein lysates derived from all the animals of the study were analysed for mouse ApoA-I protein expression as described below.

2.2.2.1 Polyacrylamide gel electrophoresis (PAGE)

Polyacrylamide gel for molecular weight-based proteins separation was prepared using premixed TGX (Tris-Glycine eXtended) acrylamide/bis-acrylamide solutions from TGX Stain-Free™ FastCast™ Acrylamide Starter Kit, 10% (Bio-Rad). A 10% resolving gel acrylamide solution was prepared combining equal volumes (4 ml) of resolver A and B solutions, to which were added 0.0005 % of TEMED (Sigma-Aldrich) and 0.005% of APS 10% (ThermoFisher Scientific) for the solution polymerization. The mixture was mixed by vortexing and immediately casted into a 1.5 mm thick glass chamber, formed with Mini-PROTEAN® Spacer Plates (Bio-Rad) stabilized on Mini-PROTEAN Tetra cell casting stand (Bio-Rad). Immediately after, 5% stacking gel acrylamide solution was made by combining equal volumes of stacker A and B solutions, 0.001% of TEMED (Sigma-Aldrich) and 0.005% of APS 10% (ThermoFisher Scientific) and rapidly vortexed and poured onto the resolving gel to fill the chamber. The comb was then inserted on top of the chamber, being and the gel was let polymerize for at least 45 minutes. Solidified gel was either stored at 4 °C or immediately used for gel electrophoresis.

For sample preparation, a volume corresponding to the appropriate protein amount (outlined in Table 4) was mixed with 3 µl of reducing agent (NuPAGE, Sigma Aldrich), to fully denature the protein and remove all higher order structure including disulphide bonds, 1:1 amount with the sample of TRIS-GLY-SDS Sample Loading Buffer (Life Sciences) and an appropriate amount of sterile water to reach a total volume of 30 µl.

The mixture has been heated for 10 minutes to 70°C to promote protein denaturation.

The solution was subsequently charged into the gel wells, and the tracer dye, the bromophenol blue contained in the loading buffer allowed to monitor the progression of the electrophoretic stroke. In a gel well was loaded pre-stained Plus Protein Dual Color Standard (Bio-Rad) necessary for the molecular weight determination of proteins after the development of blot.

The electrophoretic run was performed in a running pad containing Torus/Tricin/SDS Running Buffer 1X (Bio-Rad) at 120 V for the first 20 minutes and then at 150 V until the tracer dye had exited the race front.

Detection	Sample	Protein amount tested
Human AIM	Liver, intestine, brain and cerebellum protein lysates derived from animals 3.15 and 3.22	7, 20 and 45 µg
Mouse ApoA-I	All liver and intestine protein lysates available.	20 and 40 µg
Human AIM	RF salt-soluble protein fraction.	7 µg
	RF salt-insoluble protein fraction.	3 and 7 µg
	RF total protein fraction.	

Table 4 Summary of protein amount tested in WB for AIM detection in mice biopsy samples and in RF protein extracts and ApoA-I murine detection in mice biopsy samples.

2.2.2.2 Transfer step

At the end of the electrophoretic run, proteins were transferred from the gel to a polyvinylidene difluoride (PVDF) membrane where they are immobilized for the subsequent detection. Transfer buffer was prepared in advance according to the manufacturing protocol: 1:5 100% ethanol, 1:5 Tran-Blot Turbo Buffer (Bio-Rad), deionized H₂O up to the final volume and was let cool at 4°C.

Immun-Blot PVDF Membrane (Bio-Rad), cut to gel size, was pre-wetted in a 100% methanol bath for 1 minute under gentle agitation for its activation.

Semi-dry electrophoretic transfer protein blotting was performed using Trans-Blot® Turbo™ Transfer System (Bio-Rad) which allows fast and high-efficiency transfer. Blotting sandwich was assembled in the centre of the transfer cassette bottom placing the gel over the PVDF membrane between two stack of transfer buffer-soaked filter paper which will be in direct contact with plate electrodes (the cassette lid and bottom).

For efficient transfer of a wide variety of proteins over a broad range of molecular weights (5-150 kDa) the MIXED MW program was selected and ran for 8-9 minutes.

The quality of protein transfer was checked through stain-free visualization of the membrane.

2.2.2.3 Detection step

Following transfer, in order to block any sites on the membrane that would allow non-specific binding of antibodies and diminish background, the membrane was incubated for 1 hour at RT under constant gentle agitation in blocking solution, prepared dissolving 5% non-fat powdered milk (Bio Basic) in Tris buffered saline solution diluted in deionized H₂O added with 1% Tween (TBS-T 1X).

Afterwards, the membrane was incubated overnight at 4°C under gentle agitation with the appropriate primary antibody. Primary and secondary antibody combinations with the relative dilution to optimize the protocol are described in Table 5. The primary antibody was either diluted directly in blocking solution, or in 5% BSA TBST 1X.

Detection	Primary and secondary Antibody combination	Dilutions tested
Human AIM in biopsies protein lysates	Rabbit monoclonal Anti-hApolipoproteinA-I antibody [EP1368Y] (Abcam) primary antibody	1:500 and 1:1000
	Mouse anti-rabbit IgG-HRP	1:10000

	secondary antibody	
Human AIM in RF protein subfractions	Rabbit monoclonal Anti-hApolipoproteinA-I antibody [EP1368Y] (Abcam) primary antibody	1:1000
	Mouse anti-rabbit IgG-HRP secondary antibody	1:10000
Mouse ApoA-I in biopsies protein lysates	Goat polyclonal Anti-mouse Apolipoprotein A-I antibody (ab7614) (Abcam) primary antibody	1:500 and 1:1000
	Donkey anti-goat IgG-HRP (Santa Cruz Biotechnology) secondary antibody	1:5000 and 1:10000

Table 5 Antibody used in WB details. Various dilutions were tested to perform the optimal conditions reaction.

After the incubation, the antibody solution was removed, and the blot was washed 3 times for 10 minutes in TBST-1X under agitation to eliminate unbound antibody residues before incubation with the secondary antibody. The secondary antibody was diluted in 2.5% non-fat milk TBST-1X and incubated for 1 h at RT under gentle agitation. The membrane was rinsed 3 times for 10 minutes and placed on a clean piece of plastic wrap for signal development.

Chemiluminescent substrate solution was prepared as described in the manufacturing protocol mixing equal volumes of Clarity™ Western ECL Substrate kit components (Bio-Rad) and was incubated for 1 minute in the dark. Chemiluminescent signal was captured and analysed using the ChemiDoc™ MP Imaging System with Image Lab™ Software (Bio-Rad).

2.2.2.4 Normalization

In order to obtain reliable and reproducible semi-quantitative results, normalization using GAPDH as housekeeping protein was performed. Therefore, following blot imaging, all the steps described in Section 2.4.3.3 were repeated. Mouse monoclonal anti-GAPDH (Proteintech Group) diluted 1:20000 in 5% BSA TBST 1X and horseradish peroxidase-conjugated goat anti-mouse (Proteintech Group) diluted 1:100000 were used as primary and secondary antibodies respectively.

2.2.3 ELISA assay

In order to further examine AIM protein amount in the tissue lysates and in the RF protein extracts, the human Apolipoprotein-AI ELISA Kit (ab189576), Abcam was used (main protocol steps are summarized in figure 7).

This Simple Step ELISA® kit (Abcam) is a highly sensitive, reproducible and specific sandwich ELISA assay in which the analyte (ApoA-1M) undergoes immunocapture in solution by two different types of antibodies, namely an affinity tag labelled capture antibody and a reporter conjugated detector antibody, to form an antibody-analyte sandwich. This complex is next immobilized via immunoaffinity on an anti-tag antibody coating the wells of the microplate. After the addition of the substrate (TMB), HRP (reporter) catalyse its oxidation, generating a blue coloration proportional to the amount of bound analyte. The intensity is measured at 450 nm and the concentration of the target protein is determined using a standard curve as described in manufacturing protocol.

Due to the number of samples, two plates were needed to analyse all the samples in triplicate. For both plates, the assay was performed as follows, with the only difference that a complete standard curve was included just in the first plate.

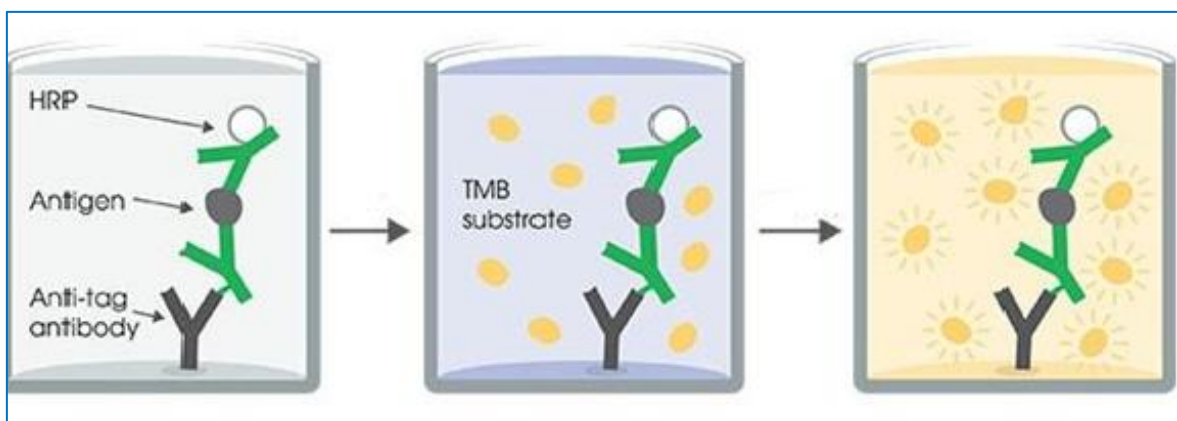


Figure 7 Overview ELISA test step. The affinity tag labelled capture antibody is recognized by a reporter conjugated detector antibody which immunocapture the sample analyte in solution with the formation of the antibody-analyte sandwich complex. This entire complex is in turn immobilized via immunoaffinity of an anti-tag antibody coating the well. TMB substrate added, generates blue coloration catalysed

by HRP during its incubation. This reaction is then stopped by addition of Stop Solution completing any colour change from blue to yellow. Signal is generated proportionally to the amount of bound analyte and the intensity is measured at 450 nm. (Image by Abcam).

2.2.3.1 Reagent preparation

All reagents were equilibrated at room temperature prior to use.

The 1X Wash Buffer PT was prepared by diluting 10X Wash Buffer PT with deionized water and mixed thoroughly and gently.

To prepare the Antibody Cocktail, capture and detector antibodies were diluted in Antibody Diluent 5BI and then mixed thoroughly and gently.

2.2.3.2 Standard preparation

For the standard curve, serial dilutions were carried out over a concentration range of 0 to 20 ng/ml of the standard sample of Apolipoprotein A1 for human use.

For this purpose, the sample standard was reconstituted by adding 500 μ l of diluent sample NS and kept at room temperature for 10 minutes.

Serial dilutions were carried out in 200ul of total NS diluent in each tube and adding the corresponding amount of standard samples to obtain the desired standard concentration.

Eight tubes have been labelled as standard and Standard 8 does not contain protein and is the blank control as described in manufacturing protocol.

2.2.3.3 Sample preparation

Liver, brain and intestine lysates, along with the proteins extracted from the RF, were diluted into Sample Diluent NS, to obtain a final concentration in the well of 50 μ g of total proteins for the tissue lysates and 2 μ g for the RF protein extracts.

2.2.3.4 Assay procedure

Once all reagents and samples were ready to use, 50 μ l of each sample and standards were added to the appropriate wells, followed by the

addition of 50 μl of the Antibody Cocktail to each well. Then the plate was sealed and incubated for 1 hour at room temperature on a plate shaker set to 400 rpm.

Afterwards, each well was washed as follows. The content of each well was aspirated by pipetting and 350 μl of 1X Wash Buffer PT were dispensed into the wells. This step was repeated three times, being careful to remove completely the liquid at each step to ensure a good performance and minimize background. After the last wash the plate was inverted and blotted against a clean paper towel to remove excess liquid.

At this point, 100 μl of TMB Substrate were added to each well to catalyse the blue colour development and the plate was incubated for 10 minutes in the dark on a plate shaker set to 400 rpm.

To stop the reaction for an endpoint reading, 100 μl of Stop Solution were added to each well and the plate was placed on a shaker for 1 minute to mix. Finally, the OD was recorded at 450 nm through microplate reader (iMark™ Microplate Absorbance Reader, Biorad).

2.2.3.5 Data analysis

The average absorbance value was calculated for the blank control, the standards and the samples. Then the average absorbance value of blank control was subtracted from all other average absorbance values and a standard curve was created by plotting the blank-corrected absorbance values (x-axis) against the human APOA-I concentration in $\mu\text{g/mL}$ related to each standard (y-axis). A four parameter (4PL) algorithm was chosen to fit a curve to the data.

The concentration of the AIM protein in each sample was determined by interpolating its absorbance value, after blank control subtraction, against the standard curve. The resulting value was then multiplied by the appropriate sample dilution factor.

2.2.4 *Ex vivo* analyses, immunohistochemistry and histology on liver tissues

Liver biopsies from the treated and control groups of APO3 study were subjected to immunohistochemical analysis for detection of human APOA-I. The corresponding slides have been kindly provided by the service facility of histology associated with the enclosure of the University of Milano Bicocca. The animals at the end of treatment were killed by asphyxia, perfused and subsequently biopsies were stored in paraffin.

The slides were deparaffined at room temperature by sequential incubations in alcohol-based solutions as described in manufacturing protocol by Vector Laboratories. Initially the slides were immersed in a 100% Xylene solution for 3 minutes (the passage was repeated twice); then the slides were immersed in a 100% xylene/ethanol 100% solution in a ratio of 1:1 for 3 minutes. Followed in incubation in ethanol 100% for 3 minutes (step repeated twice). The slides were then sequentially incubated in an ethanol solution of 95%, ethanol 70% and ethanol 50% each step lasting 3 minutes. Finally, the slides were immersed in water by performing 3 washes from one minute each.

The next phase of antigen unmasking was carried out by incubating the slides in a solution of ddH₂O and 1% of Antigen Unmasking Solution, Citrate-based (H-330) (Vector Laboratories), at 100°C in water bath for 10 minutes. At the end, the slides were allowed to cool to room temperature for 20 minutes. The sections were washed with PBS.

For immunohistochemical analysis, ImmPRESS® HRP Horse Anti-Mouse IgG Polymer Detection Kit (Vector Laboratories) was used. To inhibit the activity of endogenous peroxidase, slides were incubated in BLOXALL® Block solution (SP-6000) for 10 minutes. The slides were washed in PBS for 5 minutes two times. The blockage was performed incubating the slides in Normal Horse Serum, 2.5% (Immpress Reagent Kit, Vector Labs) for 20 min.

The slides were then incubated with primary antibody Anti-hApolipoproteinA-I antibody [EP1368Y], Abcam diluted 1:150 in Normal Horse Serum 2.5% (Immpress Reagent Kit, Vector Laboratories) for 1 hour, avoiding the drying of samples, for the human APO detection. Blank control was represented by incubation with only secondary antibody (Immpress Reagent Kit, Vector Laboratories) following the same steps of tests samples. Then, the slides were washed in PBS for 5 minutes twice and was incubated with secondary antibody HRP conjugated (Immpress Polymer Reagent, Vector Laboratories) for 30 minutes at room temperature. Subsequently, the slides were washed twice in PBS for 5 minutes and the chromogenic reaction was developed by exposing the slides to ImmPACT DAB peroxidase (HRP) substrate kit (ImmPRESS Reagent Kit, Vector Laboratories) for 3 minutes. The slides were washed twice in PBS for 5 minutes and counterstained with Gill's hematoxylin 2 (Sigma Aldrich) for 30s, de-hydrated and finally the coverslips were mounted on slides using VectaMount AQ Aqueous Mounting Medium.

All images were digitally acquired with Scanscope (Aperio). Area and signal quantification was performed using Imagescope (Aperio).

2.3 APOA1 sequence mutagenesis and molecular cloning plasmids

The following procedures have been used to develop a set of plasmids of interest through the Gibson Assembly cloning method (New England Biolabs, USA). The methods used to introduce the site-specific AIM mutation into human APOA1 WT CDS are also described.

The CDS of the human APOA1 was kindly granted by Genecopoeia, plasmid EX-C0169-M02. The backbone for all plasmids built was the plasmid pCX- HO1-F2A-EGFP product previously by our group and distributed by Addgene, USA (plasmid # 74672) represented in figure 8.

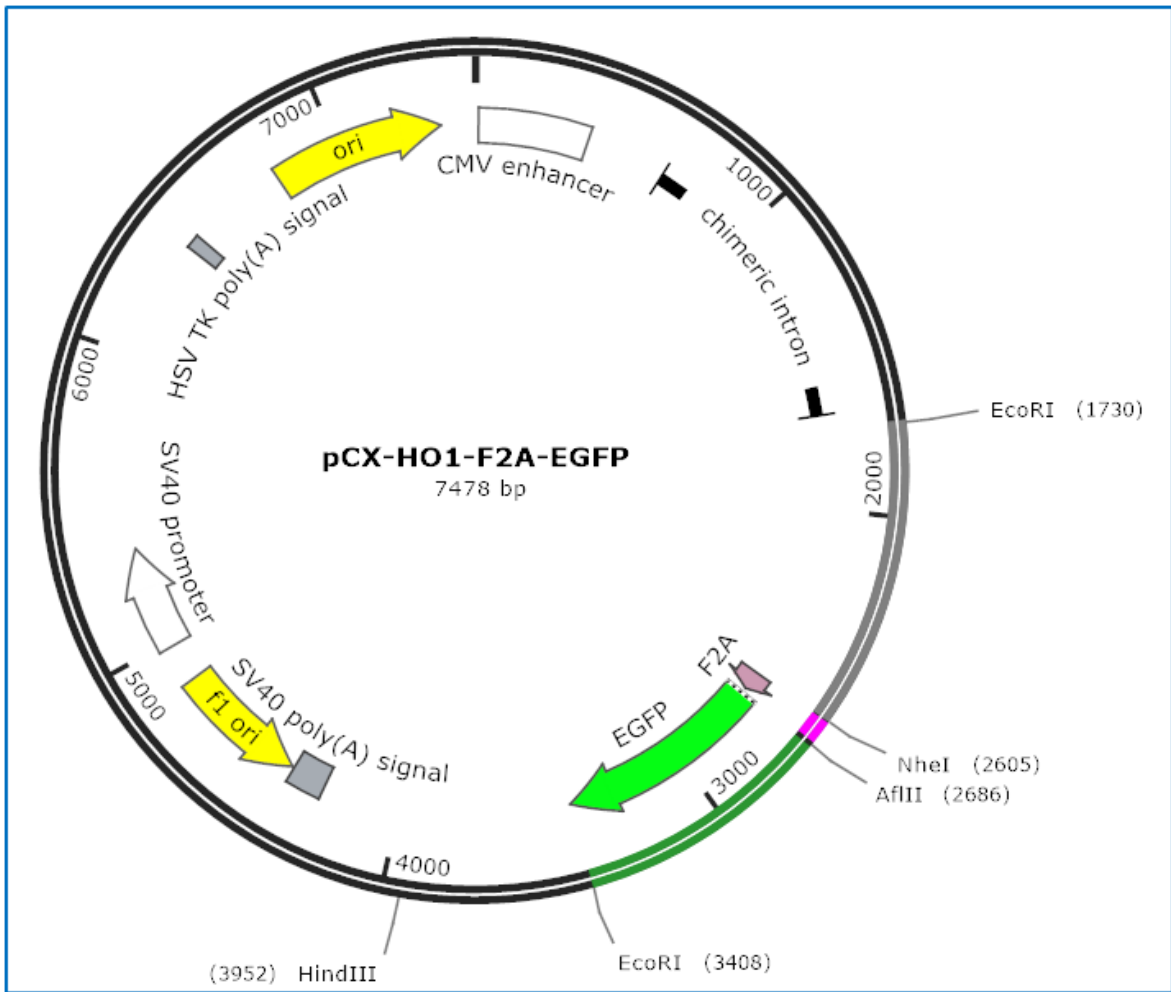


Figure 8 *pCX-HO1-F2A-EGFP* plasmid map used as backbone for subsequently plasmids built.

Initially coding sequence of the human gene APOA1 was mutagenized the by using the system pGem T-easy vector (Promega) and then the monocistronic, dicistronic, tricistronic and tetracistronic plasmids tests and relative control plasmids were built starting by *pCX- HO1-F2A-EGFP* plasmid as template.

2.3.1 F2A peptide details

2A peptides are 18–22 amino-acid long viral oligopeptides that mediate “cleavage” of polypeptides during translation in eukaryotic cells.

The designation “2A” refers to a specific region of the viral genome and different viral 2As have generally been named after the virus they were derived from. The most studied 2A peptide is found in the Aphtho virus foot-and-mouth disease virus (FMDV). The FMDV RNA genome contains

a single, long ORF encoding a Polyprotein and FMDV 2a (F2A) is known to be responsible for primary processing event in the resolution of the polyprotein to individual proteins and its co-expression ¹²⁰.

The mechanism of 2A-mediated "self-cleavage" was recently discovered to be ribosome skipping the formation of a glycyl-prolyl peptide bond at the C-terminus of the 2A. A highly conserved sequence GDVEXNPGP is shared by different 2As at the C-terminus and is essential for the creation of steric hindrance and ribosome skipping. Modelling of F2A indicated that it may form an (amphipathic) α -helix over most of its size, with a reverse turn at its C-terminus. This led to the suggestion that the α -helix, in the ribosomal exit tunnel, combined with the reverse turn, might subtly shift the peptidyl-tRNA-Gly in the peptide-transferase centre (PTC), disfavours peptide bond formation to prolyl-tRNA-Pro, while promoting hydrolysis of the peptidyl-tRNA-Gly ester bond, thereby generating the upstream product. Proline is the poorest nucleophile of all proteinogenic amino acids since its secondary amino group is conformationally and sterically constrained. It may therefore be uniquely affected by subtle changes within the ribosomal PTC. Hydrolysis of the nascent peptidyl-2A-tRNA-Gly ester bond is catalysed by translation terminating release factors, despite the presence of the Pro codon in the A-site. Since mutation of this Pro codon to codons encoding several other amino acids almost completely abrogates 2A activity, any conformational shift in the PTC driven by 2A is suggested to discriminate prolyl-tRNA-Pro from other aminoacyl-tRNAs. Studies in which the codon Pro has been changed and therefore the coding of several amino acids almost completely abrogates the activity of the 2A ^{121 122}.

2A peptides lead to relatively high levels of downstream protein expression compared to other strategies for multi-gene co-expression, and they are small in size thus bearing a lower risk of interfering with the function of co-expressed genes. 2A peptides have also been successfully employed by several different groups for polycistronic and bi-cistronic multigene expression ¹²³.

F2A sequence

- Val Lys Gln Thr Leu Asn Phe Asp Leu Leu Lys Leu Ala Gly Asp Val Glu
Ser Asn Pro Gly Pro-

2.3.2 Gibson cloning assembly

For building monocistronic, dicistronic tricistronic and quadricistronic plasmids was used Gibson Cloning Assembly kit (NEB, USA) developed by Dr. Daniel Gibson and his colleagues at the J. Craig Venter Institute and licensed to NEB by Synthetic Genomics, Inc. It allows for successful assembly of multiple DNA fragments, regardless of fragment size or end compatibility being suitable for large DNA constructs.

Gibson Assembly efficiently joins multiple overlapping DNA fragments with overlaps until 15–80 bp, created by high fidelity PCR, in a single-tube isothermal reaction (in table 6 are shown the primers used details). The Gibson Assembly Master Mix includes three different enzymatic activities that perform in a single buffer: the exonuclease creates single-stranded 3' overhangs that facilitate the annealing of fragments that share complementarity at one end (overlap region); the proprietary DNA polymerase fills in gaps within each annealed fragment; the DNA ligase seals nicks in the assembled DNA.

The end result is a double-stranded fully sealed DNA molecule that can serve as template for molecular biology applications, including direct transformation.

Each fragment of interest was amplified by PCR with the enzyme High fidelity DNA Polymerase (NEB, USA) using pairs of Primers supplied by Eurofins genomics and specially designed for Gibson cloning (www.sgDNA.com primer design tool) as described in table 6.

For each insert, the optimal annealing temperature has been identified by screening a range of 10 temperatures (62°C to 72°C) as described in table 6.

Primers	Sequence 5' 3'	T ann. (°C)	Additional information
APO-F2A-EGFP Ins1 FWD	AACGTGCTGGTTGTTGTGCTGTCTCA TCATTTTGGCAAAGatgaaagctgcg gtgctgac	64	APOA-I fragment isolation with overlaps for cloning in pCX-HO1-F2A-EGFP plasmid to built pCX- APO-F2A-EGFP.
APO-F2A-EGFP Ins1 REV	ACTTGAGAAGGTCAAAATTCAAAGTC TGTTTCACGCTAGCctgggtggtgag cttcttag		
APO-F2A-EGFP Ins2 FWD	gctagcgtgaaacagacttt	70	F2A-EGFP fragment isolation with overlaps for cloning in pCX-HO1-F2A-EGFP plasmid to built pCX- APO-F2A-GFP.
APO-F2A-EGFP Ins2 REV	CCACCTTCTGATAGGCAGCCTGCACC TGAGGAGTGAATTCTtacttgtacag ctcgtcca		
APO Empty FWD	AACGTGCTGGTTGTTGTGCTGTCTCA TCATTTTGGCAAAGatgaaagctgcg gtgctgac	64	APOA1 fragments isolation. pCX-APO-F2A-EGFP template.
APO Empty REV	CCACCTTCTGATAGGCAGCCTGCACC TGAGGAGTGAATTCTcactgggtggt gagcttct		
AIM Empty FWD	AACGTGCTGGTTGTTGTGCTGTCTCA TCATTTTGGCAAAGatgaaagctgcg gtgctgac	64	AIM fragments isolation. pGEM (post-cloning) template.
AIM Empty REV	CCACCTTCTGATAGGCAGCCTGCACC TGAGGAGTGAATTCTcactgggtggt gagcttct		
EGFP Empty FWD	AACGTGCTGGTTGTTGTGCTGTCTCA TCATTTTGGCAAAGatggtgagcaag ggcgagga	64.4	EGFP fragment isolation. EX-EGFP-M02 template.
EGFP Empty REV	CCACCTTCTGATAGGCAGCCTGCACC TGAGGAGTGAATTCTtacttgtacag ctcgtcca		
F2A Empty FWD	AACGTGCTGGTTGTTGTGCTGTCTCA TCATTTTGGCAAAGctagcgtgaaac agactttg	70	F2A fragment isolation with overlaps for cloning in pCX-HO1-F2A-EGFP plasmid.
F2A Empty REV	CCACCTTCTGATAGGCAGCCTGCACC TGAGGAGTGAATTCTgggccctgggtt ggactcca		
EGFP- F2A-APO Ins1 FWD	AACGTGCTGGTTGTTGTGCTGTCTCA TCATTTTGGCAAAGttaattaaatgg tgagcaagggcgagga	66	EGFP-F2A fragment isolation with overlaps for cloning in pCX-HO1-F2A-EGFP plasmid to built pCX-EGFP-F2A-APO plasmid.
EGFP- F2A-APO Ins1 REV	ACTTGAGAAGGTCAAAATTCAAAGTC TGTTTCACGCTAGCcttgtacagctc gtccatgc		
EGFP- F2A-APO Ins2 FWD	GTTGGCGGGAGACGTGGAGTCCAACC CAGGGCCCGAATTCatgaaagctgcg gtgctgac	66	APO fragment isolation with overlaps for cloning in pCX-HO1-F2A-EGFP plasmid to built pCX-EGFP-F2A-APO plasmid..
EGFP- F2A-APO Ins2 REV	CCACCTTCTGATAGGCAGCCTGCACC TGAGGAGTGCTTAAGtcactgggtgt tgagcttct		
APO ins Ligation FWD	TAAGAATGCTAGCgtgaaacagactt tgaatt	63	APO fragment isolation with sticky ends for cloning in pCX-EGFP-F2A-APO plasmid to built tricistronic and tetracistronic plasmid.
APO ins Ligation REV	TAGTTTATCTAGACTGGGTGTTGAGC TTCTTAGTG		

Table 6 Primers used for set plasmids cloning. The specific primers sequence with relative optimal annealing temperature is reported. The function of each primer pair is summarized.

2.3.2.1 PCR protocol

Each fragment was isolated by PCR as described in table 7 using enzyme and buffers purchased from New England Biolabs and stored at -20°C until use. For each sample the PCR reaction mix was assembled as shown in table 7 in a final volume of 25 µl.

Component	Amount
5X Q5 Reaction Buffer	5 µl
10 mM dNTPs	0.5 µl
10 µM Primer Forward	1.25 µl
10 µM Primer Reverse	1.25 µl
5X Q5 High GC Enhancer (facultative)	5 µl
Q5 High-Fidelity DNA Polymerase	0.25 µl
Nuclease-free H2O	X Up to 25 µl
DNA template (60 pg/µl)	1.5 µl

Table 7 PCR reaction mix using Q5 High-Fidelity DNA Polymerase enzyme for fragments isolation.

The reaction was performed on a thermal cycler following the program described in manufacturing protocol described in table 8.

Step	Temperature	Time
Initial Denaturation	98°C	30 seconds
35 Cycles	98°C	10 seconds
	50-72°C	30 seconds
	72°C	20-30 seconds/kb
Final Extension	72°C	2 minutes
Hold	4-10°C	

Table 8 PCR thermal cycling program for Q5High-Fidelity DNA Polymerase PCR reaction.

2.3.2.2 Gel electrophoresis

Gels with an agarose final concentration ranging from 0.8 to 2.5% were prepared, depending on the size of the fragment to be screened or isolated.

Agarose gel was prepared by dissolving the correct amount of agarose in a corresponding volume of TBE buffer 1X (TBE buffer 10X for molecular biology (PanReacAppliChem ITW Reagents) diluted 1:10 in deionized water), using brief heating in a microwave oven. Then, ethidium bromide at a final concentration of 0.01%, was added to the agarose solution to allow visualization of nucleic acids under ultraviolet light (UV). The agarose solution was then poured into a gel casting tray with the well comb in place and let sit at room temperature for 45 minutes, until it was completely solidified. The gel was then moved into the electrophoresis unit and soaked with TBE 1X.

Afterwards, an amount of each sample was mixed with an equal volume of loading buffer (30% TBE 10X, 20 % bromophenol blue, 20% H₂O, 30% glycerol (Sigma Aldrich)) before loading into the wells. The density agent and the coloured dye contained in the loading buffer allow the sample to sink into the bottom of the well and to track the DNA migration during electrophoresis. A molecular weight ladder was loaded into the first well of the gel.

Electrophoresis was carried out at room temperature at a constant voltage of 90-100 V for about 45 minutes. At the end of the run the gel was placed onto a UV trans illuminator to visualize DNA bands.

2.3.2.3 Purification inserts by gel extraction

Each fragment isolated by PCR and used for the Gibson cloning assembly reaction was purified by gel extraction using Expin™ kit, GeneAll kit as described below.

The DNA band of interest was excised using a ethanol-cleaned razor blade or scalpel on a transilluminator.

Gel volume was minimized by cutting the gel slice as small as possible and quickly.

The gel slice was weighed in a micro centrifuge tube and 3 volumes (ul) of Buffer GB to 1 volume (mg) of gel were added. For >1.5 % agarose gel, 5 volumes of buffer GB were added.

The sample was incubated at 50°C until the agarose gel is completely melted (10 min) and to help the efficient dissolving of gel, vortex the tube every 2 ~ 3 min during the incubation.

After the slice has dissolved completely and checked that the colour of the mixture is yellow (similar to Buffer GB), 1 gel volume of isopropanol to the sample was added and vortexed to mix. This step is required to increase the recover yields of DNA fragments.

The mixture was transferred to a SV column, centrifuged for 1 min and the pass-through was discarded and the SV column was re-inserted into the Collection Tube. The step was repeated again until all of the mixture has been applied to the SV column.

500 ul of Buffer GB were applied to the SV column, centrifuged for 30 sec. and the pass-through was discarded and the SV column was re-inserted into the Collection Tube. This step is for further complete removal of any traces of agarose and required only for direct use of purified DNA for very sensitive applications.

700 ul of Buffer NW were added to the SV column, centrifuged for 30 sec. and the pass-through was discarded and the SV column was re-inserted into the Collection Tube

For salt-sensitive applications, the SV was incubated for 5 min at room temperature after the addition of NW buffer, making a certain amount of wash buffer pass through the column by gravity before centrifugation.

The mixture was centrifuged for an additional 1 min to remove residual wash buffer. (If residual ethanol remains in the SV column, centrifuge again for an additional 1min at full speed before transferring to a new 1.5 ml tube because residual ethanol from buffer NW can inhibit subsequent enzymatic reaction)

Then SV column was transferred into a new 1.5 ml collection tube. 20/50 ul of Buffer EB or ddH₂O (pH:7) were applied to the centre of the membrane in the SV column, let stand for 1 min, and centrifuged for 1 min.

The concentration and the purity of DNA samples eluted were checked by NanoDrop™ Lite Spectrophotometer (Thermo Scientific™) at 260 nm and noted for subsequent reactions.

2.3.2.4 Restriction enzyme digestion

Restriction endonuclease reactions were performed on plasmid DNA either to isolate the appropriate vector backbone for subsequent cloning or with the aim to verify the insertion of the cloned DNA fragment.

All restriction endonucleases were purchased by New England Biolabs. The reaction conditions were optimized on ice according to the manufacturer's indications and are reported in table 9.

In Table 10 are outlined the enzymes used, along with specific incubation conditions, buffer and the plasmid substrate used.

Component	Amount
10 X Buffer	5 µl
Restriction enzyme	1 µl
DNA	1 µg
Nuclease-free H ₂ O	Up to 50 µl

Table 9 Restriction enzyme reaction mix.

Enzyme	Reaction details	Buffer	Plasmid substrate
EcoRI	37°C o.n.	NEBuffer™ r2.1	pGEM, pCX-HO1-2AEGFP
HindIII	37°C o.n.	rCutSmart™ Buffer	pCX-HO1-2A-EGFP (post EGFP cloning)
NheI	37°C o.n.	rCutSmart™ Buffer	EX-EGFP-M02 (post APOA1Milano cloning)
XhoI	37°C o.n.	rCutSmart™ Buffer	EX-EGFP-M02
XbaI	37°C o.n.	rCutSmart™ Buffer	Inserts digestion for Ligase reaction

Table 10 Restriction endonucleases used. In the table are indicated the different restriction enzymes used with its reaction buffer. Substrates of each reaction are reported in last column.

Each plasmid digested was checked for integrity and size on agarose gel electrophoresis (0.8%) as described in paragraph 2.3.2.2.

2.3.2.5 Gibson Assembly protocol

For a satisfactory reaction, NEB recommends a total of 0.02–0.5 pmol of DNA fragments (linearized plasmid and inserts) when 1 or 2 fragments are being assembled into a vector and 0.2–1.0 pmol of DNA fragments when 4–6 fragments are being assembled (fig.9). Efficiency of assembly decreases as the number or size of fragments increases. To calculate the number of picomoles of each fragment for optimal assembly, based on fragment size and weight, manufacturing protocol recommends the following formula:

$$\text{pmol} = (\text{weight in ng}) \times 1,000 / (\text{base pairs} \times 650 \text{ dalton})$$

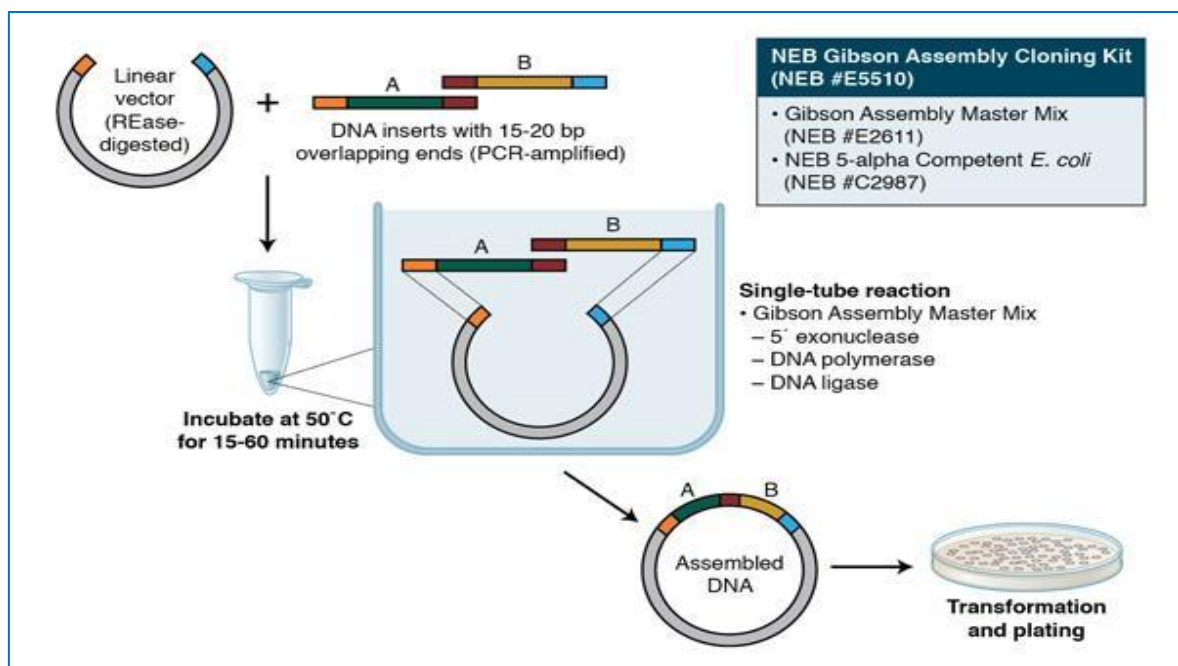


Figure 9 Gibson assembly workflow (international.neb.com).

The reaction was performed on ice as described in table 11 in a total volume of 20 μ l.

	Recommended amount of fragments for Assembly		
	2-3 Fragment Assembly	4-6 Fragment Assembly	Positive Control**
Total Amount of Fragments	0.02–0.5 pmol*X µl	0.2–1 pmol*X µl	10 µl
Gibson Assembly Master Mix (2X)	10 µl	10µl	10 µl
Deionized H ₂ O	10-X µl	10-X µl	0
Total Volume	20 µl***	20 µl***	20 µl

Table 11 Gibson assembly reaction mix.

To optimize the efficiency of the cloning reaction the production protocol recommends using 50-100 ng of linearized vector with 2-3 times the molar excess of each insert and 5 times the molar excess of any insert(s) less than 200 bp. To achieve optimal assembly efficiency using 4-6 groups of fragments, it recommends using a 1:1 molar ratio of each insert: vector.

The samples were incubated in a thermocycler at 50°C for 15 minutes when 2 or 3 fragments are being assembled or 60 minutes when 4-6 fragments are being assembled. Following incubation, the samples were stored on ice or at –20°C for subsequent transformation.

2.3.2.6 Ligase Ligation Protocol

For tricistronic and tetracistronic plasmid assembling, T4 DNA Ligase (M0202), NEB was used instead Gibson cloning assembly. This choice is mainly due to the fact that cloning two or more identical sequences in frame with a cloning system based on sequence homology such as the Gibson system, NEB could have greatly reduced the yield of the reaction.

Each insert to be cloned was previously digested and purified producing sticky ends, as described in paragraph 2.3.2.4 and the vector linearized at the insertion site of interest and purified (par. 2.3.2.4).

The components were assembled on ice as described in table 12.

Component	Amount
T4 DNA Ligase Buffer (10X)	2 µl

Vector DNA (4 kb)	50 ng (0.020 pmol)
Insert DNA (1 kb)	37.5 ng (0.060 pmol)
Nuclease-free water	to 20 μ l
T4 DNA Ligase	1 μ l

Table 12 Ligation Protocol with T4 DNA Ligase (M0202), NEB.

The reaction mix was gently mixed and incubated at room temperature for 10 minutes. The T4 DNA Ligase was heat inactivate at 65°C for 10 minutes.

Following incubation, the samples were stored on ice or at -20°C for subsequent transformation.

2.3.2.7 Transformation

2.3.2.7.1 Selection plates preparation

The recombinant plasmids were introduced into bacterial cells, in order to replicate and subsequently isolate/analyse the sample of interest. Before proceeding with the transformation, Lauria Bertani (LB) medium and LB agar plates were prepared as follows (Tab.13).

Component	Amount
Tryptone	5 g
NaCl	5 g
Yeast Extract	2,5 g
ddH2O	500 ml
For plates add agar	7g

Table 13 Recipe for LB broth medium.

Then the solution was mixed by swirling, to homogenize the solution. The flasks were sterilized by autoclaving following sterilization program at 15 psi, 121°C for 20 minutes.

After sterilization, the LB agar was allowed to cool to 50°C before the addition of the selection appropriate antibody (50 μ g/ml kanamycin for pCX-HO1-2A-EGFP, 100 μ g/ml ampicillin for pGEM-T Easy and EX-EGFP-M02). In the case of pGEM-T Easy vector cloning, the agar solution was supplemented with 0.5 mM IPTG and 80 μ g/ml X-Gal, for blue/white selection of recombinants.

Afterwards, LB agar was poured into 10 cm polystyrene Petri dishes and let solidify for about 1 hour. These operations were conducted as sterile as possible, working near the flame of a Bunsen burner.

After solidification, the plates were inverted and let sit for several hours.

2.3.2.7.2 NEB 5-alpha Competent E. coli cells transformation

NEB 5-alpha Competent E. coli cells (provided with the kit) were transformed with 2 μ l of the assembly reaction, following the transformation protocol.

Chemically Competent cells were thawed on ice.

2 μ l of the chilled assembly product were added to the competent cells and mixed gently by pipetting up and down or by flicking the tube 4–5 times. The mixture was incubated on ice for 30 minutes.

Then it has been subjected to heat shock at 42°C for 30 seconds and transferred on ice for 2 minutes. 950 μ l of room-temperature SOC media were added to the tube. The mixture was incubated at 37°C for 60 minutes in agitation at 250 rpm. The selection plates were warmed to 37°C and working near the flame of a Bunsen burner, 100 μ l of the transformed cells were spread onto LB agar plates. To obtain the maximum number of colonies, an aliquot of the solution was centrifuged for 1 min at 5000 rpm, the supernatant was removed, and the cell pellet resuspended in 100 μ l and spread on the plate. The plates were incubated overnight at 37°C.

2.3.2.8 Plasmid purification from bacterial cells

After incubation, grown single colonies were picked and transferred into 5 ml of LB medium.

Bacterial cells were allowed to grow at 37°C under constant agitation (250rpm) overnight for subsequent DNA purification.

Isolation of plasmid DNA from transformed bacterial cells was performed using the PureYield™ Plasmid Miniprep System (Promega) as follows.

In a 15-mL conical centrifuge tube, 5 ml of the bacterial culture were centrifuged at 2000 rpm for 5 minutes. Afterwards, the medium was discarded, and the cell pellet resuspended in 600 µl of deionized water.

The resuspended pellet was transferred into a 1.5-mL tube and mixed with 100 µl of Cell Lysis Buffer by inverting the tube 6 times.

Immediately after, 350 µl of cool (4-8°C) Neutralization Solution were added to the sample and the tube was inverted several times, until the mixture turned yellow and a precipitate was formed, to ensure complete neutralization.

The sample was centrifuged at maximum speed for 3 minutes in a microcentrifuge. Meanwhile, a PureYield™ Mini-column was placed on an adapter tube. At the end of the centrifuge, the supernatant was transferred into the assembled mini-column being careful to not disturb the cell debris pellet.

The assembly was centrifuged at maximum speed for 15 seconds to pull the lysate through the column.

After discarding the eluted, 200 µl of Endotoxin Removal Wash was added into the mini-column and the tube was centrifuged at maximum speed for 15 seconds.

The eluted was discarded before adding 400 µl of Column Wash Solution to the

Mini-column and centrifuging at maximum speed for 15 seconds.

The PureYield™ Mini-column was transferred to a fresh 1.5 mL tube and 30 µl of nuclease-free water were added onto the centre of the mini-column matrix for final elution. The column was let stand for 1 minute at room temperature and then was centrifuged at maximum speed for 15 seconds to elute the plasmid DNA. The eluted volume was collected to repeat the final elution step. The concentration of eluted DNA was immediately assessed measuring the absorbance at 260 nm (A₂₆₀)

using the NanoDrop™ Lite Spectrophotometer (Thermo Scientific™) and then was stored at -20°C.

2.3.2.9 Samples analysis and sequencing

A first screening of the samples was carried out by enzymatic digestion by comparing each sample with its negative (empty plasmid) and by PCR for the presence of the insert of interest in the purified plasmid.

Successively to confirm the accuracy of the recombinant DNA sequence, the samples were submitted to Eurofins Genomics for sequences analysis.

Samples were prepared according to the manufacturer's instructions using the appropriate sequencing primers listed in table 14.

Primer Sequence 5'-3'	Primer	Function
GAGCCGAAATCTGGGAGG	FWD1	Anneals on the pCX vector backbone, about 250 nt before the 5' end of the insert
GAGAAGCTGAGCCCACTG	FWD2	Anneals on the APOA-I sequence, about 80 nt before the Milano mutation.
GAAGTTCATCTGCACCACC	FWD4	Anneals on the EGFP sequence, about 200 nt from the 5' end.
GCATGGACGAGCTGTACAAG	FWD5	Multicistronic plasmids.
GGCATGGACGAGCTGTACAA	FWD6	Multicistronic plasmids.
CCTGCCACTTCTTCTGGAA	REV1	Anneals approximately in the middle of the APOA1 sequence.
GCCCTTGCTCACCATCTTA	REV2	Anneals on the EGFP sequence, about 50 nt after the 5' end.
TGTGGAATTGTGAGCGGA	REV3	Anneals on the pCX-vector backbone, about 500 nt after the 3' end of the insert.

Table 14 Primers used for sequencing. In the table are reported all the 5'-3' sequences of forward and reverse primer.

2.3.3 APOA1 mutagenesis: the Milano variant

2.3.3.1 pGEM-T Easy Vector System

The pGEM®-T Easy Vector Systems are systems to clone PCR products generated by thermostable polymerases which add a single deoxyadenosine, in a template-independent fashion, to the 3'-ends of the amplified fragments. The pGEM®-T Easy pre-linearized Vector contains 3'-T overhangs at the insertion site to provide a compatible overhang for these PCR products as shown in figure 10.

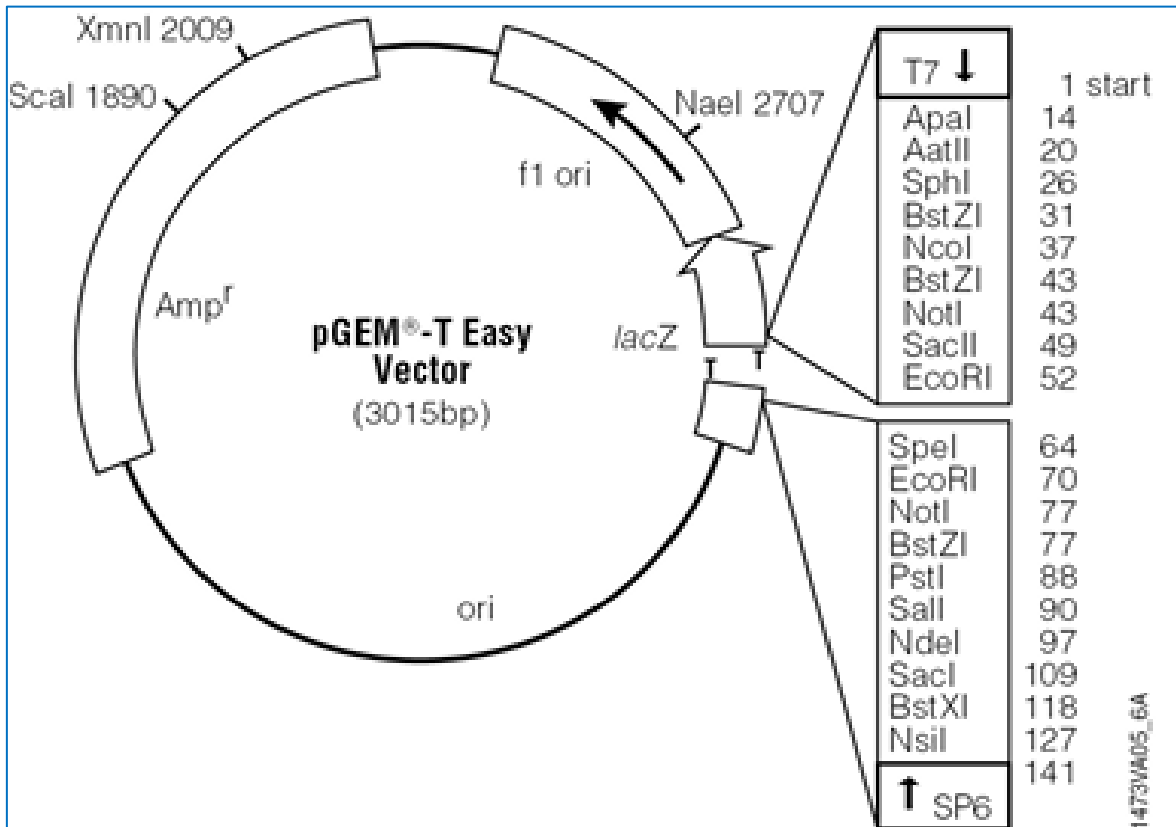


Figure 10 pGEM-T Easy vector system map.

This strategy was employed to clone the 3'-half APOA-I fragment containing the nucleotide substitution associated to the Milano variant.

2.3.3.1.1 PCR for APOA1 sequence mutagenesis

The arg173cys mutation in the APO WT CDS, present in plasmid M00APO plasmid (purchased from Genecopoeia) was inserted through site-specific PCR mutagenesis through the use of primers that anneal and carry the site-specific Milano mutation.

The HOT FIREPol[®] DNA Polymerase (Solys BioDine) was chosen for this procedure due to its capacity to generate 3' A-tailed fragments, essential for TA cloning. The better annealing temperature for the amplification was detected and for each sample the PCR reaction mix was assembled as shown in Table 15 in a final volume of 10 μ l.

Reagent	Amount
10 X HOT FIREPol® 10x Buffer BD	1 µl
25 mM MgCl ₂	1.2 µl
dNTP mix (20 mM)	0.1
Primer Forward (10 pmol/µl)	0.1
Primer Reverse (10 pmol/µl)	0.1
HOT FIREPol® (5 U/µl)	0.15
Nuclease-free H ₂ O	Up to 10 µl
DNA template (10 ng/µl)	1 µl

Table 15 HotFirePolymerase PCR reaction mix.

The reaction was performed in a thermal cycler set on the program outlined in Table 16.

Step	Temperature	Time
Initial Denaturation	95°C	15 min
34 Cycles	95°C	30 seconds
	50-72°C	30 seconds
	72°C	1min/kb
Final Extension	72°C	10 minutes
Hold	4-10°C	

Table 16 PCR thermal cycling program for HOT FIREPol® DNA Polymerase.

The PCR product was purified by gel extraction purification in according to manufacturing protocol as described above (par.2.3.2.3) and analysed by Nanodrop for purity e concentration.

2.3.3.1.2 pGEM ligation reaction protocol

The pGEM reaction ligation was assembled in a 0.5 ml tube as described in table 17, according to the manufacturer's protocol.

Reagents	Sample Reaction	Positive Control
2X Rapid Ligation Buffer, T4 DNA Ligase	5 µl	5 µl
pGEM®-T Easy Vector	1 µl	1 µl
PCR product	15 ng	-
Control Insert DNA	-	2 µl
T4 DNA Ligase (3 Weiss)	1 µl	1 µl

units/ μ l)		
Deionized water	Up to 10 μ l	Up to 10 μ l

Table 17 Ligation reaction for cloning in pGEM-T Easy Vector.

Before use, the pGEM®-T Easy Vector and the Control Insert DNA were briefly centrifuged to collect contents at the bottom of the tube and the 2X Rapid Ligation Buffer was mixed by vortexing.

The reactions were mixed by pipetting and then incubated for 1 hour at room temperature. Then cloning mix was transformed in NZ5- α competent cells (Nzytech) following the manufacturing protocol as described below.

2.3.3.1.3 NZ5- α competent cells transformation protocol

NZ5- α competent E. coli cells (Nzytech) were transformed with 5 up to 10 μ l of the assembly reaction, following the transformation protocol.

Chemically Competent cells were thawed on ice.

10 μ l of the chilled assembly product were added to the competent cells and mixed gently by pipetting up and down or by flicking the tube 4–5 times. The mixture was incubated on ice for 30 minutes.

Then it was subjected to heat shock at 42°C for 40 seconds and transferred on ice for 2 minutes. 900 μ l of room-temperature SOC media were added to the tube.

The mixture was incubated at 37°C for 60 minutes in agitation at 250 rpm. The selection plates were warmed to 37°C and Working near the flame of a Bunsen burner, 100 μ l of the transformed cells were spread onto LB agar plates. LB agar plates are obtained as described above (par.2.3.2.7.1) with the difference that the agar solution was supplemented with 0.5 mM IPTG and 80 μ g/ml X-Gal, for blue/white selection of recombinants as described in par.2.3.2.7.1.

2.3.4 Functional *in vitro* validation of plasmids built

Functional *in vitro* validation of built plasmids was carried out by transfection of HeLa cell line by electroporation (Neon Electroporation system, Thermo Scientific).

2.3.4.1 Cell line

Hela cell line, kindly provided by CNR, Pisa has been used for the functional validation of plasmids sets.

The cells were made to grow in Dulbecco's Modified Eagle's Medium (DMEM), with 4,5 mg/L D-glucose, L-glutamine, and 110 mg/L sodium pyruvate, 10% fetal bovine serum (FBS) to 37°C with 5% CO₂. It's a female epithelial cell line isolated in 1951 from a cervical carcinoma derived from a 31-year-old patient.

Hela cells have been reported to contain human papilloma virus 18 (HPV-18) sequences; P53 expression was reported to be low and normal levels of pRB (retinoblastoma suppressor) were found.

2.3.4.1.1 Handling procedure

The vial was thawed by gently shaking in a water bath at 37 °C for about 2 minutes. Subsequently it was removed from the water bath and in conditions of absolute sterility, the contents of the vial was transferred to a centrifuge tube containing 9,0 ml of complete culture medium and spin at approximately 125 x g for 5 to 7 minutes.

The pellet of cells was resuspended with the recommended complete medium and distributed in a culture flask of 75 cm² and kept in incubator at 37°C with 5% CO₂ in air atmosphere to ensure the best growth conditions.

2.3.4.1.2 Subculturing procedure

The culture medium was removed and discarded. The cell layer was briefly rinsed with 0.25% (w/v) Trypsin- 0.53 mM EDTA solution to remove all traces of serum which contains trypsin inhibitor. 2.0 to 3.0

mL of Trypsin-EDTA solution was added to flask and placed at 37°C for 5 minutes to facilitate dispersal.

8.0 mL of complete growth medium was added, and cells were aspirated by gently pipetting. Appropriate aliquots of the cell suspension were added to new culture vessels and incubated cultures at 37°C.

2.3.4.2 Electroporation

2.3.4.2.1 Cell preparation

The cells were grown in complete culture medium with 10% FBS and without antibiotics in a culture flask of 75 cm².

The cells were rinsed with PBS (without Ca²⁺ and Mg²⁺) and then trypsinized with the Trypsin/EDTA solution. An aliquot of trypsinized cell suspension was used to count cells to determine the cell density.

Four six well plates were performed by electroporation in duplicate of each plasmid built.

500,000 cells were plated for each well of the 6 well-plate (Sarsted) used.

The cells were harvest in growth medium containing serum and each cell volume corresponding to 500,000 cells was transferred to a centrifuge tube. Each tube was then centrifuged the cells at 400 × g for 5 minutes at room temperature.

Two PBS washings were then performed, centrifuging at 400 x g for 8 minutes of each.

At the last washing the PBS was completely aspirated and the cell pellet was resuspended in 100ul of Resuspension Buffer R. The pellet was gently pipetted to obtain a single cell suspension.

6 well plates pre-incubated in a 37°C, 5% CO₂ with 2ml of culture medium containing serum and supplements, but without antibiotics were already to plate the electroporated cells.

2.3.4.2.2 Neon electroporation system

The appropriate amount of plasmid DNA (5ug at a concentration of 1 to 5 µg/µl in sterile water for each reaction) was transferred in a sterile 1.5 mL microcentrifuge tube. The suspension cell was added to the tube containing plasmid DNA and then gently mixed.

Once installed the Neon Transfection System as described in the manufacturing protocol the electroporation reaction was performed for each sample with following parameters specific for the HeLa cell line summarized in table 18.

Pulse voltage (V)	Pulse width (ms)	Pulse number
1005	35	2

Table 18 Neon Electroporation System parameters for HeLa cell line electroporation.

The sample was immediately transferred from the Neon™ Tip into the prepared culture plate containing pre-warmed DMEM with FBS but without antibiotics.

The plate was gently rocked to ensure even distribution of the cells and incubated at 37°C in a humidified CO₂ incubator.

These steps were repeated for each sample.

48h after the transfection, the GFP positive (GFP+) cells were detected by Incucyte® Live-Cell analysis system, Sartorius to estimate the transfection efficiency.

2.3.4.2.3 Cell sorting and Immunocytochemistry

At the end of Incucyte® Live-Cell analysis, each sample was sorted (BD FACS Jazz) for GFP channel in collaboration with Institute of Clinical Physiology of the CNR of Pisa. Subsequently each sample sorted was plated in 4 well Nunc™ Lab-Tek™ II Chamber Slide system™ (ThermoFisher) to enrich the cellular population GFP positive for next steps of ICC. After 48h, the media were gently aspirated from the wells and each well was washed with 500 µL of sterile PBS.

Each well was fixed 500 μ L of cold methanol for 5 min. Subsequently each well was washed with 500 μ L of ice-cold PBS five minutes on a rocking platform for three times.

For immunohistochemical analysis, ImmPRESS® HRP Horse Anti-Mouse IgG Polymer Detection Kit (Vector Laboratories) was used. To inhibit the activity of endogenous peroxidase, slides were incubated in BLOXALL® Block solution (SP-6000) for 10 minutes. The slides were washed in PBS for 5 minutes two times. The blockage was performed incubating the slides in Normal Horse Serum, 2.5% (Immpress Reagent Kit, Vector Labs) for 20 min.

The slides were then incubated with primary antibody Anti-hApolipoproteinA-I antibody [EP1368Y], Abcam diluted 1:100 in Normal Horse Serum 2.5% (Immpress Reagent Kit, Vector Laboratories) for 1 hour, avoiding the drying of samples, for the human APO detection. Blank control was represented by incubation with only secondary antibody (Immpress Reagent Kit, Vector Laboratories) following the same steps of tests samples. Then, the slides were washed in PBS for 5 minutes twice and was incubated with secondary antibody HRP conjugated (Immpress Polymer Reagent, Vector Laboratories) for 30 minutes at room temperature. Subsequently, the slides were washed twice in PBS for 5 minutes and the chromogenic reaction was developed by exposing the slides to ImmPACT DAB peroxidase (HRP) substrate kit (ImmPRESS Reagent Kit, Vector Laboratories) for 3 minutes. The slides were washed twice in PBS for 5 minutes and counterstained with Gill's hematoxylin 2 (Sigma Aldrich) for 30seconds, de-hydrated and finally the coverslips were mounted on slides using VectaMount AQ Aqueous Mounting Medium.

All images were digitally acquired with Scanscope (Aperio) in collaboration with FPScience of Pisa. Area and signal quantification was performed using Imagescope (Aperio).

3 Results

3.1 Analysis of AIM distribution

In this section the results obtained from the study of the AIM protein localization in the RF protein fractions are reported. In addition, the results obtained on the analyses of the tissue biopsies of mice treated with APO rice milk (APO-rice, treated) and WT rice milk (controls) for detection of AIM are shown.

Lastly, the analyses on the expression of endogenous ApoA-I murine in intestine and liver biopsies of treated mice and controls to assess possible significant differences between the two groups are reported.

3.1.1 Rice flour's protein fractions analysis

ELISA and Western Blot analyses (par.2.4.3 and 2.4.4) were performed on salt-soluble, salt-insoluble and total protein fractions from transgenic (tgAPO) and WT RF, in order to investigate AIM protein levels and its distribution among the different protein fractions.

AIM was detected in tgAPO-RF protein extracts with the highest percentage in the salt insoluble protein fraction and total protein fractions while the content of AIM in the salt-soluble protein fraction was almost undetectable (fig.11 and 12).

In the WT RF protein fractions no signal was detected as expected (fig.11 and 12) and it allowed to establish that there was not any cross-reactivity of the antibodies used.

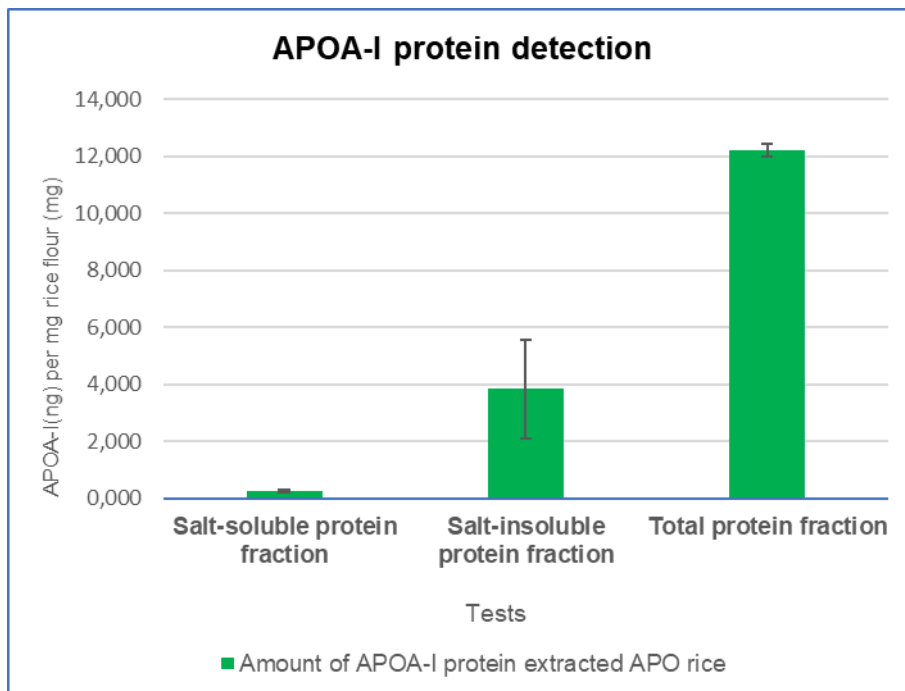


Figure 11 Two independent extractions were made for each fraction which is represented as the mean and relative standard deviation ((Human Apolipoprotein A-I ELISA Kit (ab189576)). APOA-I protein was detected mostly in the salt insoluble fraction. No signal was detected in corresponding protein fraction from WT-RF

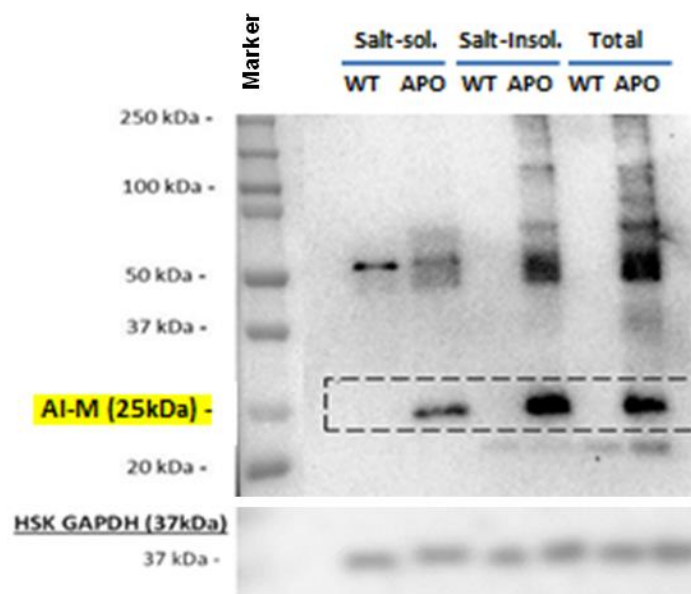


Figure 12 Immunoblot results of human APOA-I (Rabbit monoclonal Anti-hApolipoprotein A-I antibody [EP1368Y], Abcam) on RF protein extract fractions. A 25 kDa band corresponding to AIM is detected in tgAPO-RF with variable intensities in each protein fraction. Two independent tests were made for each fraction extracted. As expected, no signal was detected in the protein extracts from WT-RF.

3.1.2 Analysis of AIM protein biodistribution

AIM protein biodistribution in mice orally administered with APO-rice by oral gavage was studied by investigating its presence in protein extracts from liver, brain, cerebellum and intestine biopsies.

In order to study these aspects, a preliminary Western Blot analysis (par.2.2.2) and ELISA test (par.2.2.3) were performed on the tissue biopsies (two replicates for each sample) derived from animal 3.15, (APO-rice treated group) and from animal 3.22 (control group). Samples from animal 3.22 were used as controls and as expected, no signals were detected in these tissue lysates. This allowed to exclude any potential cross-reactivity of the antibody used between endogenous murine ApoA-I and human APOA-I.

In the treated animals the WB did not provide any signal corresponding to AIM protein (25kDa) in any of the tissues tested (fig. 13). Also in ELISA test, subsequently performed on all the available tissues to achieve a higher sensitivity (par.2.4.4) the values of the absorbance detected were similar to the background level (not shown in figure).

These results suggested that, despite the anti-atherogenic effect induced by the APO-rice treatment in the atherosclerotic mice, no protein accumulation occurred in the tissues, or that AIM protein levels were probably below the minimum detection threshold.

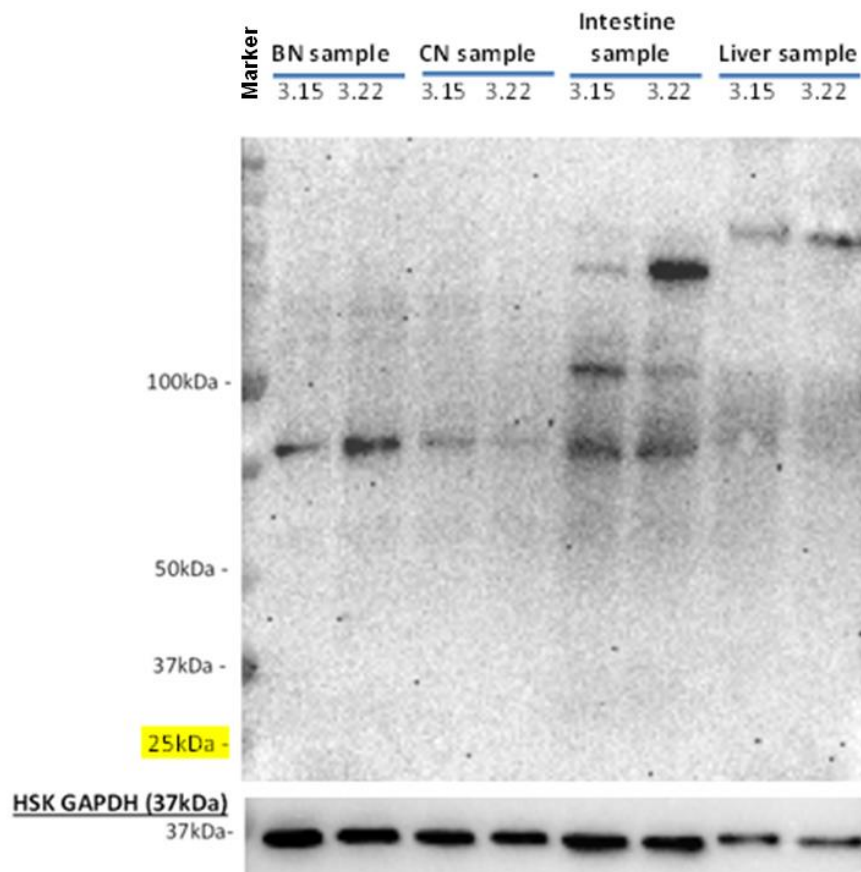


Figure 13 Immunoblot of human APOA-I (25 kDa band) (Rabbit monoclonal Anti-hApolipoprotein A-I antibody [EP1368Y], Abcam) in protein lysates of brain, cerebellum, intestine and liver biopsies harvested from treated (3.15) samples and control (3.22) samples. Two independent tests were made for each sample. No signal was detected in each sample.

3.1.2.1 Immunohistochemistry preliminary results

The immunohistochemistry (IHC) allowed the acquisition of single cell resolution by increasing spatial resolution compared to ELISA and WB conducted previously on mouse biopsies of the APO3 study.

It was performed on tissue sections of the control group animals and treated with APO milk of the pre-clinical study APO3 which were kindly granted by the service facility of histology associated with the enclosure of the University of Milano Bicocca.

For human APOA-I detection was used Rabbit monoclonal Anti-hApolipoproteinA-I antibody [EP1368Y] (Abcam), the same of WB (par.2.2.4).

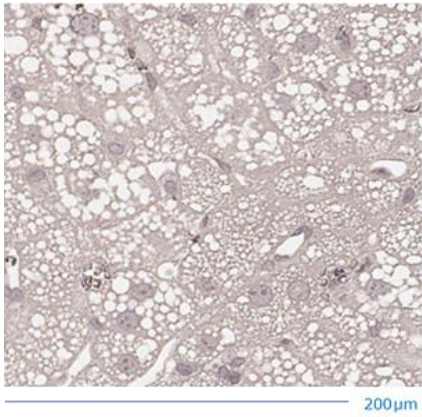
Images A and B, in figure 14 are representative of six different mouse tissue sections of the APO3 study on which the IHC was conducted.

Images A represent the blank control of two sections, one for the WT group (sample 3.22) and one for the APO treated group (sample 3.9). The section was not incubated with the primary antibody but only with the secondary antibody and serves to define the background; images B are representative of a comparison between animal tissue of control group (sample 3.22 and 3.24) and animal tissue treated with APO rice milk (sample 3.9 and 3.15) but in this case the samples in comparison are the WT group (3.22 and 3.24 samples) and the APO treated group (3.9 and 3.15 samples).

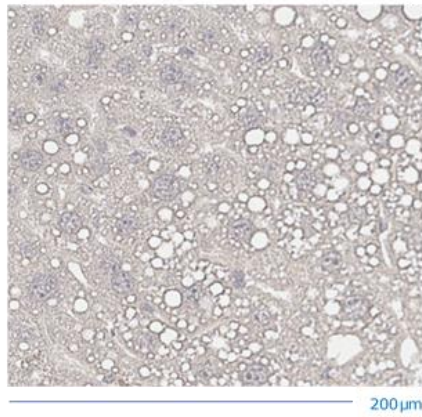
The spots represented by the most intense brown dye represent positive signals, highlighted in yellow.

A

**Blank control WT group
-Sample 3.22-**

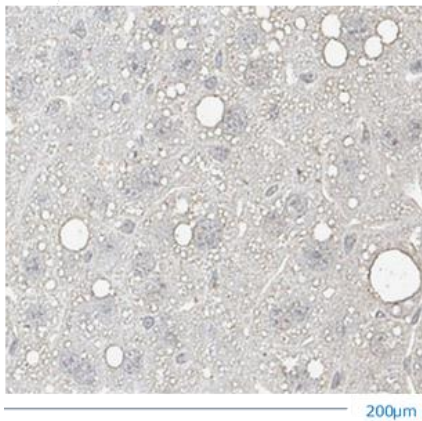


**Blank control Treated group
-Sample 3.9-**

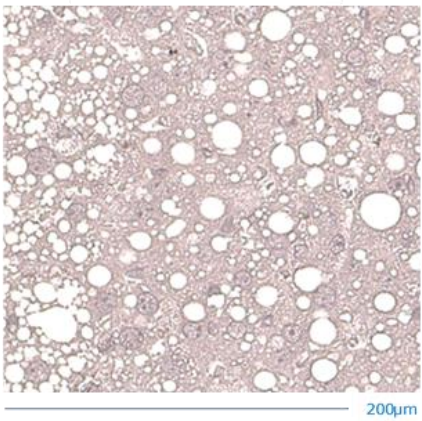


B

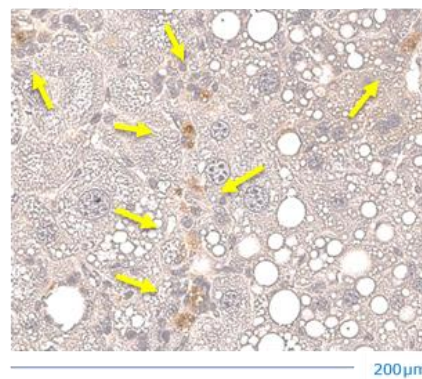
**IHC WT group
-Sample 3.22-**



**IHC WT group
-Sample 3.24-**



**IHC Treated group
-Sample 3.9-**



**IHC Treated group
-Sample 3.15-**

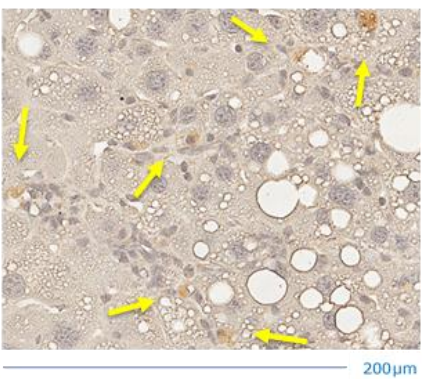


*Figure 14 Representative pictures of Immunohistochemistry assays for human AIM detection in mouse liver sections. **A**: blank control; **B**: IHC assays performed on liver section: comparison between two representative fields of control group and treated group. Highlighted in yellow positive signals detected only in APO-rice treated mice section. The positive cells are not morphologically hepatocyte-related and are of different cell types.*

As expected, the positive signal was detected only in the sections of the treated group. both the blank control and the control group sections exhibit no cross reactivity and no positive cellular signal.

Positive spots detected only in the sections of the treated animals are a further indication that the primary antibody does not cross reactive with endogenous Apo murine protein but is specific to the human APO (AIM).

3.1.3 Mouse ApoA-I protein analyses

To investigate the potential biological mechanisms induced in mice by APO-rice administration, the expression levels of endogenous ApoA-I protein were evaluated via WB (par.2.4.3).

This analysis was performed on the protein extracts from all liver and intestine lysates biopsies, since these two organs are the major sources of ApoA-I and possible significant differences between the two experimental groups could be better identified.

3.1.3.1 Preliminary results on liver samples

The results of two independent tests showed a significant increased expression of the endogenous ApoA-I murine protein (fig.15) in the liver of APO-rice treated mice, as compared to WT-milk treated mice.

The animal 3.8 was not considered because is degraded, or some problems occurred in the animal processing after the sacrifice, instead 3.11 animal was detected as outlier (graphpad.com).

The data was obtained from the semi-quantitative densitometry analysis of bands corresponding to endogenous murine ApoA-I protein, normalized to housekeeping GAPDH band signal as reported in figure 15.

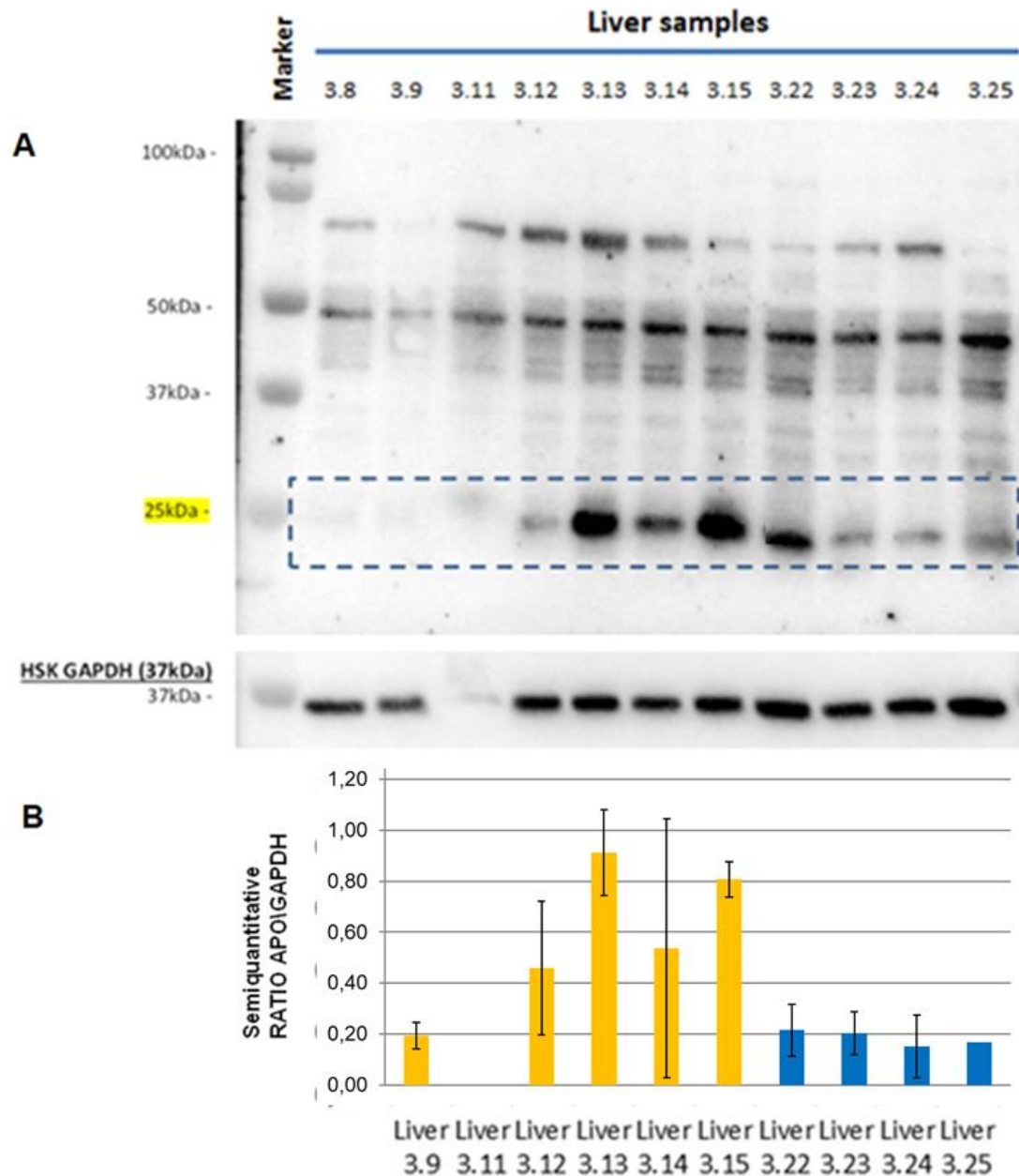


Figure 15 **A**: Immunoblotting (Goat polyclonal Anti-mouse Apolipoprotein A-I antibody (ab7614)) of mouse ApoA-I (25 kDa band) in protein lysates of liver biopsies harvested from treated (3.9-3.15) samples and control (3.22-3.25) samples. Samples 3.8 is a damage sample and therefore was not considered. **B**: chart reported the mean value of two tests performed for each liver sample of semi-quantitative densitometric analysis of mouse ApoA-I normalized to GAPDH optic signal and relative standard deviation.

A t-test performed on the mean values of the treated and control groups has established a significant difference between the two sets of samples ($p < 0.05$), as shown in figure 16.

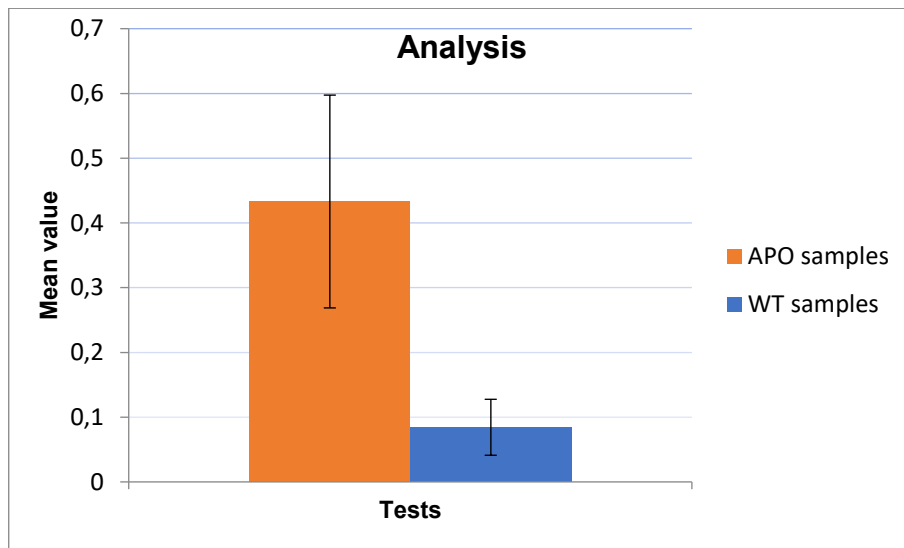


Figure 16 Chart reported the mean value of two tests performed for treated group and control group of semi-quantitative densitometric analysis of mouse ApoA-I protein normalized to GAPDH optic signal which relative standard deviation. The difference between two groups was significant.

This suggests a possible impact of orally administered AIM protein through APO-rice on the molecular regulation of its endogenous counterpart. Analysis at the level of transcriptional, post transcriptional and translation regulation of ApoA-I will be the subject of future studies for a better understanding of the mechanisms.

3.1.3.2 Preliminary results on intestine samples

Intestine samples didn't show the same pattern (fig.17) observed in liver samples with no significant differences between WT-milk and APO-rice treated mice (fig.18).

Also in this case the animal 3.8 was not considered because is degraded, or some problems occurred in the animal processing after the sacrifice.

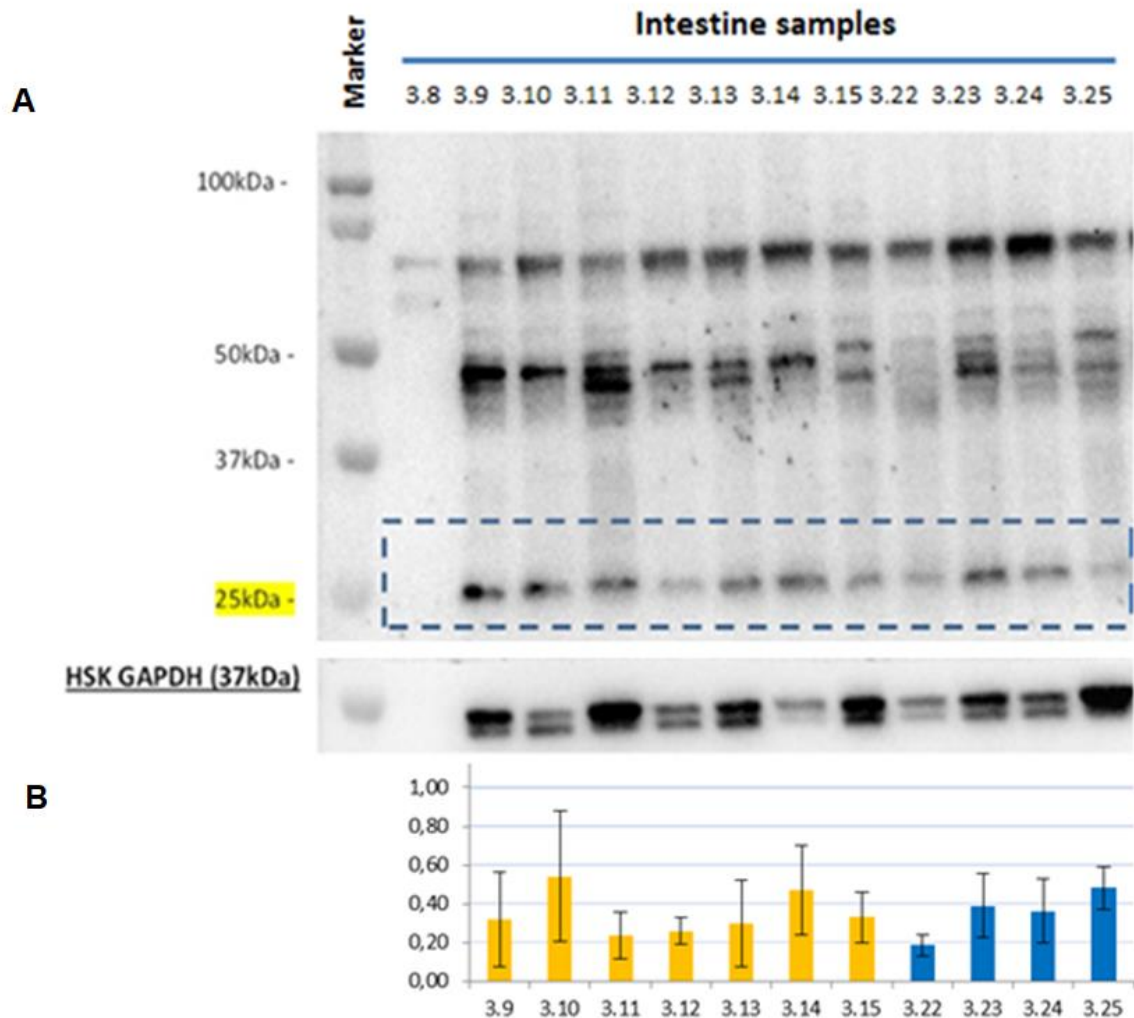


Figure 17 **A**: Immunoblotting of mouse ApoA-I (25 kDa band) (Goat polyclonal Anti-mouse ApolipoproteinA-1 antibody (ab7614)) in protein lysates of intestine biopsies harvested from treated (3.8-3.15) samples and control (3.22-3.25) samples **B**: chart reported the mean value of two tests performed for each intestine sample of semi-quantitative densitometric analysis of mouse ApoA-I normalized to GAPDH optic signal and relative standard deviation. Samples 3.8 a damage sample and therefore was not considered.

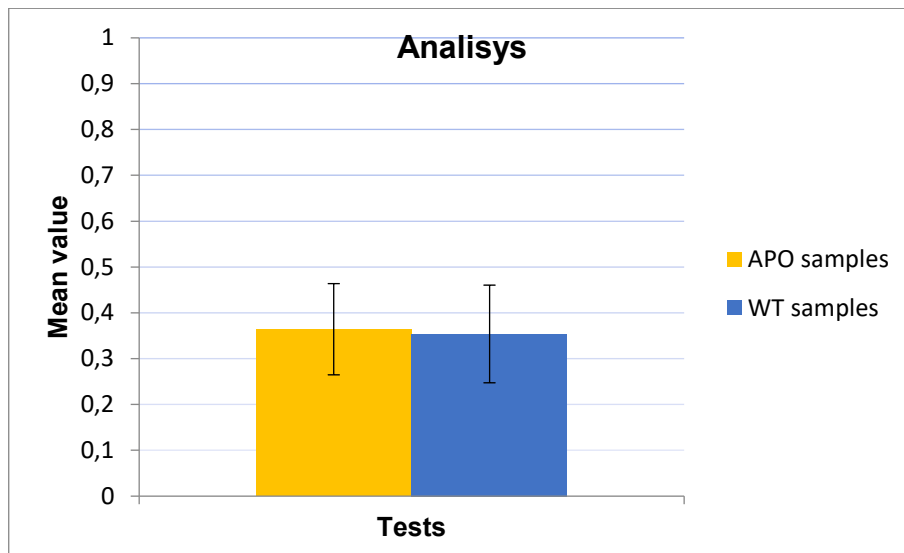


Figure 18 Chart reported the mean value of two tests performed for treated group and control group of semi-quantitative densitometric analysis of mouse ApoA-I protein normalized to GAPDH optic signal which relative standard deviation. The difference between two groups was not significant.

The antibody against Apo-endogenous-murine did not provide any signal on the protein extract from WT and APO rice protein extracts as expected and confirming the lack of cross-reactivity between murine antibody and Apo-human (figure 19). This further confirmed the hypothesis that the increased endogenous levels of Apo-murine were induced by the Apo-milk treatment.

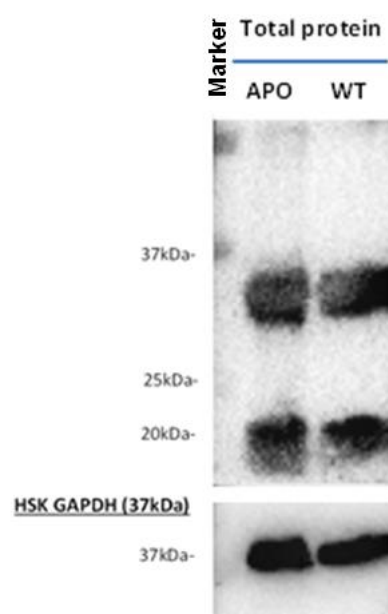


Figure 19 Immunoblotting of mouse ApoA-I (25 kDa band) (Goat polyclonal Anti-mouse ApolipoproteinA-1 antibody (ab7614)) in RF protein total fraction extracted. No signal detected corresponding to ApoA-1 protein as the expectations. No cross reactivity between Apo murine and Apo human protein with antibody used was detected as expected.

3.2 Set plasmids production for cell transfection experiments

Once the proof-of-concept studies ¹¹²provided successful results, the next step is to increase the production of the AIM protein per weight unit of rice. This led to the development and validation of a system of vectors, which will serve primarily for *in vitro* functional testing. Later, this will be used as source of CDSs to be subcloned in appropriate vectors. Then, we will carry out a specific gene-editing approach to express AIM protein for the establishment of a novel strain of engineered rice.

For all vectors built, the starting backbone was the pCX-HO1-F2A-EGFP vector (Vector backbone: pCX-C1, a modified version of pCX-EGFP plasmid from Okabe M., et al., FEBS Letters, 407 (1997) 313-319) previously produced by our group ¹²⁴) and distributed by Addgene, USA (plasmid # 74672) (fig.20) The insert HO1-F2A-EGFP (hHO-1/F2A/EGFP) with size 1674bp is under the control of pCAGGS promoter and hHO-1 5' *EcoRI*, hHO-1 3' *NheI*, EGFP 5' *AflII*, and *EcoRI* EGFP 3' cloning sites can be used. The plasmid has Kanamycin bacterial resistance and Neomycin eukaryotic resistance as shown in figure 20.

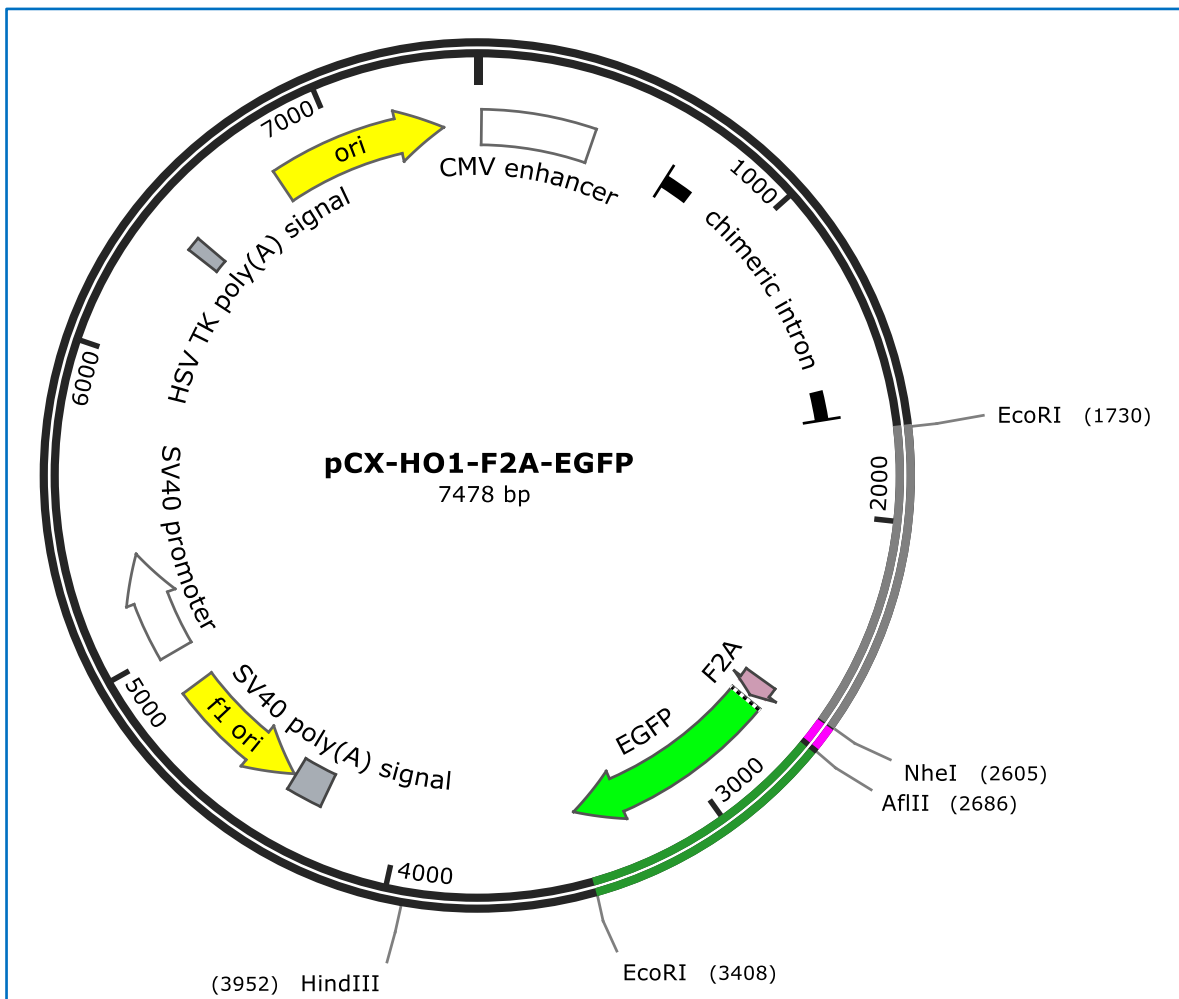


Figure 20 pCX-HO1-F2A-EGFP plasmid map. The main functional elements as well as double EcoRI restriction site are reported. In grey is highlighted HO1 sequence in frame with F2A sequence (in pink) and EGP sequence in green. (Image Created by SnapGene).

3.2.1 APOA1 sequence mutagenesis

The introduction of the Milano mutation in the APOA1 WT cDNA, obtained from the M00APO plasmid purchased from Genecopoeia, involved several experimental steps that led to the replacement of the cytosine nucleotide with a thymine in codon 173 leading to the amino acid change from arginine to cysteine.

Initially, the 3'-proximal half of APOA1 sequence, containing at its 5'-end the nucleotide of interest, was obtained by specific PCR amplification of this fragment using a pair of primers designed with the desired mismatch in the centre of the forward primer (par.2.3.3.1.1).

This reaction was performed using a Taq polymerase to facilitate the next step of cloning (TA-cloning in pGEM-T Easy vector system).

The PCR product was purified as described in par.2.3.2.3 and cloned in pGEM Teasy vector system following the protocol described (par.2.3.3.1.2).

The resulting transformed colonies with the assembled construct were screened for the correct presence of cloned insert as described in paragraph 2.3.3.1.3 by performing a PCR on the recombinant plasmids using insert-specific primers. The Figure 21 shows the electrophoresis analysis of PCR products. PCR product of the expected size 216 bp, corresponding to the presence of 3'-proximal half of APOA1 sequence, were observed in all the lines except #6, #10, #20 (fig.21).



Figure 21 Electrophoresis analysis of PCR products cloned into pGEM. Lane 1 and 22: 100 bp DNA Ladder (Solis BioDyne); Lane 2-21 (upper gel) and 23-31 (lower gel): screened samples. The insert corresponds to the 3'-proximal half of AIM sequence. Expected band size: 216 bp.

Electrophoresis analysis of PCR products cloned into pGEM. Lane 1 and 22: 100 bp DNA Ladder (Solis BioDyne); Lane 2-21 (upper gel) and 23-31 (lower gel): screened samples. The insert corresponds to the 3'-proximal half of AIM sequence. Expected band size: 216 bp.

Some positive samples were selected and checked by sequencing and submitted to Eurofins Genomics as described in par. 2.3.2.9 for Sanger sequencing to validate the accuracy of the sequence. The

electropherogram reported in figure 22 shows one of the analysed clones that matched 100% to the expected target sequence.

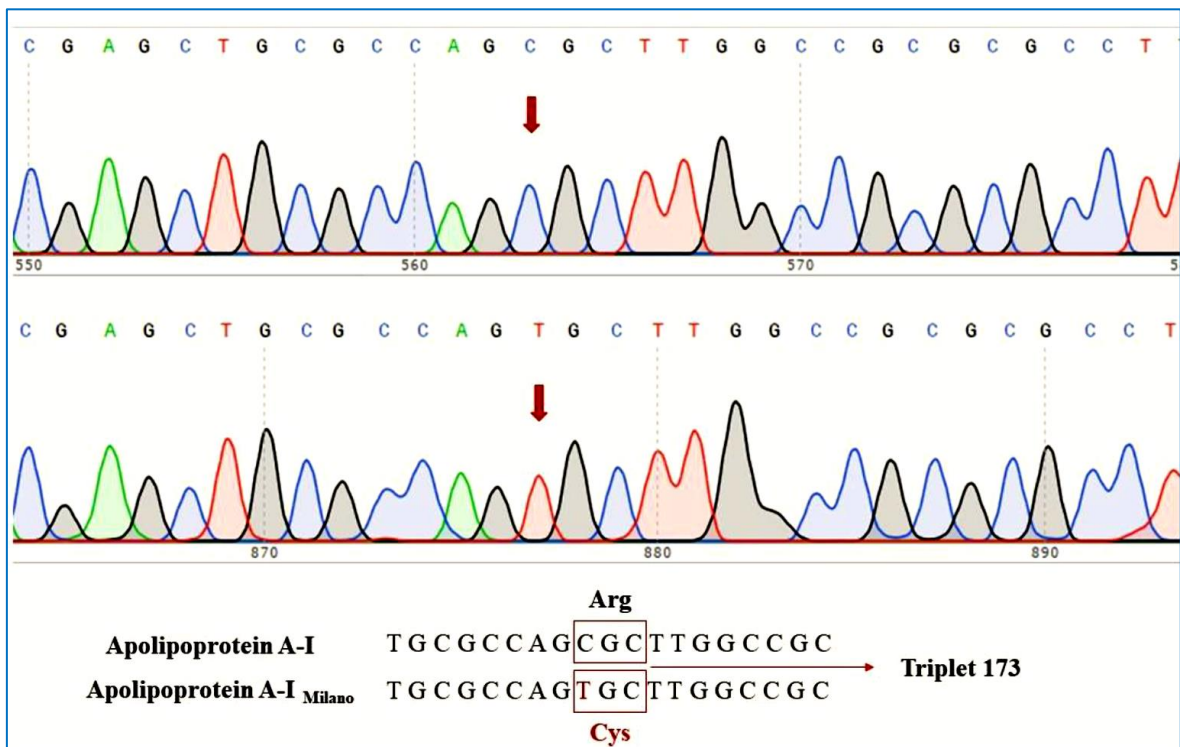


Figure 22 Electropherogram of 3'-proximal half of APOA1 with Milano mutation cloned in pGem T-easy vector system (below) compared to the APOA1 WT sequence (up).

Then, the 5'-proximal half, and the mutated 3'-proximal half fragments resulting of APOA1 sequence have been assembled into the EX-EGFP-M02 vector to obtain the full-size coding sequence of AIM. Initially, the two DNA fragments have been amplified by high fidelity PCR with specific primers designed with homologous overlaps for cloning with each other and with the backbone vector (par. 2.3.2.1) and donor vector linearized with *XhoI* restriction enzyme. Linearized vector and fragments with the appropriate overlapping ends purified were thus assembled by the Gibson Assembly cloning method following the protocol described in par.2.3.2.5.

The resulting transformed colonies with the assembled construct were screened (par.2.3.2.8) by performing a PCR on the recombinant plasmids for the correct presence of cloned insert (AIM) using insert-specific primers.

The image below shows the gel electrophoresis of PCR products. All the screened clones produced a PCR product of the expected size (804 bp), corresponding to the complete APOA1 sequence (fig.23).

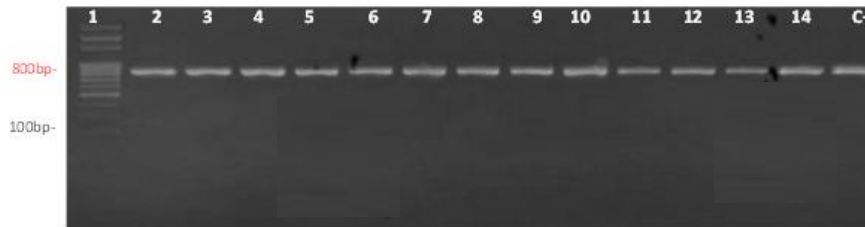


Figure 23 Electrophoretic run of AIM CDS complete PCR product. Lane 1: 100 bp DNA Ladder (Solys Biodyne); Lane 2-14: samples screened. C+: positive control represented by APO WT product. Expected band size: 804bp.

Some positive samples were selected and checked by sequencing and submitted to Eurofins Genomics as described in par. 2.3.2.9 for Sanger sequencing to validate the accuracy of the AIM sequence. The electropherogram showed in figure24 shows one of the analysed clones that matched 100% to the expected target sequence.

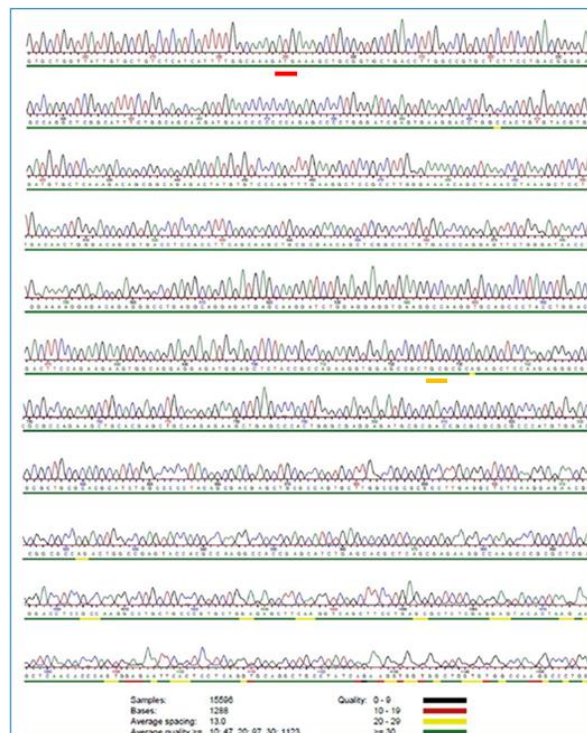


Figure 24 Electropherogram reported the complete AIM sequence. The start codon is underlined in red. The ARG->173CYS mutation is underlined in orange. The green line means the excellent quality of sequencing.

In the table 19 is reported the comparison between the aminoacidic sequences of APOA-I and that of the Milano variant (AIM). The only difference is the one concerning the amino acid Arginine in position 173 that in the AIM has been changed to Cysteine, highlighted in orange.

APO WT	1	MKAAVLT LAVL FLTGSQARHFQQDEPPQSPWDRVKDLATVYVDVLKDSGRDYVSQFEGSALGKQLNLKLLDNWDSVTST	80
AIM	1	MKAAVLT LAVL FLTGSQARHFQQDEPPQSPWDRVKDLATVYVDVLKDSGRDYVSQFEGSALGKQLNLKLLDNWDSVTST	80
	81	FSKLREQLGPVTQEFWDNLEKETEGLRQEMSKDLEEVKAKVQPYLDDFQKKWQEEEMELYRQKVEPLRAELQEGARQKLHE	160
	81	FSKLREQLGPVTQEFWDNLEKETEGLRQEMSKDLEEVKAKVQPYLDDFQKKWQEEEMELYRQKVEPLRAELQEGARQKLHE	160
	161	LQEKLSPLGGEEMRDRARAHVDALRTHLAPYSDELRRQLAARLEALKENGGARLAEYHAKATEHLSTLSEKAKPALEDLRQ	240
	161	LQEKLSPLGGEEMRDRARAHVDALRTHLAPYSDELRRQLAARLEALKENGGARLAEYHAKATEHLSTLSEKAKPALEDLRQ	240
	241	GLLPVLESFKVSFLSALEEYTKKLNTQ * 267	
	241	GLLPVLESFKVSFLSALEEYTKKLNTQ * 267	

Table 19 Comparison of the amino acid sequence of APOA-I WT, highlighted in blu, with AIM highlighted in red. As shown highlighted in red box the Milano variant carries a mutation against the arginine (R) in cysteine (C) in position 173. Red asterisk indicates the stop codon. (Alignment modified by Protein Blast, NIH).

3.2.2 Multicistronic expression plasmids construction strategy

The strategy consists of building multigenic expression plasmids containing the CDS of EGFP and the CDS of APOA1 or AIM, cloned in the same open reading frame, with the latter in multiple copies, each one spaced by the F2A, a viral sequence encoding for a oligopeptide. The pCX-HO1-F2A EGFP vector was used as a backbone for the assembly of CDSs and subsequent *in vitro* functionality tests.

The basic scheme of the final plasmid is:

**pCAGGS-CDS₁-F2A₁-(CDS₂-F2A₂)-(CDS₃-F2A₃)-CDS₄-SV 40
polyA-**

The *EcoRI* sites allowed the excision of the HO1-F2A-EGFP fragment through enzymatic digestion. Subsequently, the AIM or APOA1

fragments were cloned into the vector in single or multiple copies and in frames with the F2A and EGFP sequences exploiting the linearization of the vector downstream of the promoter obtaining the set of ultimate expression vectors for *in vitro* tests.

The following **control vectors** were also designed and assembled:

1. pCX-F2A
2. pCX-APO
3. pCX-AIM
4. pCX-EGFP
5. pCX-APO-F2A-EGFP
6. pCX-EGFP-F2A-APO
7. pCX-EGFP-F2A₁-APO₁-F2A₂-APO₂

The following **test vectors** were designed and assembled to evaluate APOA1 expression *in vitro* and subsequently perform Reverse cholesterol transport assay:

8. pCX-AIM-F2A-EGFP
9. pCX-EGFP-F2A-AIM
10. pCX-EGFP-F2A₁-AIM₁-F2A₂-AIM₂
11. pCX-EGFP-F2A₁-AIM₁-F2A₂-AIM₂-F2A₃-AIM₃

The characteristics of each plasmid built (inserts, length and function) are summarized in table 20.

	Plasmid Name	Type of insert(s)	Length (bp)	Function
0	pCX-HO1-F2A-EGFP	/	7478	Backbone plasmid
1	pCX-F2A	F2A sequence	5872	<i>In vitro</i> control vector
2	pCX-APO	APO CDS	6605	<i>In vitro</i> control vector
3	pCX-AIM	AIM CDS	6605	<i>In vitro</i> control vector
4	pCX-EGFP	EGFP CDS	6516	<i>In vitro</i> control vector
5	pCX-APO-F2A-EGFP	APO CDS in frame with F2A-EGFP insert	7414	- <i>In vitro</i> control vector - Test F2A sequence position
6	pCX-EGFP-F2A-APO	EGFP CDS in frame with F2A-APO insert	7409	- <i>In vitro</i> control vector - Test F2A sequence position
7	pCX-EGFP-F2A ₁ -APO ₁ -F2A ₂ -APO ₂	F2A-APO sequence in frame with F2A ₂ -APO ₂ in pCX-EGFP-F2A-APO plasmid	8287	- <i>In vitro</i> control vector - Test F2A sequence position
8	pCX-AIM-F2A-EGFP	AIM CDS in frame with F2A-EGFP insert	7414	- <i>In vitro</i> test vector - Test F2A sequence position
9	pCX-EGFP-F2A-AIM	EGFP CDS in frame with F2A-AIM insert	7409	- <i>In vitro</i> test vector - Test F2A sequence position
10	pCX-EGFP-F2A ₁ -AIM ₁ -F2A ₂ -AIM ₂	F2A-AIM sequence in frame with EGFP and F2A-AIM sequences in pCX-EGFP-F2A-AIM plasmid	8287	- <i>In vitro</i> test vector - Test F2A sequence position
11	pCX-EGFP-F2A ₁ -AIM ₁ -F2A ₂ -AIM ₂ -F2A ₃ -AIM ₃	F2A-AIM sequence in frame with EGFP and F2A-AIM-F2A-AIM sequences in pCX-EGFP-F2A ₁ -AIM ₂ -F2A ₁ -AIM ₂ plasmid	9172	- <i>In vitro</i> test vector - Test F2A sequence position

Table 20 In table are summarized details of each plasmid built.

3.2.2.1 Control plasmids

3.2.2.1.1. pCX-F2A plasmid

The F2A sequence was obtained by specific PCR amplification from pCX-HO1-F2A-EGFP plasmid using a pair of primers designed with homologous overlaps for cloning in the backbone plasmid (section.2.3.2).

Donor vector pCX-HO1-F2A-EGFP was linearized with *EcoRI* restriction enzyme. Then, purified linearized vector and fragment with the appropriate overlapping ends were assembled by the Gibson Assembly cloning method following the protocol described in par.2.3.2.5. The *EcoRI* restriction site was reconstituted at the 3' of EGFP sequence. The resulting transformed colonies with the assembled construct were screened for the correct presence of cloned insert (F2A) by performing a PCR on the recombinant plasmids using insert-specific primers (par.2.3.2.1). Since the F2A sequence has a size of 76bp, too small to be adequately analysed via electrophoresis of restriction enzyme digestion products or by using pairs of primers outside the cloning site, some post-bacterial transformation samples were selected and checked directly by Sanger sequencing (Eurofins Genomics) to validate the accuracy of the F2A sequence cloning (par.2.3.2.9).

The electropherogram illustrated in Figure 25 shows one of the analysed clones that matched 100% to the expected target sequence.

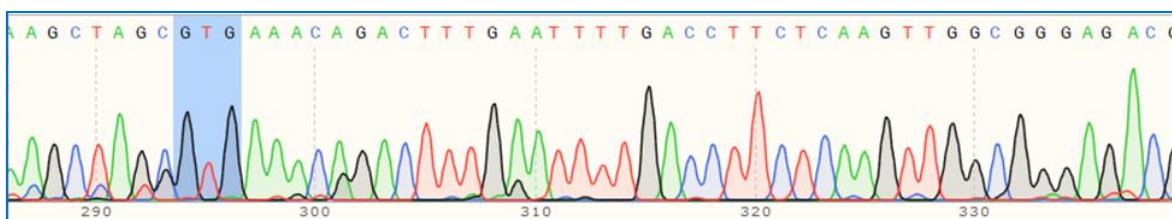


Figure 25 F2A sequence is correctly detected with Sanger sequencing in cloning assembled plasmid. The codon highlighted in blue corresponds to the first codon of F2A sequence.

The pCX-F2A plasmid contains the F2A sequence (fig.26) downstream the CAGGS promoter and thus, when transfected in eukaryotic cells, it

will not allow translation of any relevant protein product. The pCX-F2A plasmid will be used as 'empty vector' control as compared to all the other multicistronic plasmids and as further control of the possible impact of the F2A sequence on cell viability after transfection.

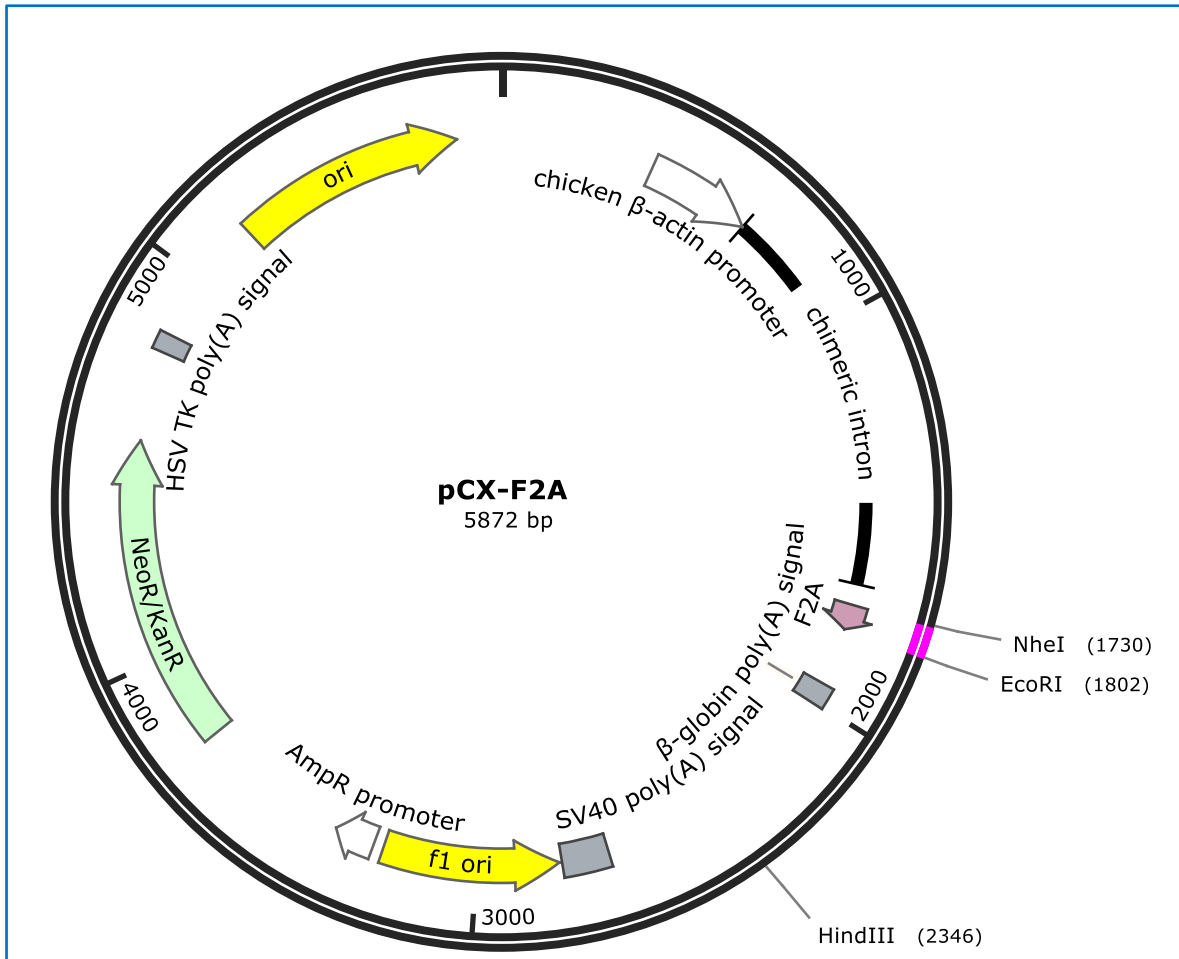


Figure 26 pCX-F2A plasmid map. The main functional elements as well as unique *EcoRI* restriction site and *NheI* restriction site are reported. In pink is highlighted F2A sequence. (Image Created by SnapGene).

3.2.2.1.2. pCX-APO plasmid

APOA1 sequence was obtained by specific PCR amplification from plasmid M002 (Genecopeia) using a pair of primers designed with homologous overlaps for cloning in the backbone plasmid (par.2.3.2.1). The donor vector pCX-HO1-F2A-EGFP was linearized with *EcoRI* restriction enzyme. Linearized vector and fragment with the appropriate

overlapping ends purified were thus assembled by the Gibson Assembly cloning method following manufacturing protocol (par.2.3.2).

The resulting transformed colonies with the assembled construct were screened (par.2.3.2.8) by performing a PCR on the recombinant plasmids for the correct presence of cloned insert (APOA1) using insert-specific primers.

The *EcoRI* restriction site was reconstituted at 3' of EGFP sequence.

The figure 27 shows the gel electrophoresis of PCR product samples.

All the screened clones produced a PCR product of the expected size (804 bp), corresponding to the complete APOA1 sequence (fig.27).

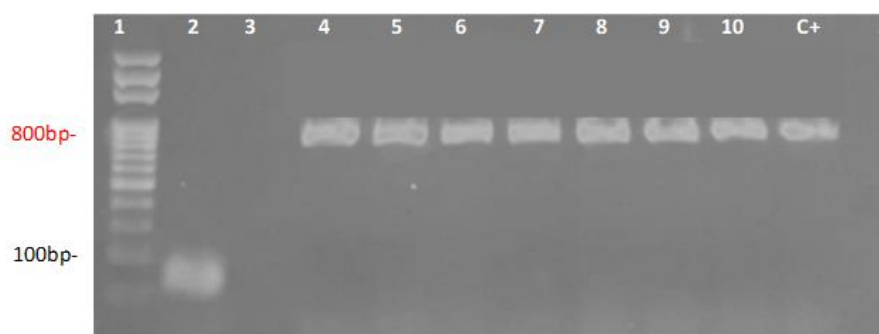


Figure 27 Electrophoretic run of APOA1 PCR product. Lane 1: 100bp DNA Ladder (Solys BioDyne); Lanes 2-10: samples screened; C+: Positive control represented by the APO fragment amplified by the plasmid M002 (Genecopoeia).

Some positive samples selected were checked by sequencing and submitted to Eurofins Genomics as described (par.2.3.2.9) for Sanger sequencing to validate the accuracy of the APO sequence. The electropherogram reported in figure 28 shows one of the analysed clones that matched 100% to the expected target sequence.

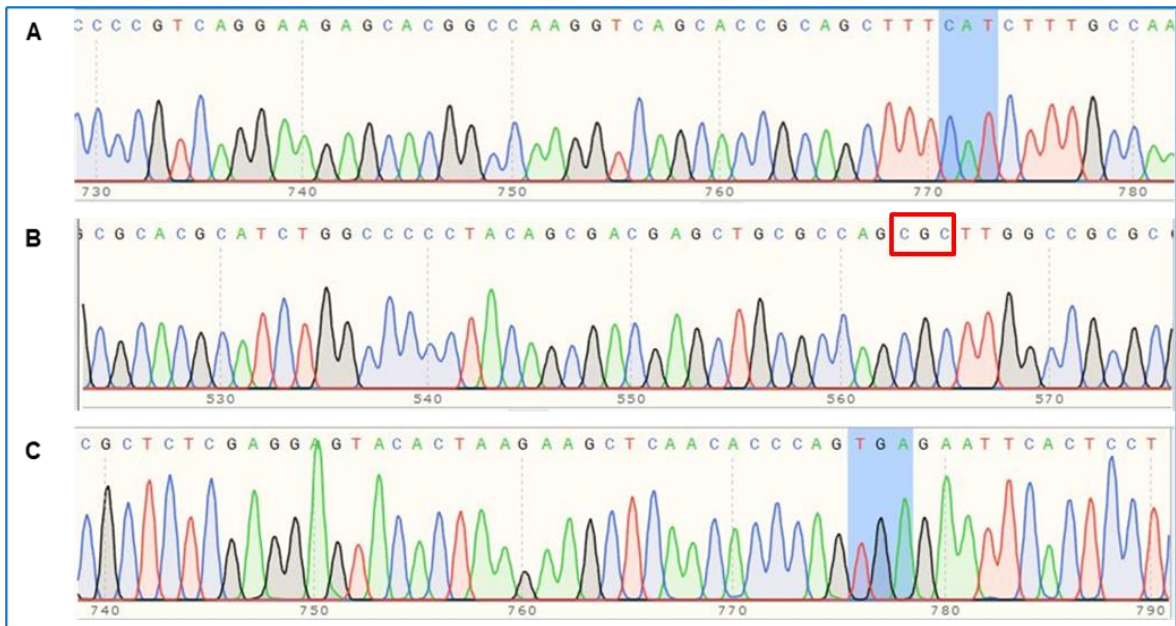


Figure 28 APOA1 sequence is correctly detected in cloning assembled plasmid. **A**: sequencing with the reverse primer of the portion including the starting codon (highlighted in blue); **B**: portion of the sequencing with primer forward which represents the codon carrying the WT variant APOA1 (underlined in red); **C**: portion of the sequencing with primer forward including the stop codon (highlighted in blue).

The resulting pCX-APO plasmid is a monocistronic plasmid expressing the APOA1 (WT) sequence (fig. 29) and it will serve as a positive control to evaluate if the residual F2A peptide that remains attached to the APOA1 in the multicistronic approach could interfere with the APOA-I biological function and as a control of the specific effects induced by the “Milano” variant as compared to the APOA1 WT sequence.

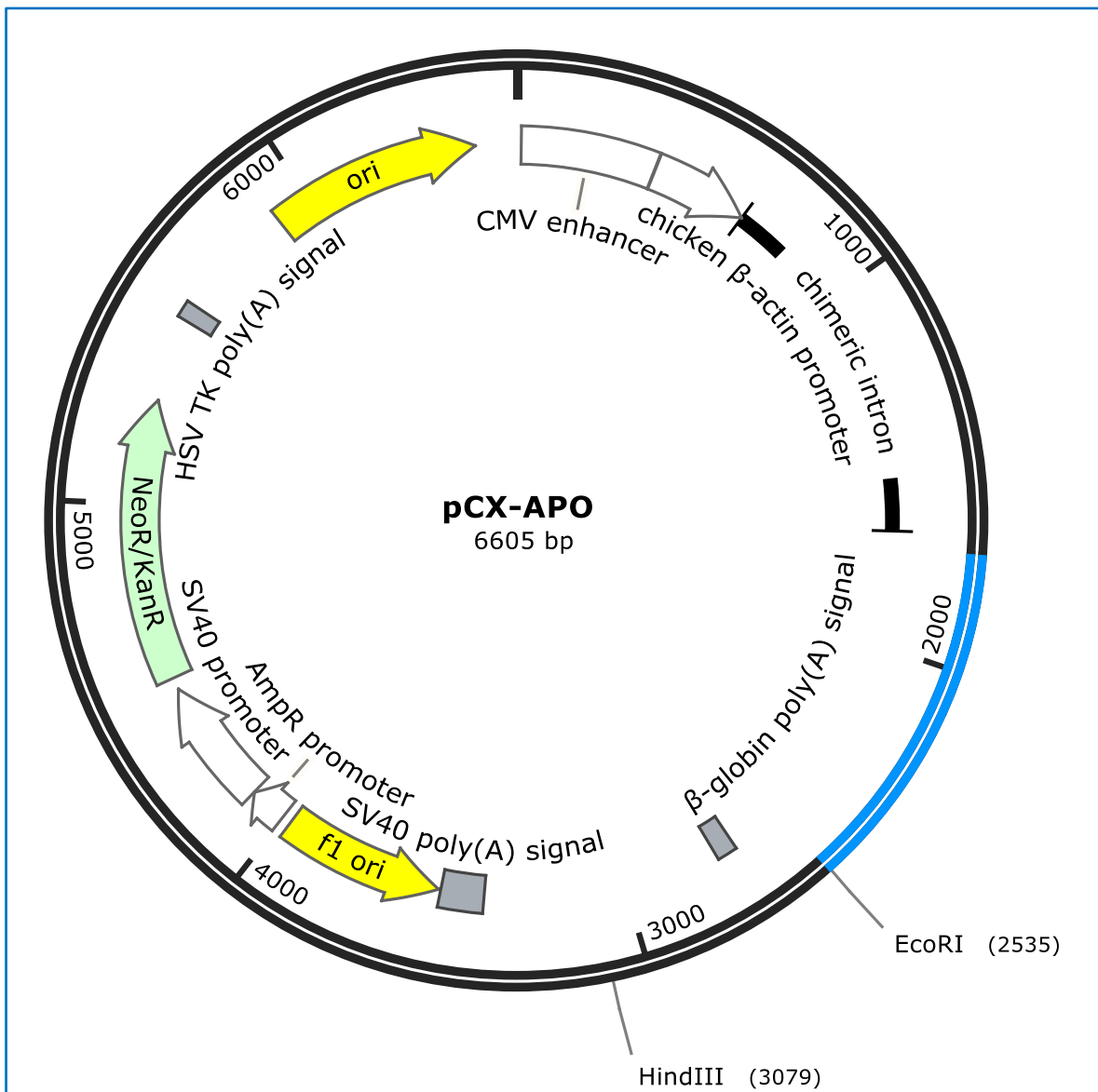


Figure 29 pCX-APO plasmid map. The main functional elements as well as unique *EcoRI* restriction site are reported. In blue is reported APO sequence. (Created by SnapGene).

3.2.2.1.3. pCX-AIM plasmid

The AIM CDS was obtained by means of specific PCR amplification from previously built pReceiver APO-GFP plasmid using a pair of primers specifically designed with homologous overlaps for cloning in the backbone plasmid (par.2.3.2.1).

The donor vector pCX-HO1-F2A-EGFP was linearized with *EcoRI* restriction enzyme and purified and fragment with the appropriate overlapping ends were thus assembled by the Gibson Assembly cloning method following the protocol described in par.2.3.2.5. The *EcoRI*

restriction site was reconstituted at the 3' of EGFP sequence. The resulting transformed colonies with the assembled construct were screened for the correct presence of cloned insert (AIM) by performing a PCR on the recombinant plasmids using insert-specific primers (par.2.3.2.8).

The figure 30 shows the gel electrophoresis analysis of PCR product samples. All the screened clones produced a PCR product of the expected size (804 bp), corresponding to the complete APOA1 sequence.

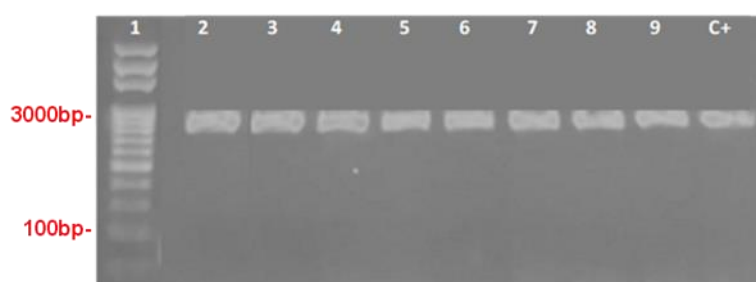


Figure 30 Electrophoretic run of AIM PCR product. Lane 1: 100bp DNA Ladder (Solys BioDyne); Lanes 2-9: samples screened; C+: Positive control represented by the AIM fragment amplified from the previously built plasmid pReceiver AIM-GFP.

Some positive samples were selected and checked by sequencing and submitted to Eurofins Genomics as described in par. 2.3.2.9 for Sanger sequencing to validate the accuracy of the AIM sequence. The electropherogram reported in figure 31 shows one of the analysed clones that matched 100% to the expected target sequence.

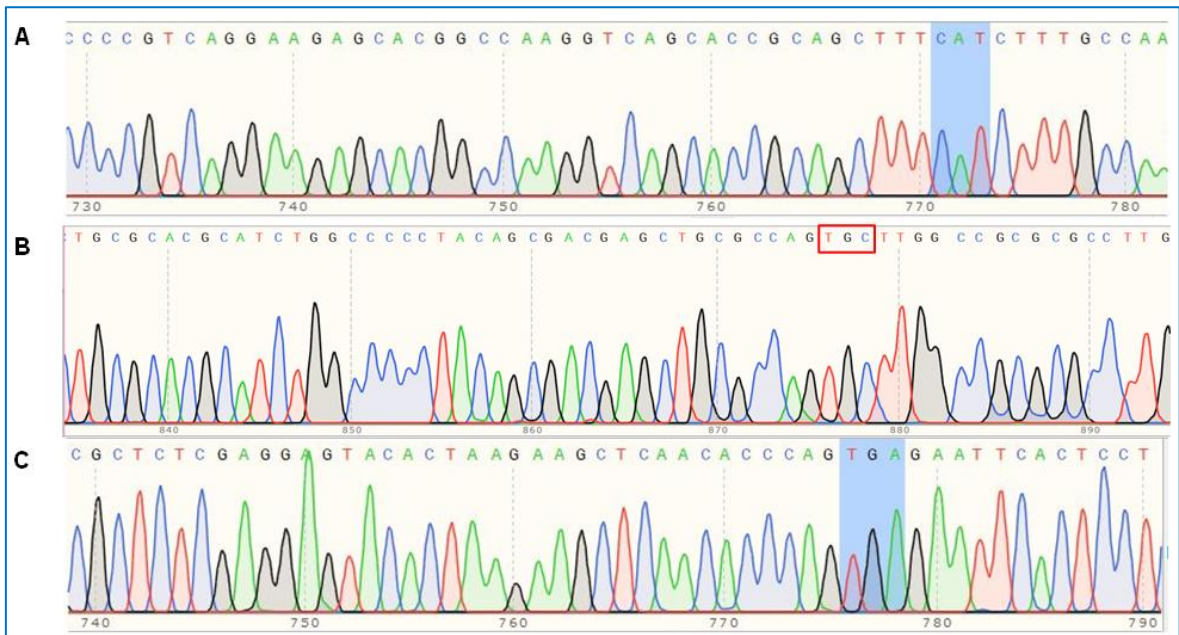


Figure 31 AIM sequence is correctly detected in cloning assembled plasmid. **A**: sequencing with the reverse primer of the portion including the starting codon (highlighted in blue); **B**: portion of the sequencing with primer forward which represents the codon carrying Milano mutation (underlined in red); **C**: portion of the sequencing with primer forward including the stop codon.

The resulting pCX-AIM is a monocistronic plasmid (fig. 32) expressing the AIM sequence, and it will serve as control to evaluate if the residual F2A peptide that remains attached to the AIM in the multicistronic approach could interfere with the AIM biological function.

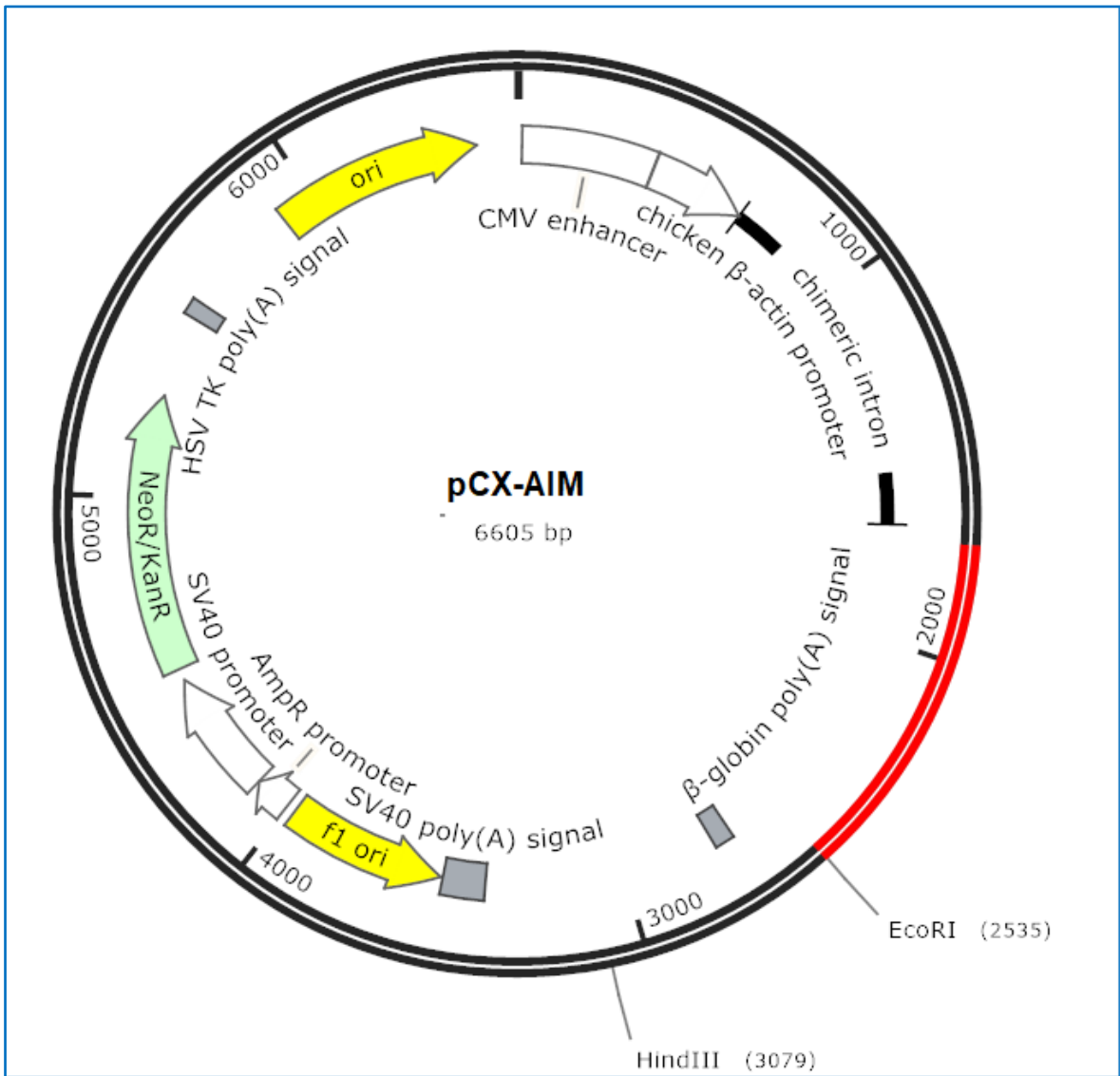


Figure 32 pCX-AIM plasmid map. The main functional elements as well as unique EcoRI restriction site are reported. In red I reported AIM sequence. (Created by SnapGene).

3.2.2.1.4. pCX-EGFP plasmid

The donor vector pCX-HO1-F2A-EGFP was linearized with *EcoRI* restriction enzyme.

Purified linearized vector and fragment with the appropriate overlapping ends were thus assembled by the Gibson Assembly cloning method following the protocol described in section 2.3.2. The *EcoRI* restriction site was reconstituted at 3' of the EGFP sequence. The resulting transformed colonies with the assembled construct were screened for the correct presence of cloned insert (EGFP) (par.2.3.2.8) by performing a PCR on the recombinant plasmids using specific primers.

The figure 33 shows the gel electrophoresis of PCR product samples. All the screened clones produced a PCR product of the expected size 1650 bp, corresponding to the fragment amplified with primers outside of cloning site containing complete EGFP sequence.

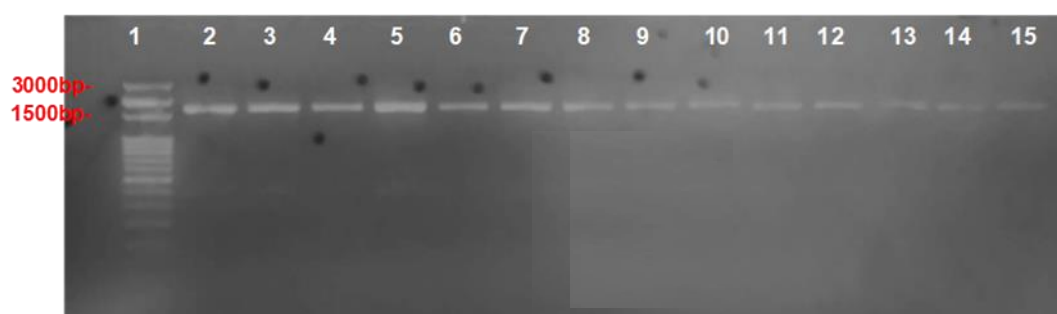


Figure 33 Electrophoretic run of control PCR fragment. Lane 1: 100bp DNA Ladder (Solys BioDyne); Lanes 2-15: samples screened. Fragments were amplified with primers outside the cloning site. Fragment size expected 1650bp.

Some positive samples were selected and checked by sequencing and submitted to Eurofins Genomics as described in par. 2.3.2.9 for Sanger sequencing to validate the accuracy of the EGFP sequence. The electropherogram reported in figure 34 shows one of the analysed clones that matched 100% to the expected target sequence.

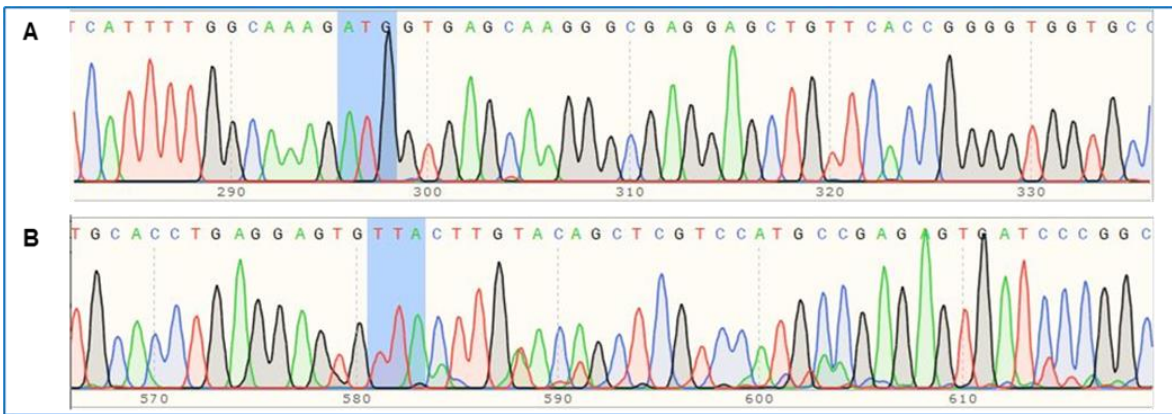


Figure 34 EGFP sequence is correctly detected in cloning assembled plasmid. A: sequencing with the forward primer of the portion including the starting codon (highlighted in blue); B: portion of the sequencing with primer reverse including the stop codon (highlighted in blue).

The resulting pCX-EGFP plasmid (fig.35) is a monocistronic plasmid expressing the EGFP sequence, and it will be used as a positive control of the monocistronic plasmids expression and as a general control for testing transfection efficiency of this series of vectors.

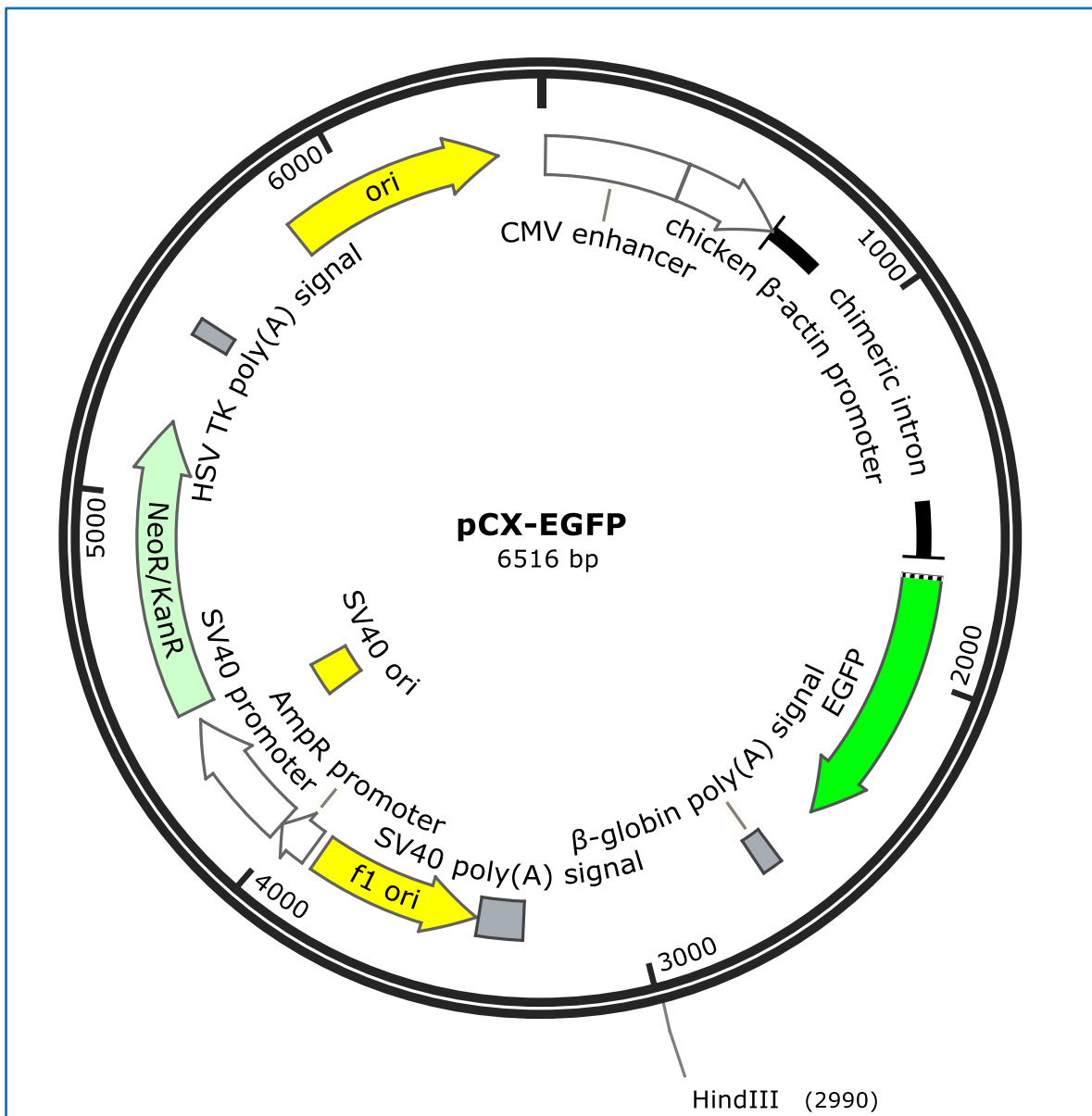


Figure 35 pCX-EGFP plasmid map. The main functional elements are reported.

3.2.2.1.5. pCX-APO-F2A-EGFP plasmid

The complete fragment composed of the APOA1 WT (APO) CDS cloned in frame with the F2A and EGFP encoding sequences was obtained with two simultaneous steps of the Gibson Assembly cloning method.

Initially, the APOA1 fragment without stop codon and F2A-EGFP fragment were amplified by high fidelity PCR with specific primers designed with homologous overlaps for cloning with each other and with the backbone vector (par.2.3.2.1). pCX-HO1-F2A-EGFP donor vector was linearized with *EcoRI* restriction enzyme. Purified linearized vector

and fragments with the appropriate overlapping ends were thus assembled by the Gibson Assembly cloning method following the protocol described in section 2.3. The resulting transformed colonies with the assembled construct were screened (par.2.3.2.8) by restriction enzyme digestion for checking the size of the linearized plasmid (7414bp) as shown in figure 36 and by performing a PCR on the recombinant plasmids for the correct presence of cloned inserts (APOA1 in frame with F2A-EGFP) using insert-specific primers as shown in figure 37.

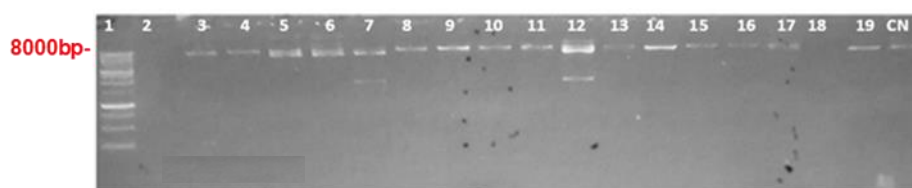


Figure 36 Electrophoretic analysis of linearized recombinant plasmid samples with *EcoRI* enzyme. Lane 1:1kb DNA Ladder (Solys BioDyne); Lanes 2-19: samples screened. The correct assembled plasmid sample has a size of 7414bp. CN: negative control is represented by the plasmid pCX-APO previously built linearized with *EcoRI*.

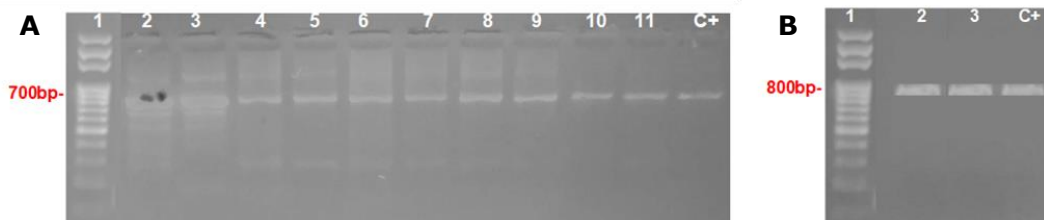


Figure 37 Electrophoretic analysis of control PCR. **A:** EGFP fragment amplification, Lane1: 100bp DNA Ladder (Solys BioDyne); Lane 2-11: samples screened. Fragments were amplified with EGFP specific primers. Fragment size expected 720bp. C+: Positive control represented by the EGFP fragment amplified by the plasmid pCX-EGFP previously built. **B:** APOA1 fragment amplification, Lane1: 100bp DNA Ladder (Solys BioDyne); Lane 2-3: positive samples previously screened for EGFP fragment. Fragments were amplified with APOA1 specific primers. Fragment size expected 801bp. C+: Positive control represented by the APOA1 fragment amplified by the plasmid pCX-APO previously built.

Some positive samples were selected and checked by sequencing and submitted to Eurofins Genomics as described in par.2.3.2.9 for Sanger sequencing to validate the accuracy of the APO-F2A-EGFP sequence.

The electropherogram reported in figure 38 shows one of the analysed clones that matched 100% to the expected target sequence.

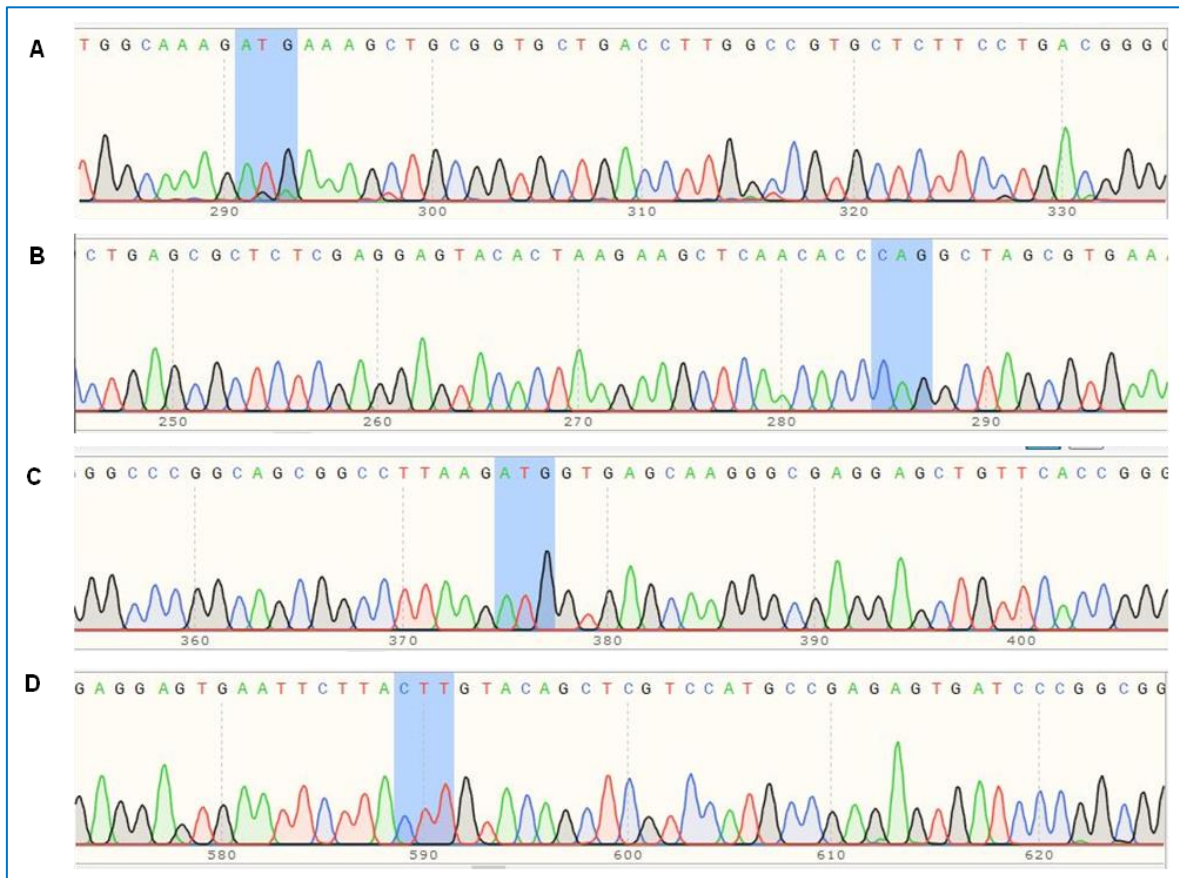


Figure 38 APOA1 sequence, F2A sequence and EGFP sequence is correctly detected in frame in cloning assembled plasmid. **A**: APOA1 sequencing with the forward primer of the portion including the starting codon (highlighted in blue); **B**: APOA1 sequencing with the forward primer of the portion including the final codon (highlighted in blue); **C** EGFP sequencing with the forward primer of the portion including the starting codon (highlighted in blue); **D**: EGFP sequencing with the reverse primer of the portion including the stop codon (highlighted in blue) with reconstitution of the cloning site *EcoRI* at 3' cloning site.

In the figure 39 are shown the effects, at amino acid sequence level, of the removal of the stop codon (coding for amino acid Q) of the APOA-1 sequence in the newly assembled pCX-APO-F2A-EGFP plasmid. In fact, in this case, APOA-I amino acid sequence ends at the penultimate codon and is immediately followed by the amino acid F2A sequence in frame (in red). This, as described above, for the peculiar function of the F2A sequence (par.2.3.1) will allow the transcription of a single

transcript and the co-translation of two distinct proteins (APO and EGFP) in transfected cells.

pCX-APO	1	MKAAVLT LAVLFLTGSQARHFQQDEPPQSPWDRVKDLATVYVDVLKDSGRDYVSQFEGSALGKQLNLKLLDNWDSVTST	80
pCX-APO-F2A-EGFP	1	MKAAVLT LAVLFLTGSQARHFQQDEPPQSPWDRVKDLATVYVDVLKDSGRDYVSQFEGSALGKQLNLKLLDNWDSVTST	80
	81	FSKLREQLGPVTQEFWDNLEKETEGLRQEMSKDLEEVKAKVQPYLDDFQKKWQEEEMELYRQKVEPLRAELQEGARQKLHE	160
	81	FSKLREQLGPVTQEFWDNLEKETEGLRQEMSKDLEEVKAKVQPYLDDFQKKWQEEEMELYRQKVEPLRAELQEGARQKLHE	160
	161	LQEKLSPLGEEMRDRARAHVDALRTHLAPYSDEL	240
	161	LQEKLSPLGEEMRDRARAHVDALRTHLAPYSDEL	240
	241	GLLPVLESFKVSFLSALEEYTKKLN	267
	241	GLLPVLESFKVSFLSALEEYTKKLN	291

Figure 39 Comparison of the amino acid sequence of ApoA-1 in pCX_APO with that of the pCX-APO-F2A-EGFP vector. As shown highlighted in grey, in the plasmid pCX-APO-F2A-EGFP the APOA-1 sequence ends at the penultimate codon (coding for amino acid Q) and is followed by the F2A sequence in frame highlighted in pink. The asterisk in red indicates the stop codon. In the red box is highlighted the WT variant codifying for amino acid Arginine (R). (Alignment by Protein Blast, NIH).

3.2.2.1.6. pCX-EGFP-F2A-APO plasmid

Since a portion of F2A sequence after the co-translational cleavage of the polypeptide remains as extension to the C-Terminal of its upstream product, a set of plasmids were constructed in which the position of the EGFP CDS and the APO CDS is inverted with respect to those described above. In this way it will be possible to assess whether the F2A sequence after the cleavage of the polypeptide can affect the expression and functionality of the APOA-I protein.

3.2.2.1.6.1 pCX-EGFP-F2A plasmid: first step

The EGFP sequence without the stop codon was obtained by specific PCR amplification from previously built pCX-EGFP plasmid using a pair of primers designed with homologous overlaps for cloning in the backbone plasmid (par.2.3.2.1).

The donor vector pCX-F2A was linearized with *NheI* restriction enzyme. Purified linearized vector and fragment with the appropriate overlapping ends were thus assembled by the Gibson Assembly cloning method following the protocol described in section 2.3.2. The resulting transformed colonies with the assembled construct were selected and checked by sequencing and submitted to Eurofins Genomics as described in par.2.3.2.9 for Sanger sequencing to validate the accuracy of the EGFP sequence. The electropherogram reported in figure 41 shows one of the analysed clones that matched 100% to the expected target.

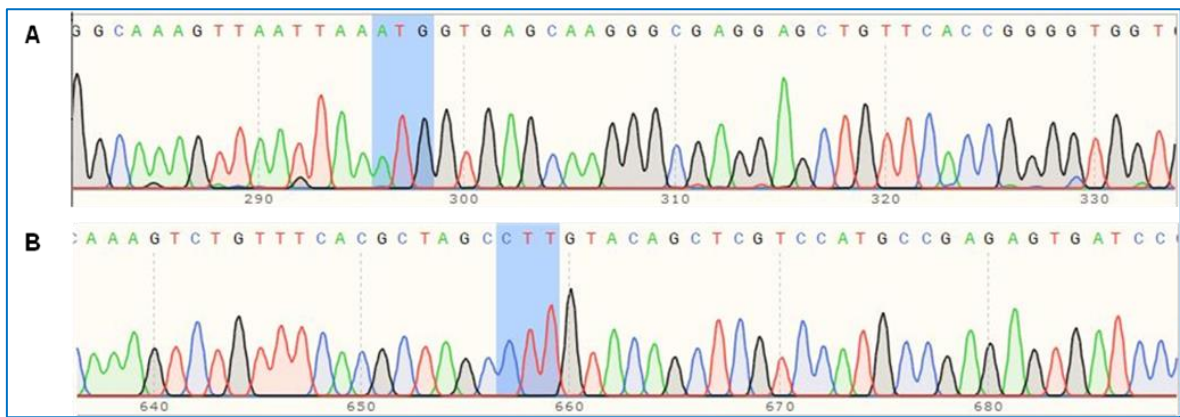


Figure 41 EGFP sequence is correctly detected in frame with F2A sequence in cloning assembled plasmid. A: sequencing with the forward primer of the portion including the starting codon (highlighted in blue); B: portion of the sequencing with primer reverse including the final codon (highlighted in blue).

3.2.2.1.6.2 pCX-EGFP-F2A-APO plasmid: final step

The APO sequence with stop codon was obtained by specific PCR amplification from previously built pCX-APO plasmid using a pair of primers designed with homologous overlaps for cloning in the backbone plasmid (par.2.3.2.1). The donor vector pCX-EGFP-F2A was linearized with *EcoRI* restriction enzyme. Purified linearized vector and fragment with the appropriate overlapping ends were thus assembled by the Gibson Assembly cloning method following the protocol described in section 2.3.2. *EcoRI* restriction site was reconstituted at 3' of F2A sequence as unique restriction site. *AflIII* restriction site was generated at 3' of APO sequence as unique restriction site. The resulting transformed colonies with the assembled construct were screened for the correct presence of cloned insert (APO) (par.2.3.2.8) by performing restriction enzyme digestion and PCR using insert-specific primers on the recombinant plasmids.

The figure 42 shows the gels electrophoresis analyses of enzymatic digestion (Fig. 42A) and PCR (Fig. 42B) analyses.

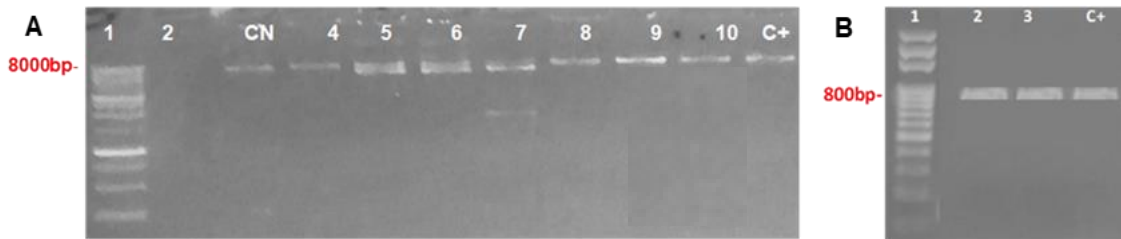


Figure 42 Electrophoretic run of control fragments. **A**: linearized recombinant plasmid samples with *Afl*II restriction enzyme. Lane 1: 1kb DNA Ladder (Solys BioDyne); Lanes 2-10: samples screened. The correct assembled plasmid sample has a size of 7414bp. CN: negative control represented by pCX-EGFP-F2A plasmid *Nhe*I linearized; C+: Positive control represented by the digestion with the same enzyme of pCX-APO-F2A-EGFP previously built. **B**: APOA1 fragment amplification, Lane 1: 100bp DNA Ladder (Solys BioDyne); Lane 2-3: positive samples previously screened for correct linearization. Fragments were amplified with APOA1 specific primers. Fragment size expected 804bp. C+: Positive control represented by the APOA1 fragment amplified by the plasmid pCX-APO previously built.

Positive samples were selected and checked by sequencing and submitted to Eurofins Genomics as described in par.2.3.2.9 for Sanger sequencing to validate the accuracy of the EGFP sequence. The electropherogram reported in figure 43 shows one of the analysed clones that matched 100% to the expected target sequence.

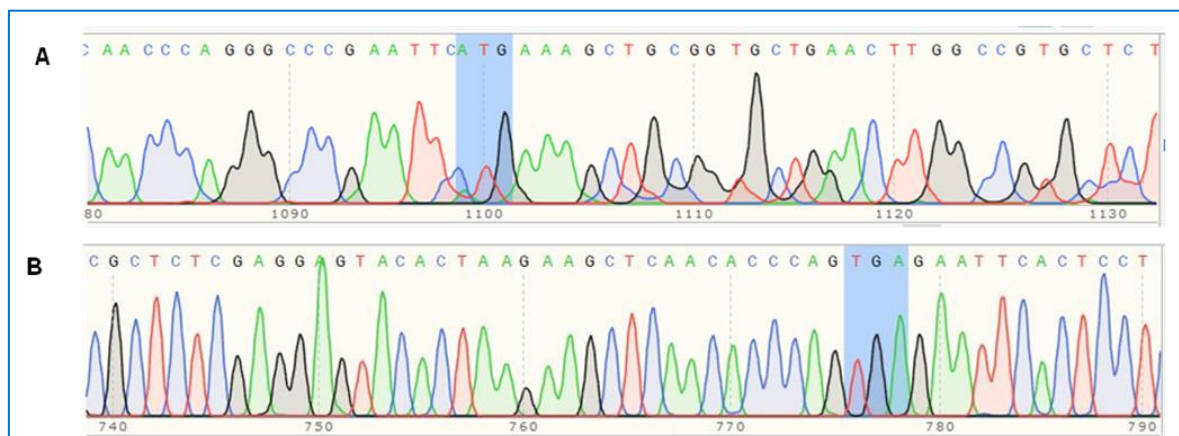


Figure 43 APO sequence is correctly detected in cloning assembled plasmid in frame with F2AEGFP sequence. A: sequencing with the forward primer of the portion including the starting codon (highlighted in blue); B: portion of the sequencing with primer forward including the stop codon (highlighted in blue).

As already highlighted figure 43, in the figure below (fig. 44) is shown at amino acid sequence level the removal of the stop codon (coding for amino acid K) of the EGFP sequence in the pCX-EGFP-F2A-APO vector

built. In fact, in this case, EGFP amino acid sequence ends at the penultimate codon and is immediately followed by the amino acid F2A sequence in frame (in red). This, as described above, for the peculiar function of the F2A sequence (par.2.3.1) will allow the transcription of a single transcript and the co-translation of two distinct proteins (EGFP and APO) after cells transfection.

pCX-EGFP	1	MVSKGEELFTGVVPIILVELDGDVNGHKFSVSGEGEGDATYGKLTCLKFICTTGKLPVPWPTLVTTLTLYGVQCFSRYPDHMK	80
pCX-EGFP-F2A-APO	1	MVSKGEELFTGVVPIILVELDGDVNGHKFSVSGEGEGDATYGKLTCLKFICTTGKLPVPWPTLVTTLTLYGVQCFSRYPDHMK	80
	81	QHDFFKSAMPEGYVQERTIFFKDDGNYKTRAEVKFEGDTLVNRIELKGIDFKEDGNILGHKLEYNYNHNVYIMADKQKN	160
	81	QHDFFKSAMPEGYVQERTIFFKDDGNYKTRAEVKFEGDTLVNRIELKGIDFKEDGNILGHKLEYNYNHNVYIMADKQKN	160
	161	GIKVNFKIRHNIEDGSVQLADHYQQNTPIGDGPVLLPDNHYLSTQSALS KDPNEKRDMVLLFVTAAGITLGMDELYK*	239
	161	GIKVNFKIRHNIEDGSVQLADHYQQNTPIGDGPVLLPDNHYLSTQSALS KDPNEKRDMVLLFVTAAGITLGMDELYKA	240

	241	SVKQTLNFDLLKLAGDVESNPGP	263

Figure 44 Comparison of the amino acid sequence of EGFP with that of the pCX-EGFP-F2A-APO vector. As shown highlighted in dark green, in the plasmid pCX-EGFP-F2A-APO, the EGFP sequence ends at the penultimate codon (coding for amino acid K) and is followed by the F2A sequence in frame highlighted in pink. The asterisk in red indicates the stop codon. (Alignment by Protein Blast, NIH).

The resulting pCX-EGFP-F2A-APO is a dicistronic plasmid (fig.45) expressing the EGFP and the APOA-1 (WT) sequences in a F2A-based multicistronic system. The plasmid will serve as a control to evaluate if the F2A position (downstream or upstream to the APOA-1 sequence) could impact on APOA-I biological function.

Furthermore, it will be used as a control of the specific effects induced by the "Milano" variant as compared to the APOA-1 (WT) sequence and of the effect of two APO sequences on the RCT compared to only one or more sequences of the Milano variant as in the case of multicistronic vectors.

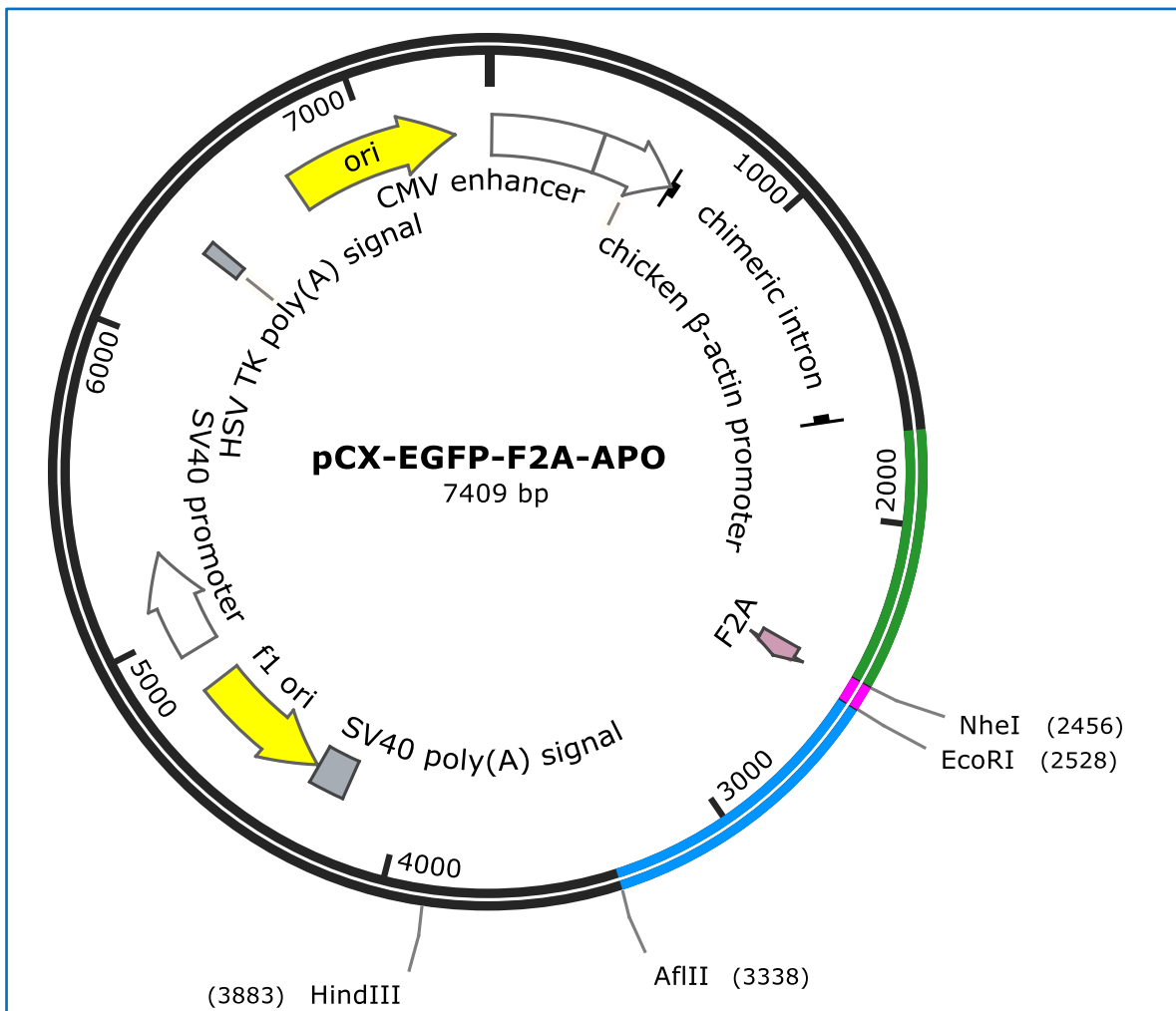


Figure 45 pCX-EGFP-F2A-APO plasmid map. The main functional elements as well as *NheI*, *EcoRI* and *AflIII* restriction sites are reported. In green is reported EGFP sequence in frame with F2A sequence (pink) and APO sequence (blue). (Created by SnapGene).

3.2.2.1.7. pCX-EGFP-F2A₁-APO₁-F2A₂-APO₂

The F2A-APO fragment, without the stop codon, was obtained by specific PCR amplification from previously assembled pCX-EGFP-F2A-APO (reported in 3.2.2.1.6.2 paragraph) plasmid introducing the unique *NheI* restriction site at 5' of the F2A-APO fragment and the unique *XbaI* restriction site at 3' of the F2A-APO fragment. Since *NheI* and *XbaI* enzymes generate compatible ends, the *NheI*-*XbaI* digested F2A-APO fragment and the *NheI*-linearized backbone were assembled by classical cloning technique (not via Gibson assembly) with the Ligase enzyme reaction following the protocol described in par.2.3.2.6. *NheI* restriction site was reconstituted at 5' of F2A sequence. The resulting transformed

colonies with the assembled construct were screened for the presence of cloned insert (F2A₁-APO₁) (par.2.3.2.8) by performing enzyme restriction digestion with *HindIII* enzyme on the recombinant plasmids. The figure 46 shows the gel electrophoresis analysis of enzyme digestion product samples. The negative control is the backbone plasmid pCX-EGFP-F2A-APO linearized with the same enzyme (7408bp). The expected size of cloning product is 8286bp.

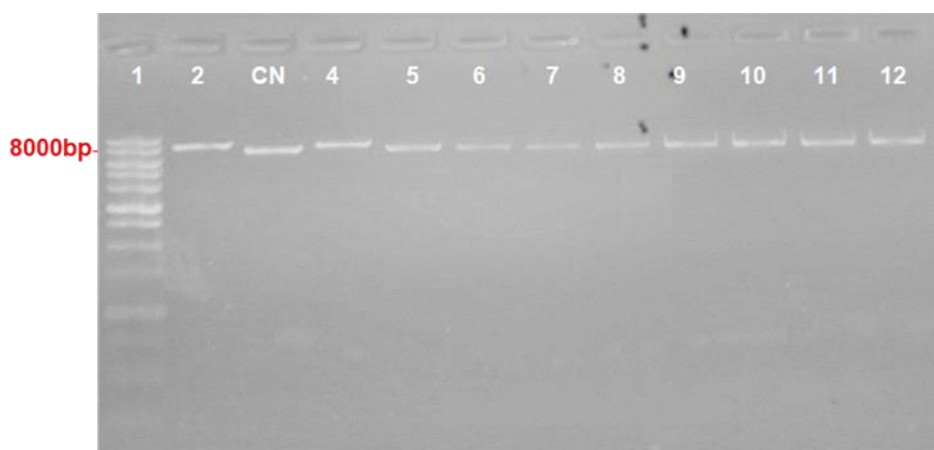


Figure 46 Electrophoretic run of linearized recombinant plasmid samples with *HindIII* restriction enzyme. Lane 1:1kb DNA Ladder (Solys BioDyne); Lanes 2-12: samples screened. The correct assembled plasmid sample has a size of 8287bp. CN: negative control represented by pCX-EGFP-F2A-APO plasmid previously built digested with the same enzyme.

Positive samples were selected and checked by sequencing and submitted to Eurofins Genomics as described in par.2.3.2.9 for Sanger sequencing to validate the accuracy of the F2A₁-APO₁ fragment. The electropherogram reported in figure 47 shows one of the analysed clones that matched 100% to the expected target sequence.

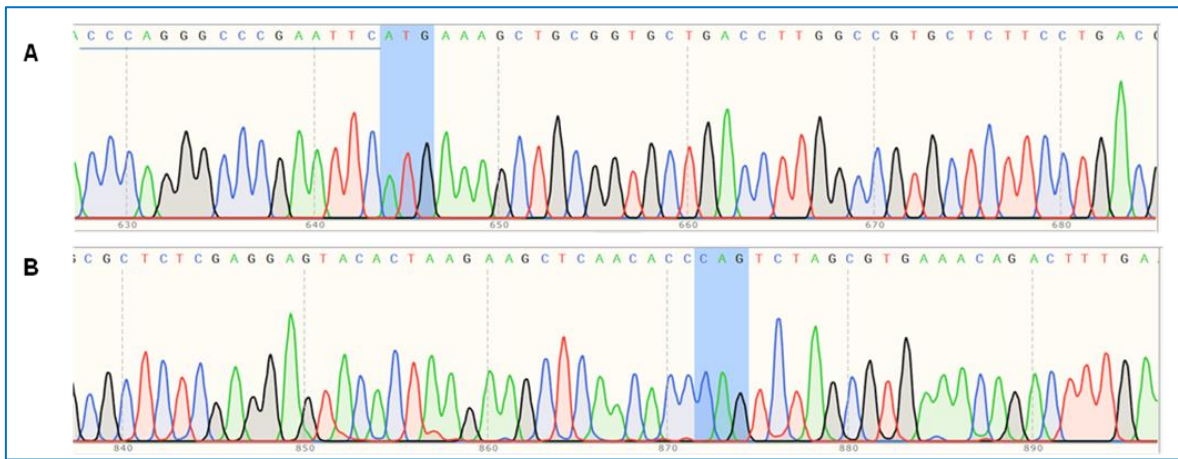


Figure 47 APO sequence is correctly detected in cloning assembled plasmid in frame with EGFP sequence and F2A₂-APO₂ sequence. **A**: sequencing with the forward primer of the portion including APO1 starting codon (highlighted in blue) and a portion of F2A₁ sequence underlined in blue; **B**: portion of the sequencing with primer forward including APOA1 final codon.

The resulting pCX-EGFP-F2A₁-APO₁-F2A₂-APO₂ is a tricistronic plasmid (fig.48) co-expressing EGFP together with two copies of APOA-I (WT) sequences. It will be used as a control as specify above for its corresponding dicistronic plasmid pCX-EGFP-F2A-APO and also as further control of the specific effects induced by the "Milano" variant in tricistronic plasmid expressing two sequences of AIM on the AIM expression and on the reverse cholesterol transport assay.

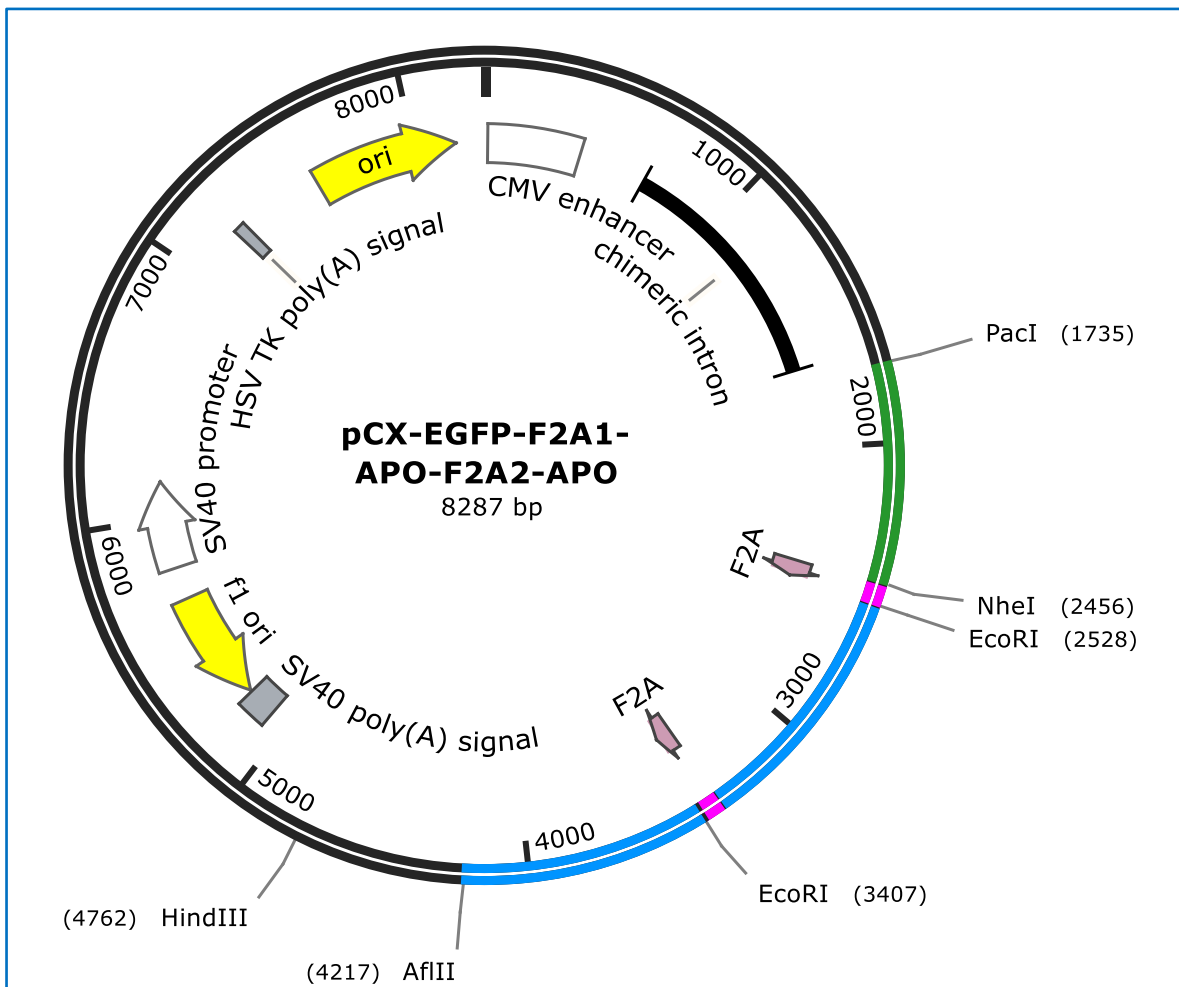


Figure 48 *pCX-EGFP-F2A₁-APO₁-F2A₂-APO₂* plasmid map. The main functional elements as well as *NheI*, *EcoRI* and *AflII* restriction sites are reported. In green is reported EGFP sequence in frame with two sequences of F2A (pink) and APO (blue). (Created by SnapGene).

3.2.2.2 AIM-expressing multicistronic plasmids

3.2.2.2.6 *pCX-AIM-F2A-EGFP* plasmid

The complete fragment composed of the AIM CDS in frame with sequence F2A and EGFP CDS was obtained with two simultaneous steps of the Gibson Assembly cloning method.

Initially, the AIM fragment without stop codon and the F2A-EGFP fragments were amplified by high fidelity PCR with specific primers designed with homologous overlaps for cloning with each other and with the backbone vector (par.2.3.2.1). The *pCX-HO1-F2A-EGFP* donor vector was linearized with *EcoRI* restriction enzyme.

Purified linearized vector and fragments with the appropriate overlapping ends were thus assembled by the Gibson Assembly cloning method following the protocol described in section 2.3.2. *EcoRI* restriction site was reconstituted at 3' of EGFP sequence. The resulting transformed colonies with the assembled construct were screened (par.2.3.2.8) by restriction enzyme digestion for checking the linearized plasmid size and by performing a PCR on the recombinant plasmids for testing the correct presence of cloned inserts (AIM in frame with F2A-EGFP) using insert-specific primers (fig.49).

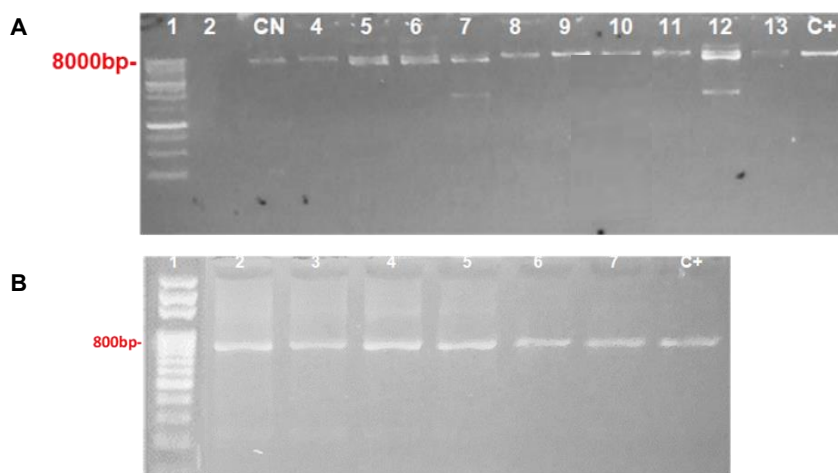


*Figure 49 Electrophoretic run of control fragments. A: linearized recombinant plasmid samples with *NheI* restriction enzyme. Lane 1:1kb DNA Ladder (Solys BioDyne); Lanes 2-13: samples screened. The correct assembled plasmid sample has a size of 7414bp. CN: negative control represented by pCX-HO1-F2A-EGFP backbone plasmid digested with the same enzyme; C+: Positive control represented by pCX-APO-F2A-EGFP previously built digested with the same enzyme. B: AIM fragment amplification, Lane1: 100bp DNA Ladder (Solys BioDyne); Lane 2-7: positive samples previously screened for correct linearization. Fragments were amplified with APOA1 specific primers. Fragment has a expected size of 801bp; C+: Positive control represented by the AIM fragment amplified by the plasmid pCX-AIM previously built.*

Positive samples were selected and checked by sequencing and submitted to Eurofins Genomics as described in par.2.3.2.9 for Sanger sequencing to validate the accuracy of the AIM fragment in frame with F2A and EGFP sequence. The electropherogram reported in figure 50 shows one of the analysed clones that matched 100% to the expected target sequence.

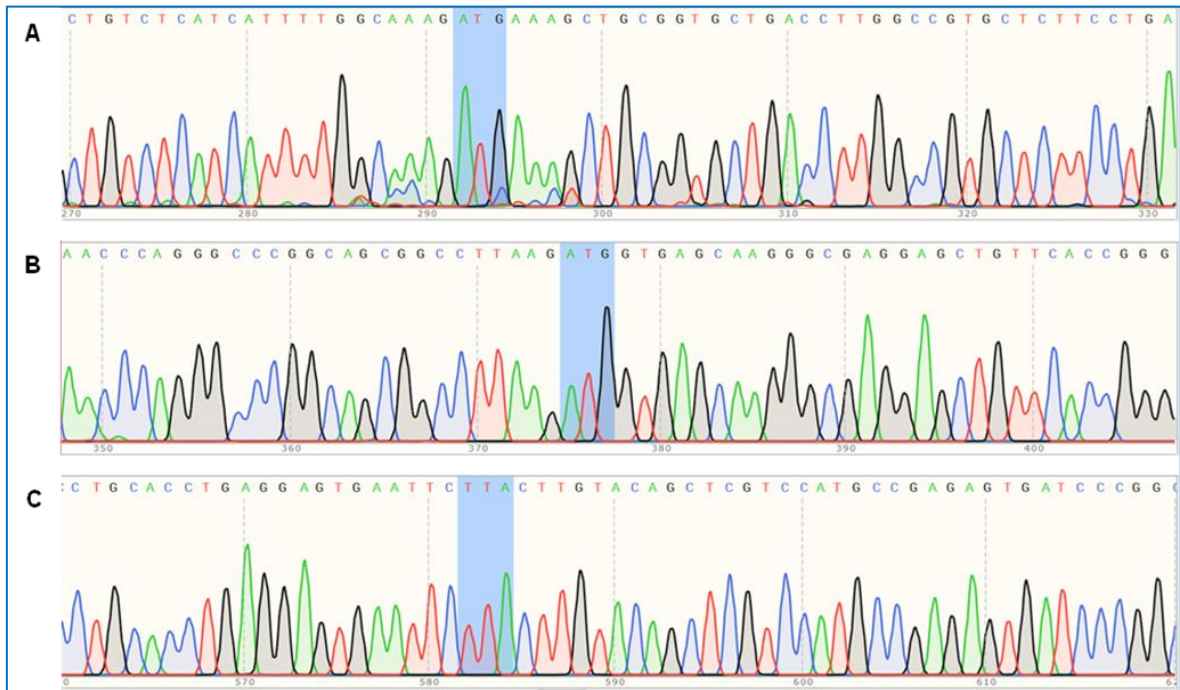


Figure 50 AIM sequence, F2A sequence and EGFP sequence is correctly detected in frame in cloning assembled plasmid. **A:** AIM sequencing with the forward primer of the portion including the starting codon (highlighted in blue); **B:** EGFP sequencing with the forward primer of the portion including the starting codon (highlighted in blue); **C:** EGFP sequencing with the reverse primer of the portion including the stop codon (highlighted in blue) with reconstitution of the cloning site EcoRI at 3' cloning site.

As already highlighted in figure 50, in the figure below (fig.51) is shown at amino acid sequence level the removal of the stop codon (coding for Q amino acid) of the AIM sequence in the pCX-AIM-F2A-EGFP vector built. In fact, in this case, AIM amino acid sequence ends at the penultimate codon and is immediately followed by the amino acid F2A sequence in frame (in red). This, as described above, for the peculiar function of the F2A sequence (par.2.3.1) will allow the transcription of a single transcript and the co-translation of two distinct proteins (AIM and EGFP) after cells transfection.

pCX-AIM 1	MKAAVLT LAVL FLTGSQARHFVQQDEPPQSPWDRVKDLATVYVDVLKDSGRDYVSQFEGSALGKQLNLKLLDNWDSVTST	80
pCX-AIM-F2A-EGFP 1	MKAAVLT LAVL FLTGSQARHFVQQDEPPQSPWDRVKDLATVYVDVLKDSGRDYVSQFEGSALGKQLNLKLLDNWDSVTST	80
81	FSKLREQLGPVTQEFWDNLEKETEGLRQEMSKDLEEVKAKVQPYLDDFQKKWQEEMELYRQKVEPLRAELQEGARQKLHE	160
81	FSKLREQLGPVTQEFWDNLEKETEGLRQEMSKDLEEVKAKVQPYLDDFQKKWQEEMELYRQKVEPLRAELQEGARQKLHE	160
161	LQEKLSPLGEEMRDRARAHVDALRTHLAPYSDELQRLAARLEALKENGGARLAEYHAKATEHLSTLSEKAKPAEDLRQ	240
161	LQEKLSPLGEEMRDRARAHVDALRTHLAPYSDELQRLAARLEALKENGGARLAEYHAKATEHLSTLSEKAKPAEDLRQ	240
241	GLLPVLESFKVSFLSALEEYTKLNTQ*-----	267
241	GLLPVLESFKVSFLSALEEYTKLNTQASVKQTLNFNLLKLAGDVESNPGP	291

Figure 51 Comparison of the amino acid sequence of AIM in pCX-AIM with that of the pCX-AIM-F2A-EGFP vector. As shown highlighted in yellow, in the plasmid pCX-AIM-F2A-EGFP the AIM sequence ends at the penultimate codon (coding for amino acid glutamine, Q) and is followed by the F2A (in pink). The asterisk in red indicates the stop codon. In the red box is highlighted the Milano mutation R173C. (Alignment by Protein Blast, NIH).

The resulting pCX-AIM-F2A-EGFP is dicistronic plasmid (fig.52) expressing the AIM together with EGFP sequences. It will serve as a control to evaluate the potential interference of the residual downstream F2A peptide on AIM expression and function, and it will be also used to evaluate the specific effects induced by the “Milano” variant as compared to the wild-type APOA-I on the reverse cholesterol transport assay.

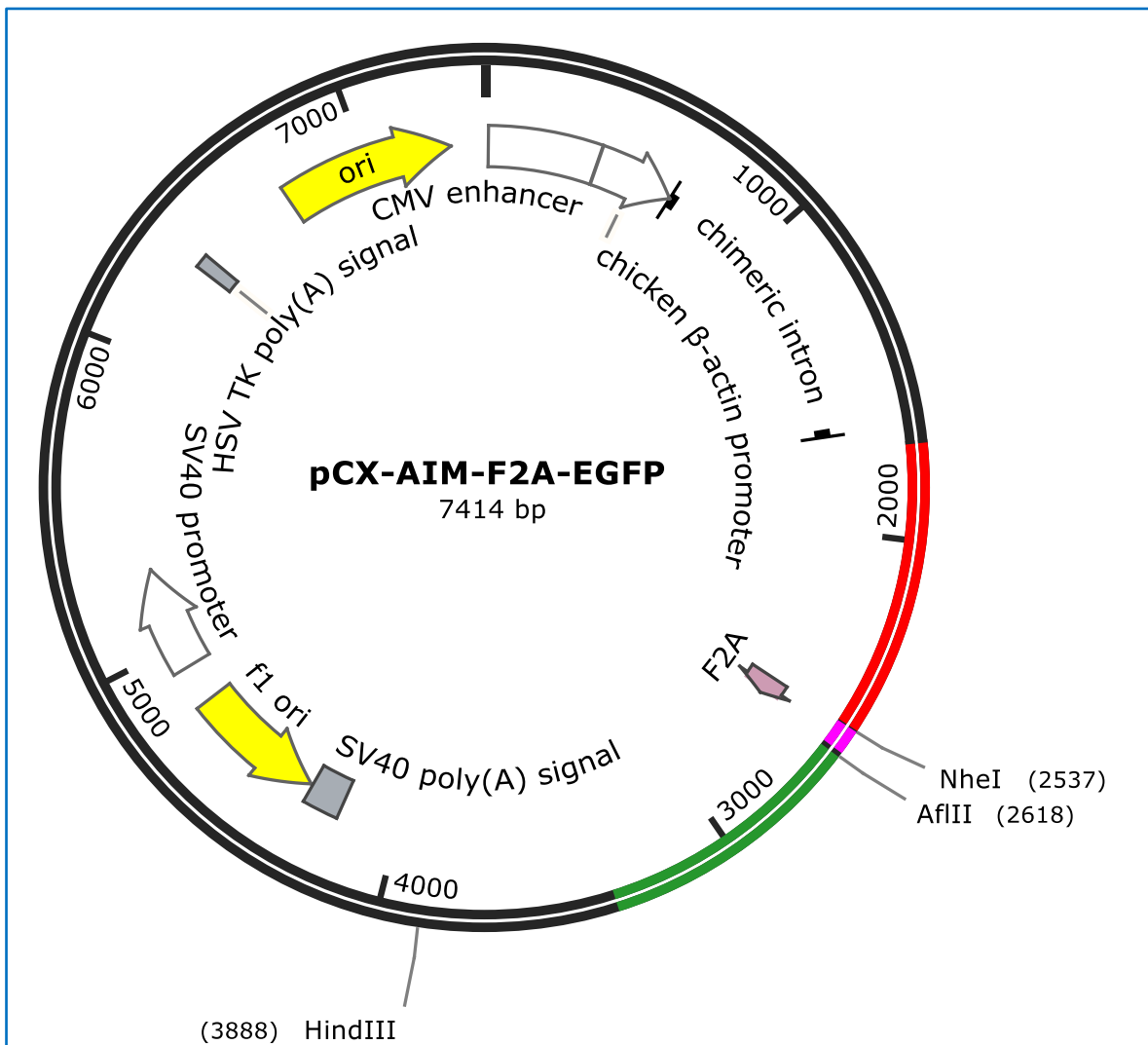


Figure 52 pCX-AIM-F2A-EGFP plasmid map. The main functional elements as well as *NheI* and *AflIII* restriction site are reported. In blue is red AIM sequence in frame with F2A sequence (pink) and EGFP sequence (green). (Created by SnapGene).

3.2.2.2.7 pCX-EGFP-F2A-AIM plasmid

The AIM CDS with stop codon was obtained by specific PCR amplification from previously assembled pCX-AIM plasmid (described in par.3.2.2.1.3) using a pair of primers designed with homologous overlaps for cloning in the backbone plasmid (par.2.3.2.1). The previously assembled donor vector pCX-EGFP-F2A was linearized with *EcoRI* restriction enzyme. Purified linearized vector and fragment with the appropriate overlapping ends were thus assembled by the Gibson Assembly cloning method following the protocol described in section 2.3.2. *EcoRI* restriction site was reconstituted at 3' of F2A sequence as unique restriction site.

The *AflIII* restriction site was generated at 3' of APO sequence as unique restriction site. The resulting transformed colonies with the assembled construct were screened for the presence of cloned insert (AIM) (par.2.3.2.8) by performing enzyme restriction digestion with *NheI* on the recombinant plasmids.

The figure 53 shows the agarose gel electrophoresis analysis of digested product samples.

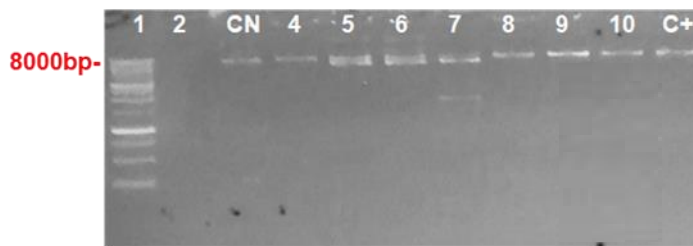


Figure 53 Electrophoretic run of linearized recombinant plasmid samples with *NheI* enzyme. Lane 1: 1kb DNA Ladder (Solys BioDyne); Lanes 2-10: samples screened. The correct assembled plasmid sample has a size of 741bp. CN: negative control is represented by the plasmid *pCX-EGFP-F2A* previously built linearized with *EcoRI*.

Positive samples were selected and checked by sequencing and submitted to Eurofins Genomics as described in par.2.3.2.9 for Sanger sequencing to validate the accuracy of the EGFP sequence. The electropherogram reported in figure 54 shows one of the analysed clones that matched 100% to the expected target sequence.

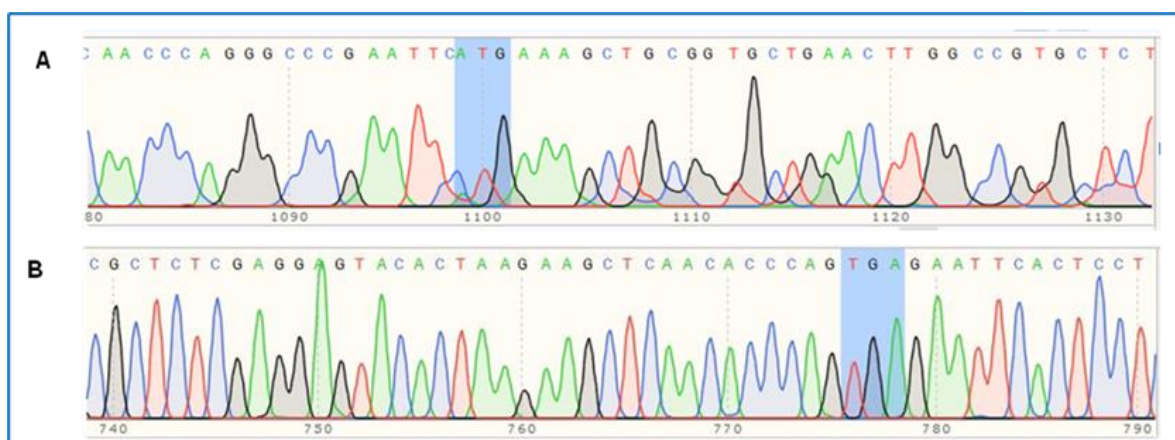


Figure 54 AIM sequence is correctly detected in cloning assembled plasmid in frame with F2AEGFP sequence. **A**: sequencing with the forward primer of the portion including the starting codon (highlighted in blue); **B**: portion of the sequencing with primer forward including the stop codon (highlighted in blue).

As already highlighted in figures 54, in the figure below (fig.55) is shown at amino acid sequence level the removal of the stop codon (coding for amino acid K) of the EGFP sequence in the pCX-EGFP-F2A-AIM vector built. In fact, in this case, EGFP amino acid sequence ends at the penultimate codon and is immediately followed by the amino acid F2A sequence in frame (in red). This, as described above, for the peculiar function of the F2A sequence (par.2.3.1) will allow the transcription of a single transcript and the co-translation of two distinct proteins (EGFP and AIM) after cells transfection.



Figure 55 Comparison of the amino acid sequence of EGFP with that of the pCX-EGFP-F2A-AIM vector. As shown highlighted in dark green, in the plasmid pCX-EGFP-F2A-AIM, the EGFP sequence ends at the penultimate codon (coding for amino acid K) and is followed by the F2A sequence in frame highlighted in pink. The asterisk indicates the stop codon. (Alignment by Protein Blast, NIH).

The resulting pCX-EGFP-F2A-AIM is a dicistronic plasmid (fig.56) expressing the EGFP and the AIM sequences. It will be used to evaluate if the F2A position (downstream or upstream to the AIM sequence) could impact on AIM biological function.

It will also be used as a control to evaluate the expression and specific effects induced by the "Milano" variant sequence expressed on the reverse cholesterol transport assay compared to the wild-type variant and to multi-copies expressing AIM plasmids.

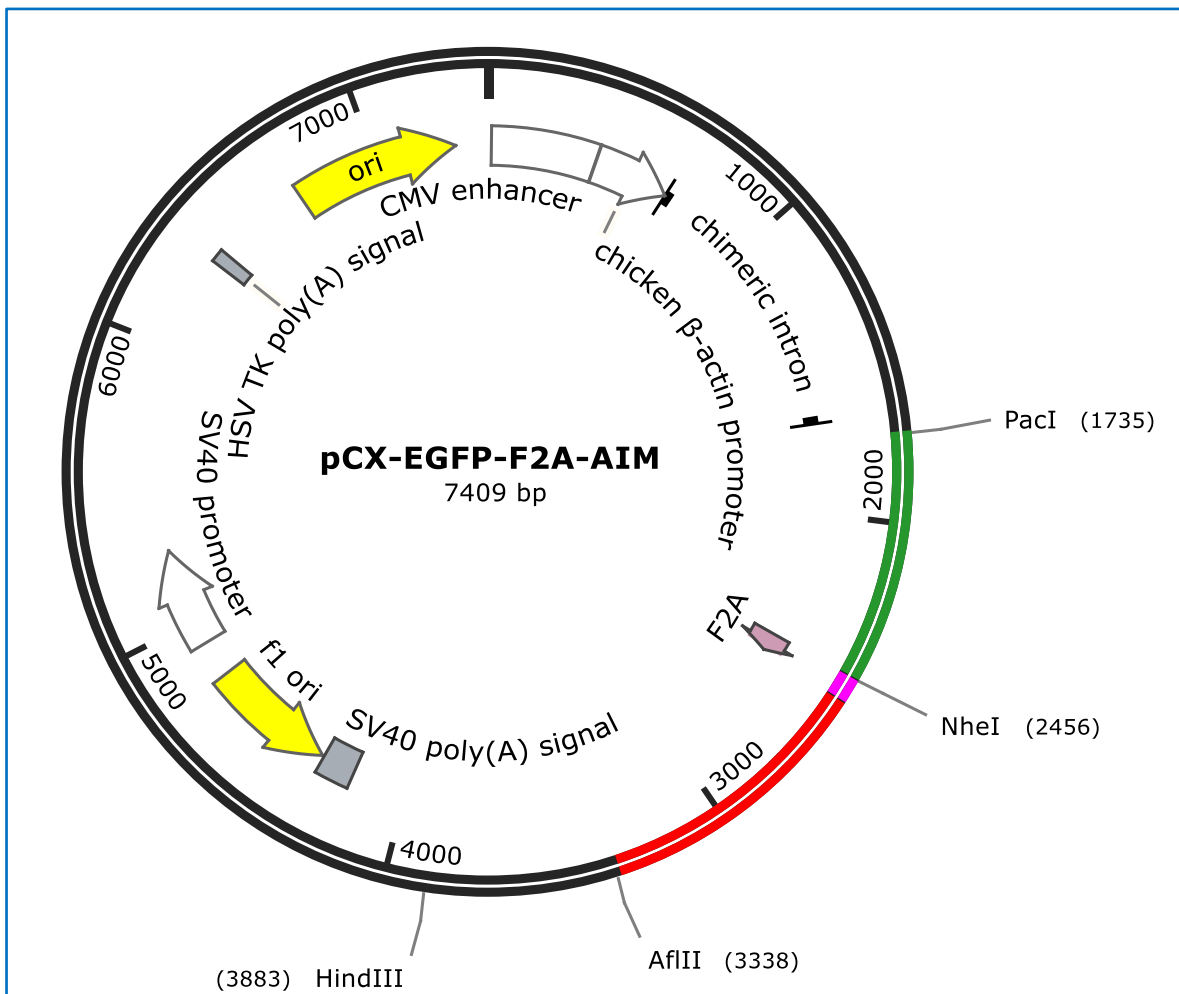


Figure 56 pCX-EGFP-F2A-AIM plasmid map. The main functional elements as well as PacI, NheI and AflII restriction sites are reported. In green is reported EGFP sequence in frame with F2A sequence (pink) and AIM sequence (red). (Created by SnapGene).

3.2.2.2.8 pCX-EGFP-F2A₁-AIM₁-F2A₂-AIM₂ plasmid

The F2A-AIM fragment, without the stop codon, was obtained by specific PCR amplification of previously assembled pCX-EGFP-F2A-AIM plasmid (reported in par.3.4.3.2.2) introducing the unique *NheI* restriction site at 5' of the F2A-AIM fragment and the unique *XbaI* restriction site at 3' of the same fragment. Since *NheI* and *XbaI* enzymes generate compatible ends, the *NheI-XbaI* digested F2A-AIM fragment and the *NheI*-linearized backbone were purified and purified and assembled through classical cloning (not via Gibson assembly) with the Ligase enzyme reaction following the protocol described in par. 2.3.2.6. *NheI* restriction site was reconstituted at 5' of F2A sequence. The resulting transformed colonies with the assembled construct were

screened for presence of cloned insert (F2A₁-AIM₁) (par.2.3.2.8) by performing enzyme restriction digestion with *HindIII* enzyme on the recombinant plasmids.

The figure 57 shows the agarose gel electrophoresis analysis of digestion product samples. The negative control is the backbone plasmid pCX-EGFP-F2A-AIM linearized with the same enzyme (7414bp) and the positive control is represented from pCX-EGFP-F2A₁-APO₁-F2A₂-APO₂ linearized with the same enzyme (8287bp).

The expected size of cloning product is 8287bp.

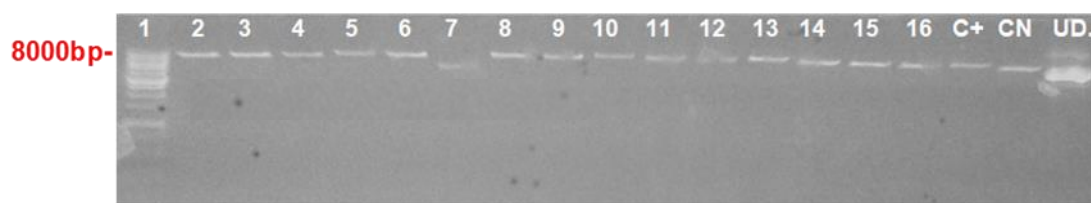


Figure 57 Electrophoretic run of linearized recombinant plasmid samples with *HindIII* restriction enzyme. Lane 1:1kb DNA Ladder (Solys BioDyne); Lanes 2-16: samples screened. The correct assembled plasmid sample has a size of 8287bp. C+: Positive control represented by pCX-EGFP-F2A₁-AIM₁-F2A₂-AIM₂ plasmid (8287bp) digested with the same enzyme. CN: negative control represented by pCX-EGFP-F2A-AIM plasmid previously built digested with the same enzyme. UD: undigested pCX-EGFP-F2A₁-APO₁-F2A₂-APO₂ plasmid.

Positive samples were selected and checked by sequencing and submitted to Eurofins Genomics as described in par.2.3.2.9 for Sanger sequencing to validate the accuracy of the F2A₁-AIM₁ fragment in frame with EGFP and F2A₂-AIM₂ sequences. The electropherogram reported in figure 58 shows one of the analysed clones that matched 100% to the expected target sequence.

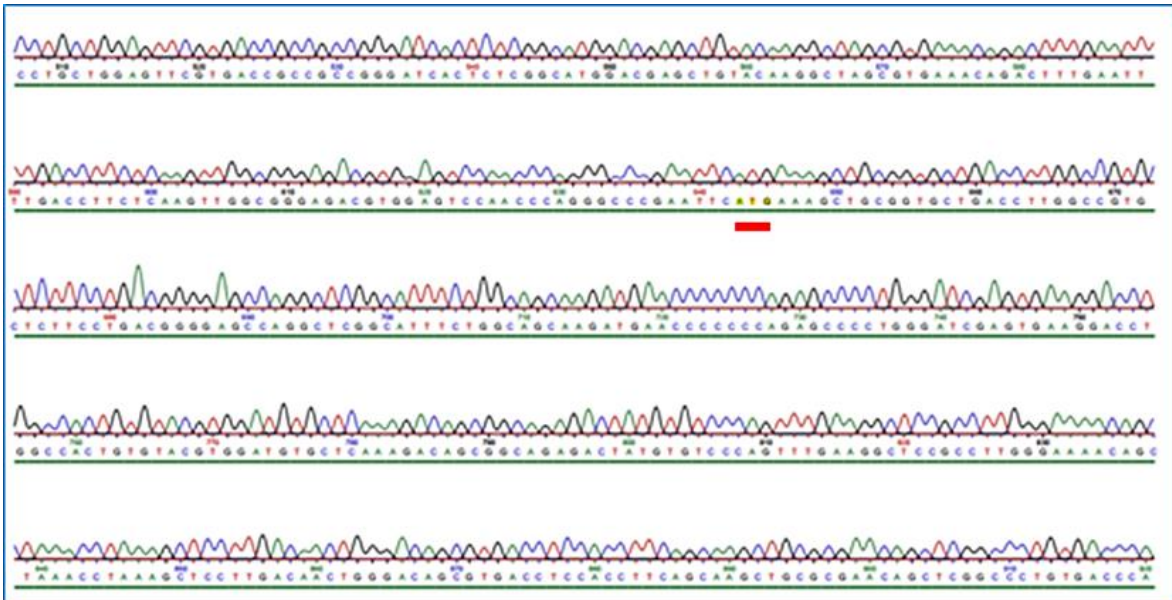


Figure 58 F2A₁AIM₁ sequence is correctly detected in cloning assembled plasmid in frame with EGFP sequence and F2A₂AIM₂ sequence. Electropherogram represents the sequencing with the forward primer of the portion including AIM₁ starting codon (underlined in red) and a portion of upstream F2A₁ sequence.

The resulting pCX-EGFP-F2A1-AIM1-F2A2-AIM2 is a tricistronic plasmid (fig.59) co-expressing the EGFP sequence together with two copies of AIM sequences. It will be used to evaluate if the addition of an AIM CDS to the multi-cistronic F2A will increase the biological effects induced by AIM sequence when transfected in eukaryotic cells. Furthermore, it will serve as control to test the specific effects induced by two Milano” variant sequences on the general AIM expression and on the Reverse cholesterol transport assay.

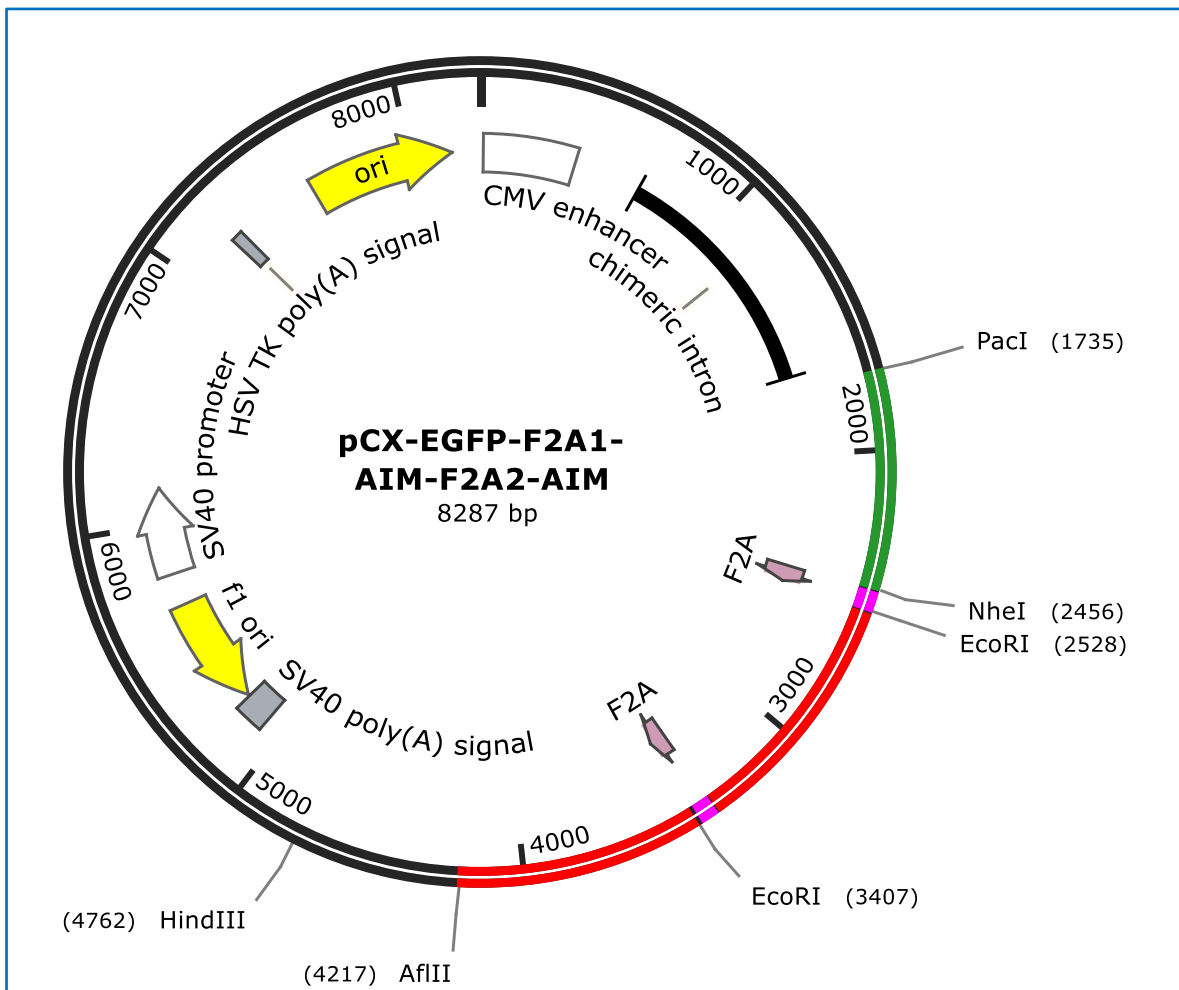


Figure 59 *pCX-EGFP-F2A₁-AIM₁-F2A₂-AIM₂* plasmid map. The main functional elements as well as *NheI*, *EcoRI* and *AflII* restriction sites are reported. In green is reported EGFP sequence in frame with two sequences of F2A (pink) and AIM (red). (Created by SnapGene).

3.2.2.2.9 *pCX-EGFP-F2A₁-AIM₁-F2A₂-AIM₂-F2A₃-AIM₃* plasmid

The F2A-AIM fragment, without stop codon, was obtained by specific PCR amplification from previously assembled *pCX-EGFP-F2A₁-AIM₁-F2A₂-AIM₂* plasmid (described in par.3.4.3.2.3) introducing the unique *NheI* restriction site at 5' of the F2A-AIM fragment and the unique *XbaI* restriction site at 3' of the fragment. The same strategy of cloning reported in 3.4.3.2.3 paragraph was then applied. *NheI* restriction site was reconstituted at 5' of F2A sequence. The resulting transformed colonies with the assembled construct were screened for presence of

cloned insert (F2A-AIM) (par.2.3.2.8) by performing an enzyme restriction digestion with *HindIII* enzyme on the recombinant plasmids. The figure 60 shows the agarose gel electrophoresis analysis of digestion product samples. The negative control is the backbone plasmid pCX-EGFP-F2A₁-AIM₁-F2A₂-AIM₂ linearized with the same enzyme (8287bp).

The expected size of cloning product is 9172bp.

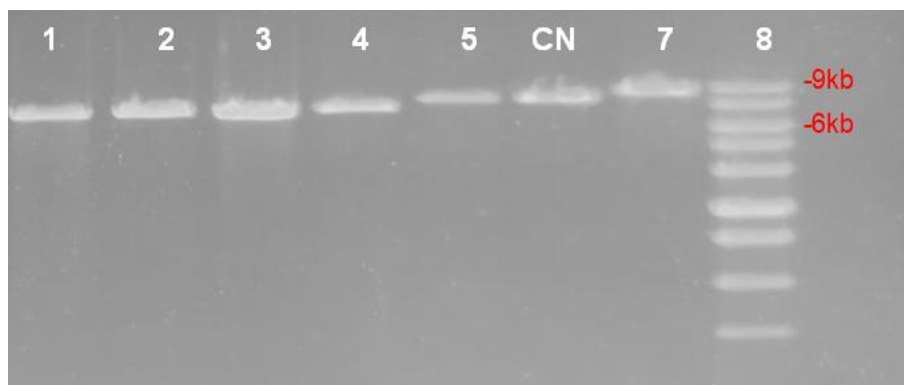


Figure 60 Electrophoretic run of linearized recombinant plasmid samples with *HindIII* restriction enzyme. Lane 8:1kb DNA Ladder (Solys BioDyne); Lanes 1-7: samples screened. The correct assembled plasmid sample has a size of 9172bp. CN: negative control represented by pCX-EGFP-F2A₁-APO₁-F2A₂-APO₂ plasmid.

Positive samples (lane 7) were selected and checked by sequencing and submitted to Eurofins Genomics as described in par.2.3.2.9 for Sanger sequencing to validate the accuracy of the F2A₁-AIM₁ fragment in frame with EGFP and two downstream (F2A-AIM) sequences. The electropherogram reported in figure 61 shows one of the analysed clones that matched 100% to the expected target sequence.

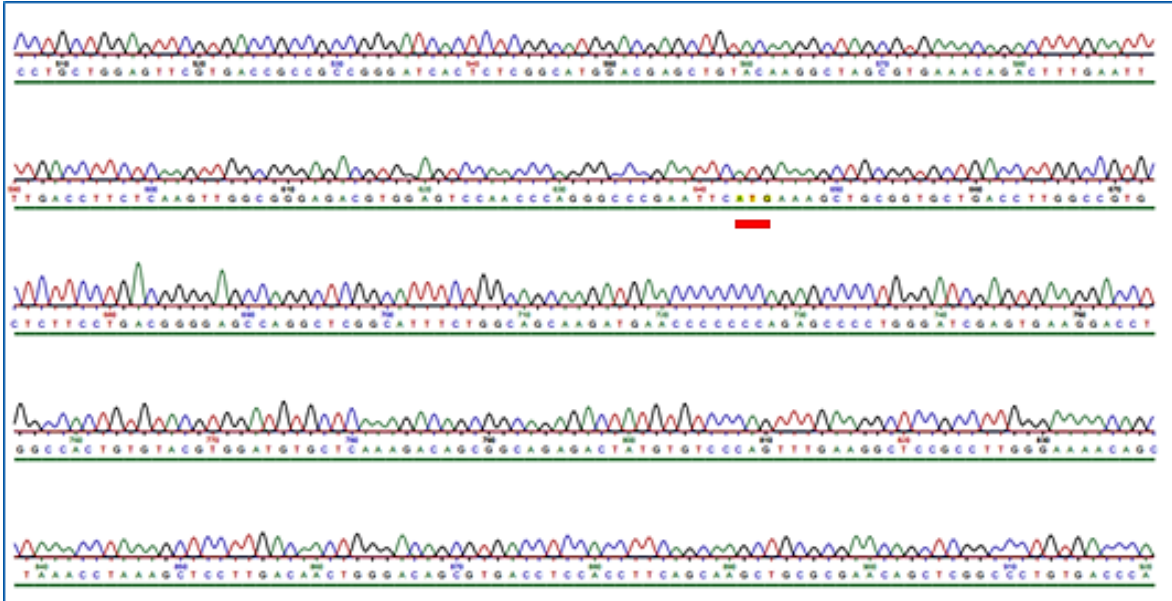


Figure 61 $F2A_1AIM_1$ sequence is correctly detected in cloning assembled plasmid in frame with EGFP sequence and $F2A_3AIM_3$ sequence. Electropherogram represents the sequencing with the forward primer of the portion including AIM_1 starting codon (underlined in red) and a portion of upstream $F2A_1$ sequence.

The resulting pCX-FGFP- $F2A_1$ - AIM_1 - $F2A_2$ - AIM_2 - $F2A_3$ - AIM_3 is a tetracistronic plasmid (fig. 62) co-expressing three copies of AIM sequences together with EGFP. It will be used to test the specific effects induced by three copies of Milano" variant sequences on the general AIM expression and on the reverse cholesterol transport assay.

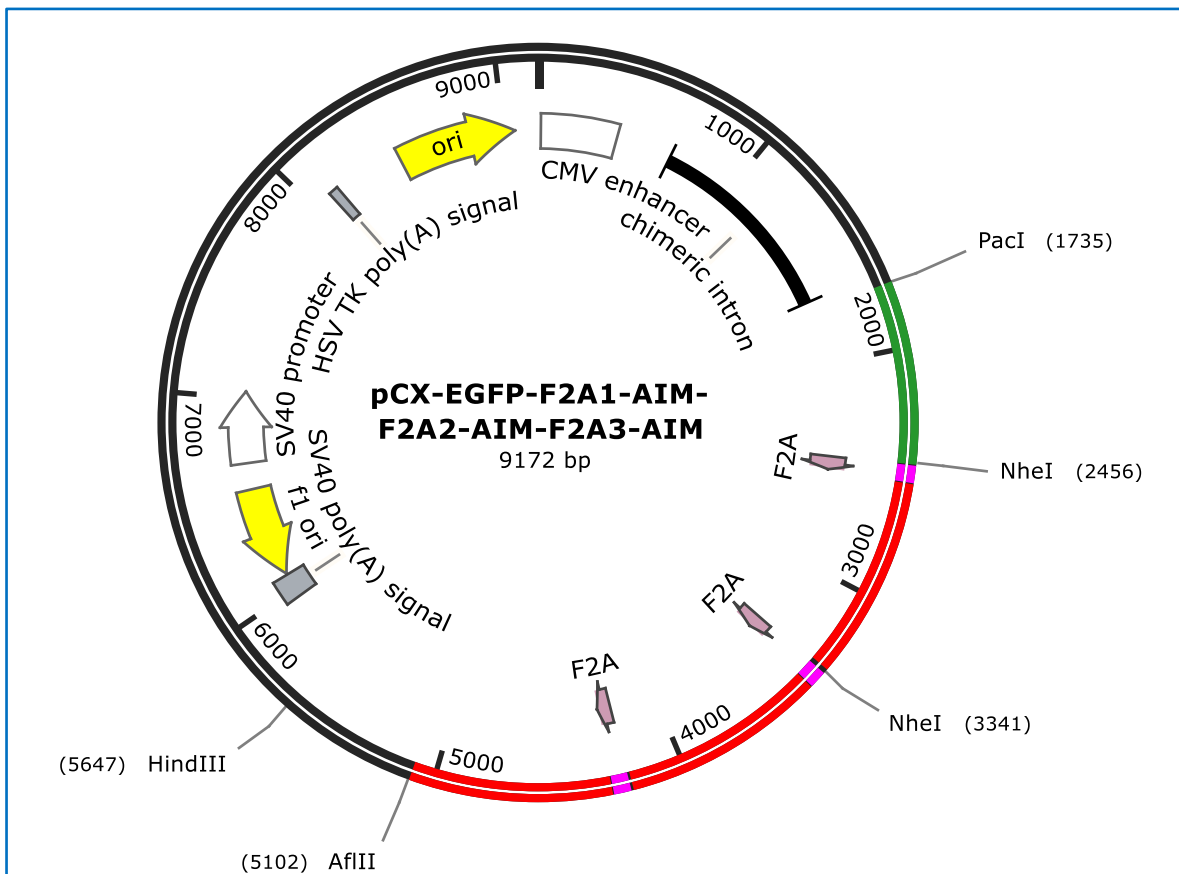


Figure 62 *pCX-EGFP-F2A₁-AIM₁-F2A₂-AIM₂-F2A₃-AIM₃* plasmid map. The main functional elements as well as *NheI*, and *AflII* restriction sites are reported. In green is reported EGFP sequence in frame with three sequences of F2A (pink) and AIM (red). (Created by SnapGene).

The different size of all plasmids built is summarized in figure 63.

All plasmids were digested with *HindIII* enzyme, a unique restriction enzyme with restriction site outside of cloning sites.

As expected, there is no difference in size between the plasmids carrying the APOA-I WT and those carrying the Milano variant.

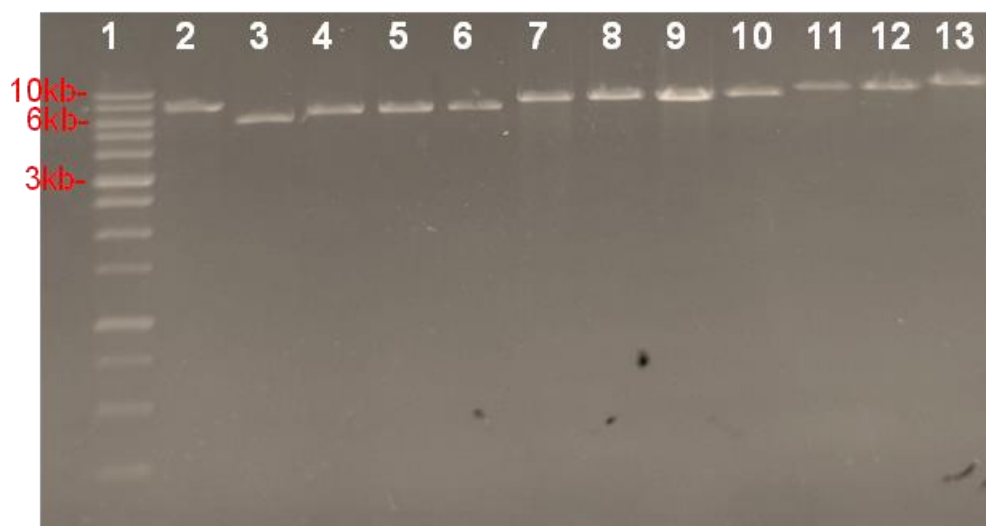


Figure 63 Electrophoretic run of linearized recombinant plasmids built with *HindIII* restriction enzyme. Lane 1: 1kb DNA Ladder (Solys BioDyne); Lanes 2-13: samples checked.

Lane 2: pCX-HO1-F2A-EGFP plasmid; lane 3: pCX-F2A plasmid; lane 4: pCX-EGFP; lane 5: pCX-APO; lane 6: pCX-AIM; lane 7: pCX-APO-F2A-EGFP; lane 8: pCX-AIM-F2A-EGFP; lane 9: pCX-EGFP-F2A-APO; Lane 10: pCX-EGFP-F2A-AIM; Lane 11: pCX-EGFP-F2A₁-APO₁-F2A₂-APO₂; lane 12: pCX-EGFP-F2A₁-AIM₁-F2A₂-AIM₂; lane 13: pCX-EGFP-F2A₁-AIM₁-F2A₂-AIM₂-F2A₃-AIM₃.

3.3. Preliminary results of *in vitro* functional validation of plasmids set

3.3.1. Transfection efficiency evaluation

The transfection efficiency and therefore the ability of any plasmid carrying GFP to express it, were tested by scanning the cells electroporated with plasmids set (performed in duplicate for each condition) at Incucyte® Live-Cell analysis system (Sartorius) at 48 h from the transfection.

The figure 64 shown some example outputs from the scan at the Incucyte® Live-Cell analysis system (Sartorius). As can be seen, in the various conditions under which cells were transfected with plasmids carrying EGFP CDS, most cells express the EGFP protein.

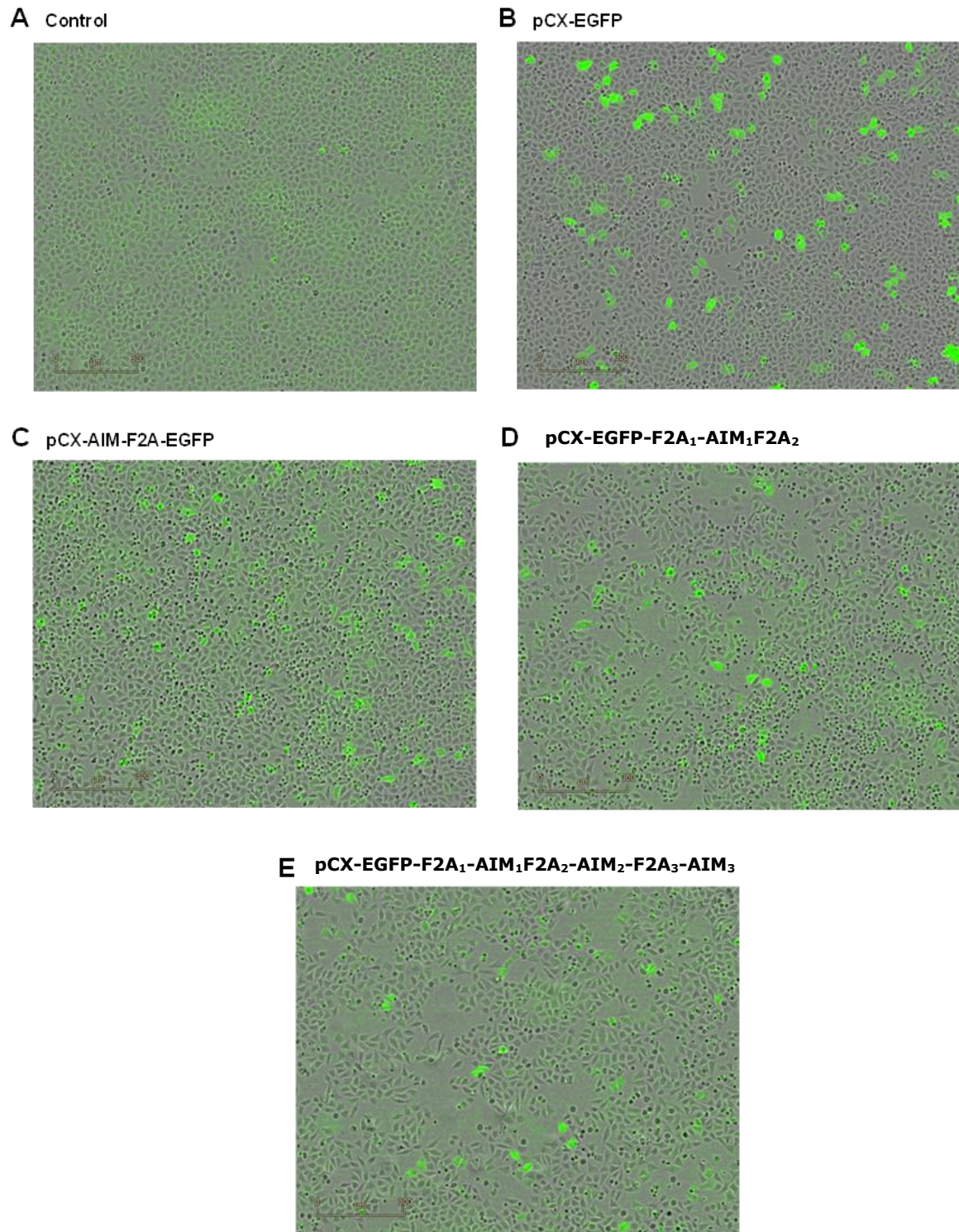


Figure 64 Example of five different outputs electroporation conditions of both replicates. The post analysis Incucyte Live-cell system output highlights the expression of EGFP protein (bright green spots in figure) in cells transfected with vectors carrying the EGFP CDS. **A**: control sample that is cell line transfected only with the vehicle; **B**: cell line transfected with the pCX-EGFP plasmid; **C**: cell line transfected with pcx-AIM-F2A-EGFP plasmid; **D**: cell line transfected with pCX-EGFP-F2A₁-AIM₁F2A₂-AIM₂; **E**: cell line transfected with plasmid pCX-EGFP-F2A₁-AIM₁F2A₂-AIM₂-F2A₃-AIM₃.

From the quantity and quality point of view of cell viability, in the various conditions of transfection in both replicates, the cells have all reached a confluence in the plates between 80 and 85% with a non-significant difference between the various conditions. From the Incucyte® Live-Cell analysis system output in the control sample (transfected only with the vehicle), we could be deduced that the electroporation reaction was not toxic to the cells and the parameters adopted for the reaction were correct.

Moreover, transfection with the pCX-F2A plasmid (not shown in figure 64), used as an additional control of cell viability since the F2A sequence has a viral origin and may exhibit some toxicity, showed no significant impact on the viability of the transfected cells.

As expected, the EGFP protein expressed by cells transfected with the plasmid expressing only EGFP (pCX-EGFP) is higher than that expressed by cells transfected with dicistronic, tricistronic and tetracistronic vectors, shown in figure 65 with relative standard deviation. For the function of the F2A sequence in these vectors, for the same amount of transcribed mRNA, two/three proteins are translated namely EGFP and APO/AIM (in one or more copies) and not just one as for pCX-EGFP.

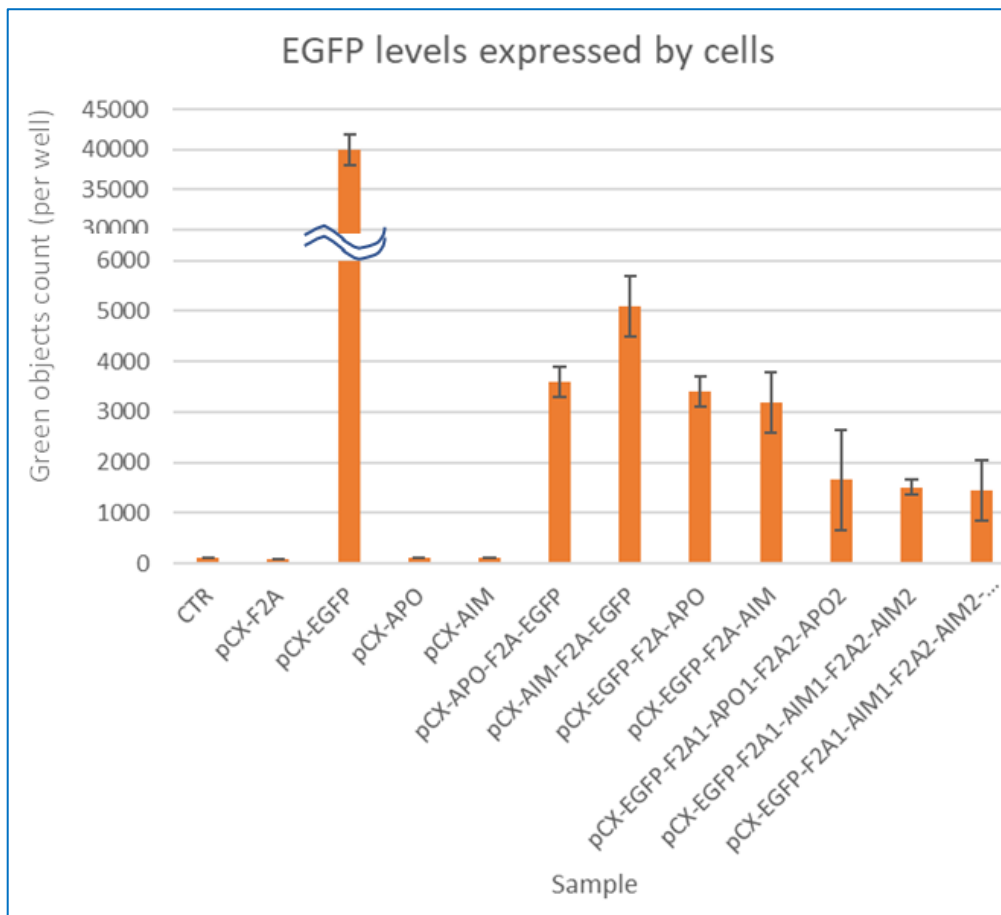


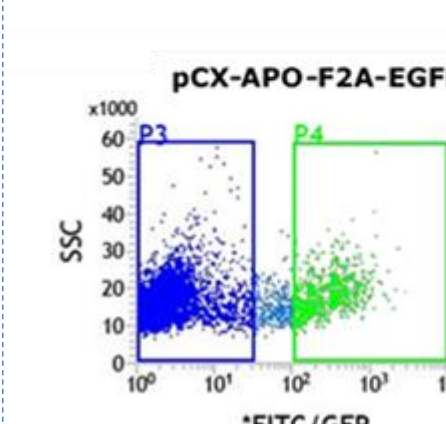
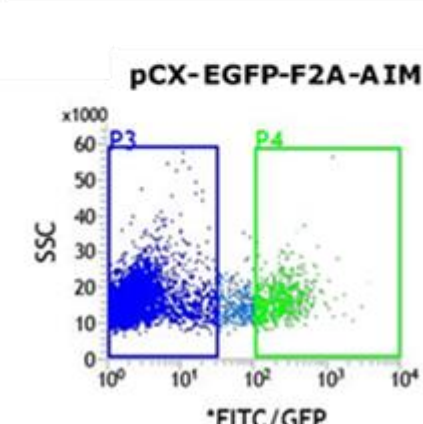
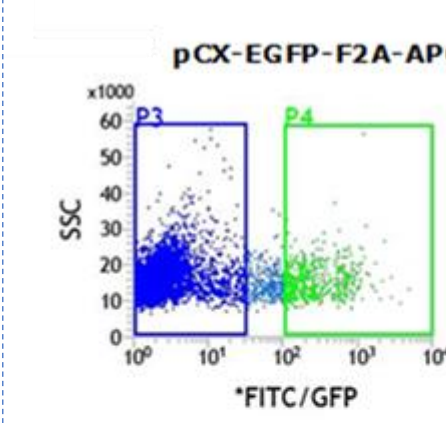
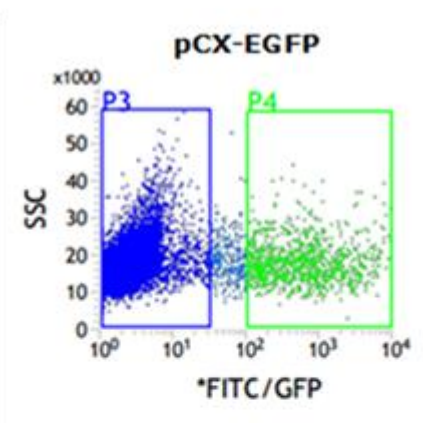
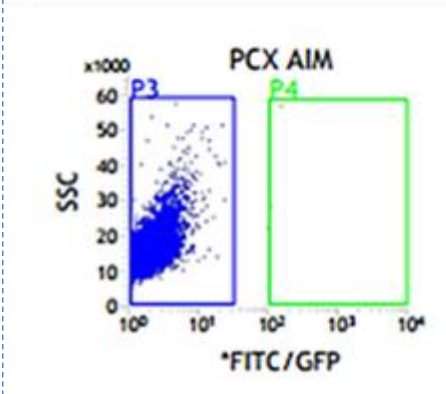
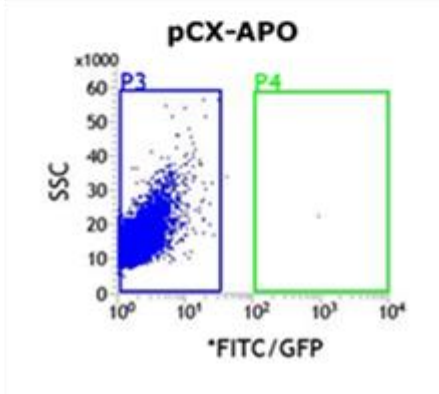
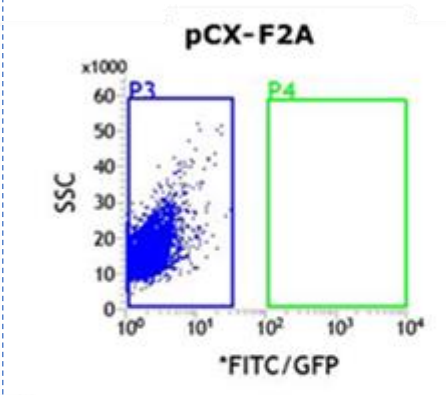
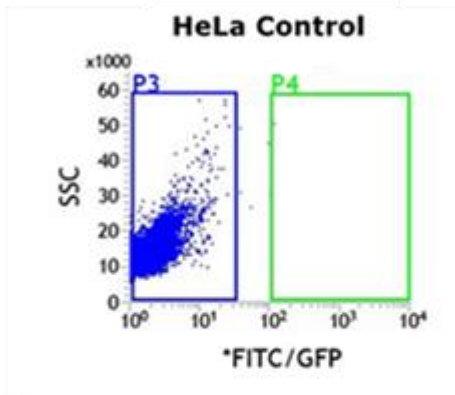
Figure 65 Nuclear EGFP expression in HeLa cells transfected with set plasmids built. Abscissa: sample plasmid electroporated; ordinate: fluorescent object count per well at 48h after transfection. The chart reported the mean value of three independent experiments performed for each electroporation condition and relative standard deviation.

The results illustrated in Figures 64 are representative of the three independent experiments. To optimize the downstream conditions for the immunohistochemistry assay for the analysis of EGFP and APO protein expression in transfected cells, we varied the conditions at Single cell Sorting about the number of starting cells transfected and the amount of plasmid used, doubling both quantities. The same IncuCyte analysis at 48h from transfection before Single cell Sorting analysis proportionally confirmed the data previously illustrated in figures 64 and 65.

The transfection efficiency results previously obtained were also confirmed by Single cell sorting (BD FACS Jazz) for GFP channel in

collaboration with Institute of Clinical Physiology of the CNR of Pisa as showed in figure 66.

■ Blue box: negative cell population
■ Green box: positive cell population



Blue box: negative cell population

Green box: positive cell population

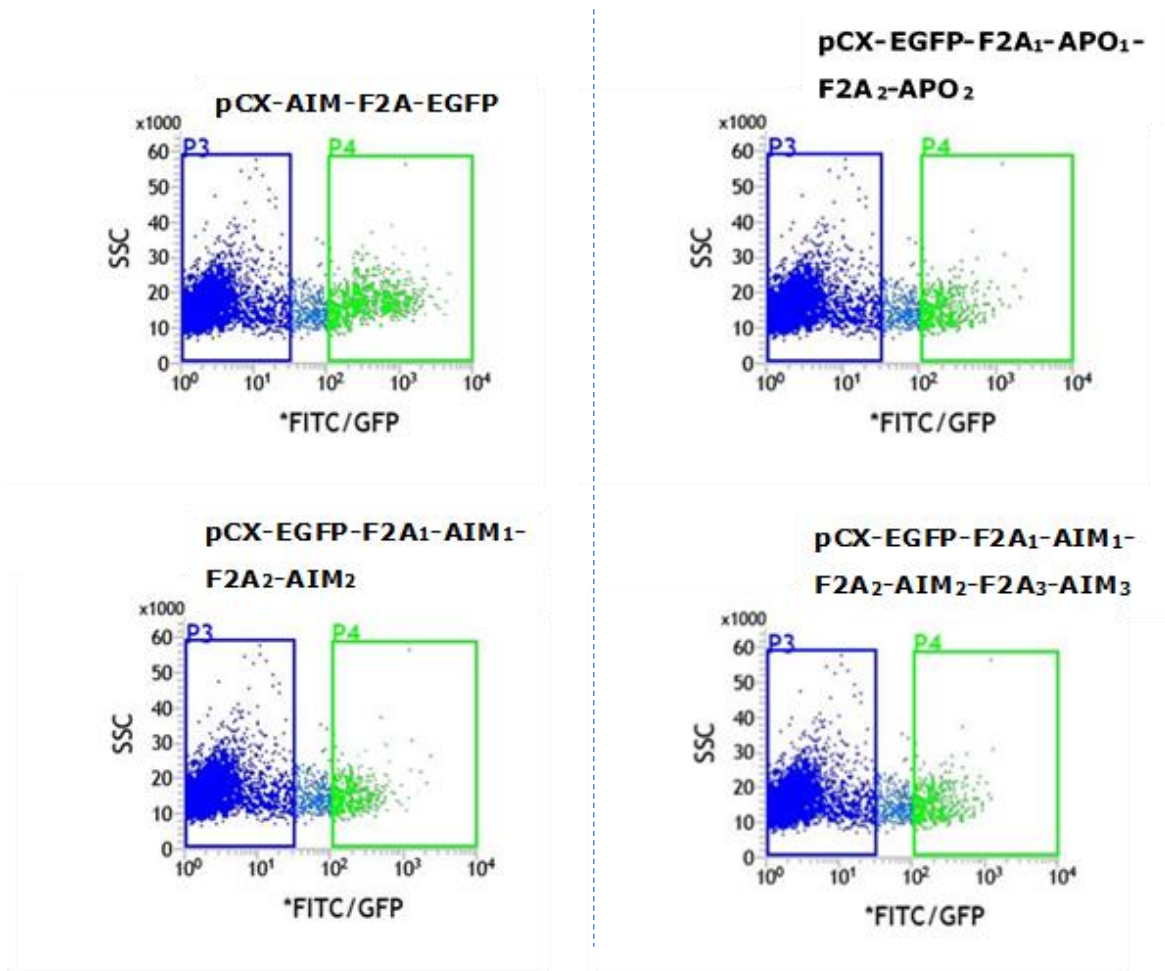


Figure 66 The graphs summarized in the figure show the results of a replicate processed at cell sorting. Two experimental replicates were carried out, each with the analysis of the set of plasmids showed in the figure. Each cell of the cell population under examination is sorted based on cell graininess and complexity (SSC parameter on the Y axis in each graph) and on the green fluorescence (FITC / GFP X axis in each graph).

Single cell sorting separates a population of cells into sub-populations based on fluorescent labelling as showed in figure 66.

The blue box (P3) represents the negative cell population sorted for each sample analysed. The green box (P4) represents the positive cell sorted for each sample analysed. Two boxes are separated by a borderline portion in which the cells do not have a completely clear fluorescence and are therefore not considered as GFP positive cells

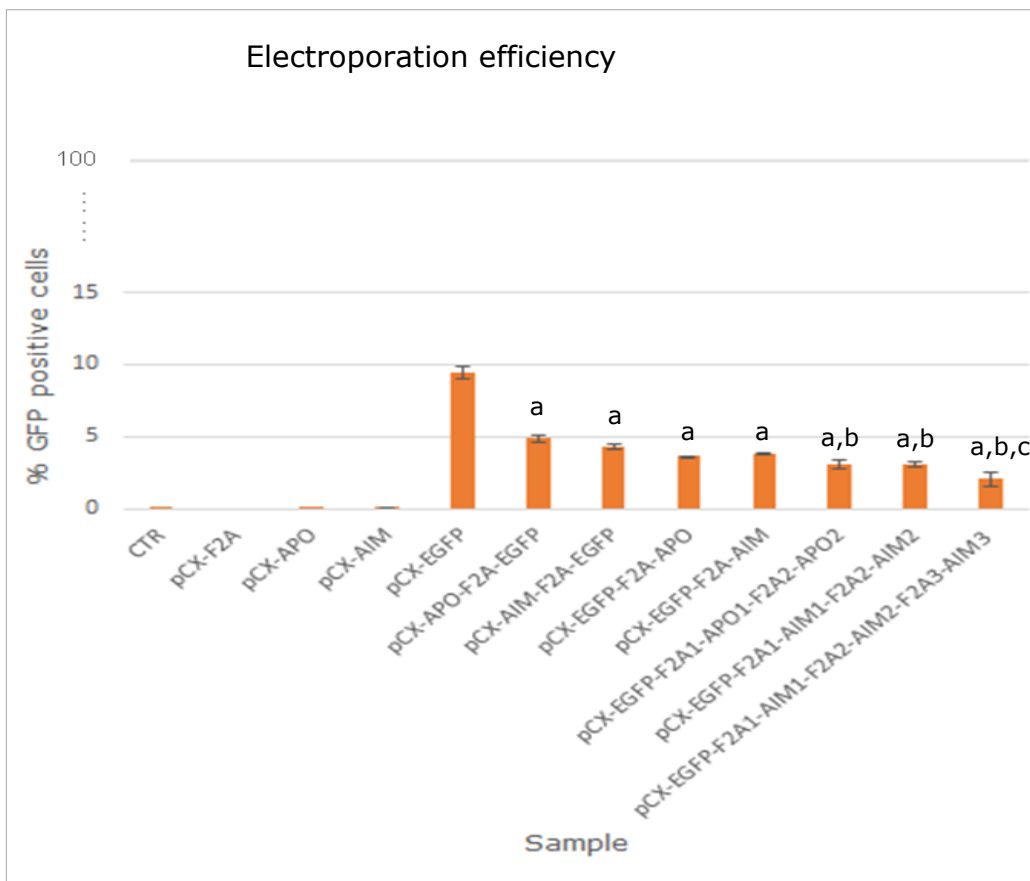


Figure 67 The graph summarizes the comparison between the percentage of GFP positive cells for each sample analysed by single cell sorting. Two independent tests were performed on each sample that are represented as mean and relative standard deviation. "a": significance against pCX-EGFP (p -value $<0,0001$); "b": significance against the di-cistronic plasmids (p -value $<0,001$); "c": significance against the tri-cistronic plasmids (p -value $<0,001$).

Tukey's multiple comparisons test was performed by GraphPadPrism 7 to evaluate the significance of the results obtained.

By means of this test each sample was related to the other with respect to the percentage of GFP positive cells detected at single cell sorting (BD FACS Jazz) and their significance was assessed.

CTR sample, and samples electroporated with pCX-F2A, pCX-APO, pCX-AIM were not considered in the significance assessment as the plasmids not carrying the EGFP CDS are all GFP-negative. The difference between the sample electroporated with the pCX-EGFP plasmid and all the samples electroporated with the other plasmids (di-cistronic, tri-cistronic and tetra-cistronic plasmids) was also significant although expressing a single GFP CDS (p -value <0.0001), the significance was

showed on the graph with letter "a" on the corresponding bar. Lastly, the difference between the percentage of GFP positive cells transfected with the di-cistronic vector carrying the EGFP CDS sequence was also significant compared to the other tri-cistronic plasmids and tetra-cistronic plasmids (p-value < 0,001) (the significance was showed on the graph with letter "b" on the corresponding bar) (p-value < 0,001); also the difference between the percentage of GFP positive cells electroporated with the tri-cistronic vector carrying the EGFP CDS sequence was also significant compared to the tetracistronic plasmid (p-value < 0,001) and the significance was showed on the graph with letter "c" on the corresponding bar.

3.3.2. Evaluation AIM protein expression: ICC results

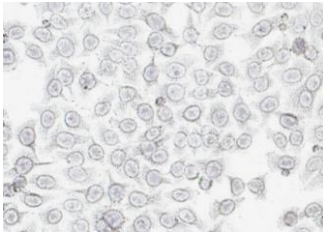
The controls of assay are represented in figure 68 (images A). The CTR electroporation control was represented by HeLa cells electroporated without any plasmids but only with the vehicle (electroporation buffer R2 provided with ThermoFisher electroporation kit). ICC Control, instead, was the blank control of ICC assay and it was represented by HeLa cell electroporated with pCX-APO plasmid, but the section was not incubated with the primary antibody but only with the secondary antibody and serves to define the background.

Images B are representative of a comparison between samples electroporated with plasmid carrying a single copy of APOA1 / AIM (pCX-EGFP-F2A-APO plasmid, pCX-EGFP-F2A-AIM plasmid, pCX-AIM-F2A-EGFP plasmid) and those electroporated with plasmid carrying multiple copies of APOA1 / AIM in series (pCX-EGFP-F2A₁-AIM₁-F2A₂-AIM₂ plasmid and pCX-EGFP-F2A₁-AIM₁-F2A₂-AIM₂-F2A₃-AIM₃ plasmid). In addition, it can be informative to evaluate and confirm previously data about the absent impact on AIM protein expression of the position of the F2A sequence with respect to the AIM CDS.

The spots represented by the most intense brown dye represent positive signals, highlighted in blue.

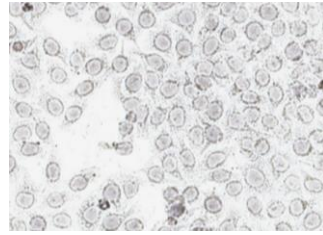
A

CTR
Electroporation
Control



200µm

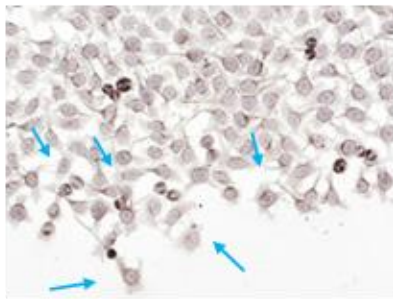
ICC Control
(Blank)
pCX-APO plasmid



200µm

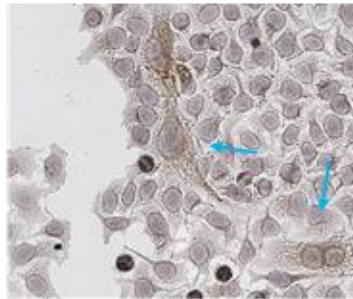
B

pCX-EGFP-F2A-APO
plasmid



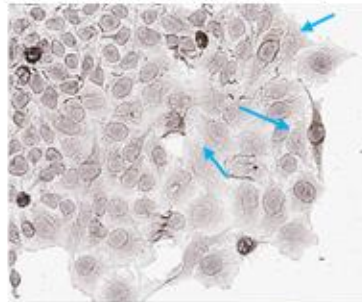
50µm

pCX-EGFP-F2A-AIM
plasmid



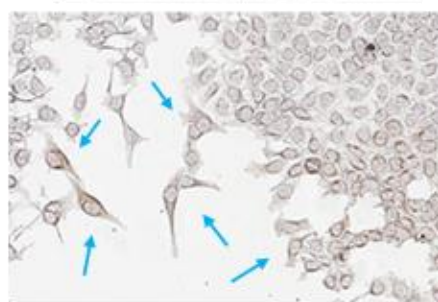
200µm

pCX-AIM-F2A-EGFP
plasmid



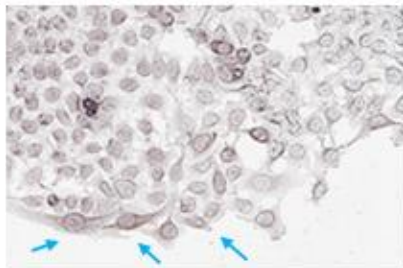
200µm

pCX-EGFP-F2A₁-AIM₁-F2A₂-
AIM₂ plasmid



50µm

pCX-EGFP-F2A₁-AIM₁-F2A₂-AIM₂-
F2A₃-AIM₃ plasmid



50µm

Figure 68 Representative pictures of Immunocytochemistry assays for APO/AIM detection in slides with previously electroporated cells fixed. **A**: blank control; **B**: ICC assays performed on slides with previously electroporated cells fixed: comparison between representative fields of samples electroporated with plasmid carrying a single copy of APOA1 / AIM and those electroporated with plasmid carrying multiple copies of APOA1 / AIM in series. Highlighted in blue positive signals detected only in sample electroporated with plasmids carrying APO/AIM CDS.

4 Discussion

The natural variant APOA-^{Milano} (AIM), discovered at the end of the 80s by Cesare Sirtori in a population of Limone sul Garda, is characterized by the substitution in position 173 of the amino acid arginine with a cysteine. This is believed to promote the formation of disulphide bonds and the resulting formation of protein dimers, which increase its stability and promote its greater interaction with lipids and cholesterol and the enzyme LCAT, main characteristics responsible for its anti-atherogenic effect.

This research project had its basis in a proof-of-concept study ¹¹² that assessed the delivery capacity and therapeutic efficacy of a new production and delivery system of the AIM muteins by means of genetically modified rice plants (*Oryza sativa* species, "Rosa Marchetti" variety). Rice plants were engineered to express and accumulate recombinant protein selectively in the seed due to its expression under the control of the prolamin promoter, the regulatory region of a gene encoding for endogenous rice protein expressed in endosperm. AIM, delivered as a lyophilised powder resulting from seed rice grinding by GRG Gene Technology SA (Minusio, Switzerland), was tested in healthy mice and in an atherosclerotic mouse model *Apoe*^{-/-} mice fed with WD by oral administration at an AIM daily dose of 0.83 mg/Kg for 3 weeks (dosage under patent PCT/IB2006/054948). Despite the continuous feeding with WD, the treatment with APO rice seeds protein extracts ('the rice milk') significantly reduced the size of the atherosclerotic plaque and lipid composition in the aortic sinuses and aortic arch of *Apoe*^{-/-} mice compared to *Apoe*^{-/-} mice treated with wild-type rice milk of the same variety. In addition, the treatment with AIM rice milk

significantly decreased the number of activated macrophages (CD68 positive) in the liver of *ApoE*^{-/-} mice fed with WD compared to mice treated with WT rice milk, also confirming the anti-inflammatory properties of APO as well as the well-known anti-atherogenic activity.

The delivery of therapeutic AIM full-length proteins via oral administration of APO rice to the disordered organism, without any need of purification, might overcome limitations about main 'APOA-I based therapies' and improve the use of these molecules as therapeutic agents for cardiovascular patients.

In fact, the production process of drugs containing APOA-I, or its variants is, to date, very laborious and expensive, since it is usually carried out by purification from human plasma or bacteria that express the recombinant protein⁹³. The very high cost of drug production is also due to the necessary protein purification which must be efficient and safe. From the purification of the protein are in fact obtained monomers, which must then be dimerized by biochemical synthesis processes, since dimerization is essential for the therapeutic efficacy of the administration of APOA-I. Also, in most cases the administration of formulations consists of intravenous infusions that are also very invasive for the patient and for his daily routine.

The work presented in this thesis has three main topics: characterizing at a protein level the rice seeds as a bioreactor and effective delivery system of the therapeutic agent; evaluating the biodistribution of the AIM in the organs of treated mice referred to previously; improving the amount of protein to be administered per gram of rice conveyed through the production of a new rice "superfood" making sure to administer the maximum amount of protein at the same weight of lyophilized powder in order to extend this use to humans. With this purpose, a new set of vectors expressing the AIM and its control vectors has been built, to be tested first *in vitro* in order to study the molecular mechanisms of the protein itself by cell transfection and then as a source of sequences for new genetic engineered rice.

In this project the production of AIM offers an important and innovative alternative for the efficient expression of recombinant protein without the need for any downstream purification phase as it is synthesized directly in the oral delivery vehicle.

This approach greatly reduces the production costs of the therapeutic agent while minimizing the risk of contamination with pathogens, since edible plants generally are well tolerated in the intestine and do not contain harmful molecules and they also do not act as hosts for human or animal infectious agents. Indeed, the use of plants as a delivery system for the production and efficient delivery of therapeutic agents is a cheaper system than mammalian cell cultures or microbial fermentation. Furthermore, the expression of the recombinant protein can be induced in specific organs of the plant, including the edible parts, thus increasing the compliance for the patients and further reducing the need for downstream processes that could affect the formulation.

In particular, for this project, the rice plant has been chosen as a bioreactor, since rice seeds do not contain significant amounts of potential allergens (e.g., gluten) and it is a well-tolerated cereal with wide diffusion among the various crops around the world. Lower production costs compared to cell-based systems together with greater stability of recombinant proteins produced in seeds allowing long-term storage at room temperature without the use of the cold chain for transport, have already directed the biopharmaceutical industries to exploit bioreactors such as rice for the production of nutraceutical and biopharmaceutical compounds ¹²⁵. This, however, does not exclude, despite our demonstration study on rice, that this approach can be extended to other edible plants such as soybean or others. Moreover, given the renowned anti-inflammatory power of APO, our approach can also be extended for use in veterinary use for domestic animals or live stocks, for example in the form of lyophilized powder to be added to animal feeds.

We carried out an effective and more accurate evaluation of human APOA-I protein in rice seeds than the previous one by analysing the

protein component of the salt soluble, salt insoluble and total protein fractions of the rice flour, according to the fractionation approach published by Lang et al. in 2013 ¹¹⁶, for the detection of APOA-I in the various fractions. Analysis of AIM by ELISA and WB of extracted fractions revealed, as expected, no signal in those protein fractions extracted from WT rice flour. On the other hands, in APO-rice flour the protein APOA-I was mostly detected in the salt insoluble protein fraction with a minimal detection in the salt soluble protein fraction. The WB analyses also revealed a different band profile when comparing APO- and WT-rice flour's protein extracts with a complete absence of signal corresponding to AIM protein (which has an apparent weight of approximately 25KDa) in WT-rice. On the other hands, samples corresponding to APO-rice flour salt insoluble and total protein extracts revealed a band of 25KDa, corresponding to APOA-I, and bands with an apparent molecular weight greater than 25kDa (absent in all the WT-rice flour extracts). This very specific pattern of bands suggests that the AIM protein is present in APO-rice flour salt insoluble and total protein extracts. Furthermore, the presence of specific bands greater than 25KDa supports the speculation that these bands refer to the multimerization capacity by AIM, characteristic for its therapeutics potential; further investigations are needed to confirm and support this hypothesis.

Although AIM is an exogenous protein for rice, with no orthologous gene known in this species, the fact that the protein is mainly detected in the salt insoluble protein fraction suggests that the APOAI-M is processed as written in its genetic information and as expected by its biological properties. In fact, in those organisms harbouring the genetic information for APOA-I, the encoded protein has elevated affinity for lipids and cholesterol, which are mainly found in the salt insoluble protein component of the rice seeds.

Studies conducted by Takaiwa F et al. in 2017 ¹²⁶ showed that a key factor influencing both therapeutic efficacy and oral bioavailability of recombinant proteins expressed in rice seeds is the intracellular

localization of such exogenous proteins in the bioreactor organism. Rice and other cereals' seeds contain organelles, called protein bodies (PBs), that are not only a natural storage compartment specialized for the accumulation of proteins essential for the germination and development of the plant, but they also proved to be an adequate intracellular deposition for recombinant proteins. Moreover, bioencapsulated proteins in PBs exhibited high resistance to digestive enzymes in the gastrointestinal tract as compared to other intracellular compartments and they were highly stable at room temperature, thus allowing the oral administration of PBs containing recombinant proteins as therapeutic or nutraceutical agents ¹²⁶. In rice seeds glutelins, which represent about the 80% of total rice protein, are the main seed storage proteins of PBs (type II). In the study conducted by Lang et al. ¹¹⁶, the rice seeds protein fractions (salt soluble, salt insoluble and total protein) were analysed, and they were found that the salt insoluble fraction is more represented by glutelins. These led us to speculate a possible co-localization between glutelins and recombinant protein AIM in PBs. This scenario would confirm the importance of this delivery system as the APO could be protected from enzymatic digestions during its transit through the gastrointestinal tract thus remaining orally bioavailable. Co-localization studies of AIM and glutelins in the genetically modified APO-rice seeds will be performed to demonstrate this hypothesis.

It should also be noted, however, that as endosperm is part of the fatter component of the seed, to understand precisely the processing of the AIM and its intestinal absorption in the body following oral administration. Investigations about whether the human intestine could be able to bio-capture the ingested APO for delivering within the liver parenchyma, as observed in mice, are the object of future studies once the work of cloning presented here will be finalized.

The data obtained in WD-fed *Apoe*^{-/-} mice demonstrated a strong effect of orally delivered AIM, by means of genetically engineered APO-rice milk, on reducing atherosclerotic plaques ¹¹² and a slighter but significant, reduction of hepatic inflammation in the liver. However,

despite these observations, the ELISA evaluation of the presence of human AIM in the liver, intestine (major accumulation organs and proteins production), brain and cerebellum of treated mice did not reveal any signal. The low protein abundance in the tissues is consistent with observations of Roma et al.²³ on AIM metabolism *in vivo*, revealing a catabolic rate significantly higher than the monomeric form of the mutated protein, compared to the wild type. More sensitive techniques are needed to attribute the observed therapeutic effect to a possible intestinal absorption of the AIM protein and thus be able to detect it in the samples analysed.

On the other hand, it should be also considered the possibility that AIM could be partially digested in its transit toward the liver. In this case, the ELISA technique could not be able to detect the correct epitopes present within the liver and the intestine as well as in other organs.

Through IHC we have increased the spatial resolution with single cell resolution compared to ELISA and WB previously performed on mice biopsies. This has allowed the localization of a few positive cells within an entire section. The technique showed a fairly clear sign of positivity in the sections of the treated animals which was not present in the blank or in the section of the control animals. This signal, which was predominantly intracellular, was recurrent in liver structures that morphologically are not traceable to hepatocytes, and this was evidence first of all that the antibody used not cross-reactive with endogenous murine ApoA-I.

Experiments conducted previously by the Romano et al. group on the plasma of treated and control mice did not reveal the presence of APO. We can speculate that it is due to the fact that the animals after the sacrifice have been perfused and also to the rapid turnover of the Milano variant. The evidence, however, at the hepatic level could lead to think that the AIM was captured, once passed the intestine, by liver cells that morphologically were not hepatocytes and not all of the same cell type. To get more information about the specific cell type, new

experiments will have to be performed using antibodies that specifically mark the different cell types present to co-localize with the APO signal. From single cell detection by IHC, the positive signal spots detected in the sections of APO-treated group, are very few compared to the total of the cells and not equally distributed throughout the section. It can therefore be speculated that one of the reasons why the protein was not detected with a precise and sensitive technique such as ELISA may also be due to the fact that, in terms of the amount of protein present/absorbed is however too low to be detected in ELISA where it is subjected to analysis in protein homogenate tissue.

A further control of the experiment to be carried out in the near future to further validate the results is by the use of a primary antibody called isotype control antibody that will allow to evaluate the further specificity of the APO signal observed. In fact, the absence of the antigen-antibody signal will be the proof that the signal observed with the primary against the APO is specific only for the human APO protein and not for endogenous murine ApoA-I.

Our findings on the effects of oral delivery of AIM in the atherosclerotic mouse model are consistent with the encouraging ones obtained by the Fogelman research group on the oral delivery of APO-mimetic peptides also on atherosclerotic murine models, support the hypothesis that, in its transit through the digestive tract, the AIM has not been completely degraded or in any case its biological function was not compromised ¹²⁷. This sort of protection could be due to the administered formulation in which the exogenous protein is accumulated mainly in the PBs of rice seeds.

In addition, Han et al. ¹²⁸ recently reported that HDL produced by the intestine were able to protect liver from inflammation and fibrosis, also in presence of a high fat diet exposure stimulus. These results further support the potential of our innovative drug delivery system and encourage us for further investigation.

One of the next goals will be to carry out a more detailed investigation on intestinal absorption also by using more sensitive techniques such as

mass spectrometry on intestinal tissue samples or *in vitro* simulation of gastrointestinal food digestion and absorption ¹²⁹. We have in fact recently obtained the authorization for animal testing of APO-rice formulation for a project on Inflammatory Bowel Disease (IBD) in collaboration with USZ in Zurich that will allow us to better understand the *in vivo* transit of APOA-I across the intestine.

The improvement of atherosclerotic lesions in mice administered with APO-rice could suggest an improvement in the ability to RCT, strictly depending on both APOA-I and liver function. This would result in an increase in cholesterol efflux from non-hepatic sites, including foam cells in atherosclerotic plaques, for its return to the liver where it is then processed and excreted ¹¹².

In this regard, to better understand the systemic impact of APO treatment, possible changes in expression levels of endogenous murine ApoA-I have been explored in liver and intestine biopsies of treated mice. Analyses in WB showed significant differential expression of the hepatic murine ApoA-I (par.3.1.3.1) of the treated mice compared to the controls suggesting a potential positive feedback impact of the AIM treatment on molecular regulation of its endogenous counterpart.

Some preliminary results (unpublished data) obtained by colleagues of the University of Milan Bicocca on gene expression of endogenous APO murine in treated mice didn't confirm the same trend observed in WB, suggesting therefore that there are involved post-transcriptional and post-translational regulations of endogenous protein.

Certainly, further investigations are needed to better understand this interesting biological result obtained. Given the administration of a relatively low dosage for the mouse and therefore more so if extended to the human organism, the nearest objective is to produce a new variety of rice (iAPO-rice) with a higher concentration of AIM to be administered per gram of rice. The new "superfood" will be performed by an advanced and safer genetic modification technique such as a CRISPR Cas specific site in the new rice plant making sure that the gene expression of recombinant protein is controlled by a strong expressed

promoter selectively in a compartment of the edible plant likely to remain the seed.

In view of this, a series of plasmids expressing AIM and the related controls were built to be tested before *in vitro* to evaluate the molecular mechanisms of the protein through cell transfection and to test its peculiar ability that is the RCT by an *in vitro* Reverse cholesterol transport assay, and as a source of sequences to catalyse the site-specific mutation in the new engineered superfood that will be built.

For this purpose, multicistronic plasmids with two / three AIM CDS in frame could be useful in the future to test even more APOA-I variants eg. Paris variant together with Milan variant. To date there are no data on a possible therapeutic potential of a similar system, but it could be interesting to investigate it.

The preliminary results from the *in vitro* functional tests showed no toxicity of both the transfection reaction and the F2A sequence in plasmids. Furthermore, by Incucyte live cell system (Sartorius) analysis the EGFP protein was expressed from all the plasmids carrying its CDS as expected.

It must be considered that the experimental setting chosen to obtain these preliminary results is based on transient cell transfection, a procedure leading to intrinsic heterogeneity in terms of number of cells transfected and levels of expression in each transfected cell for each population analysed. With this consideration in mind, we could speculate on some explanation for the behaviour of transfected cells.

The data were also confirmed by single cell sorting (BD FACS Jazz). Cells transfected with EGFP CDS-carrying plasmids express the EGFP protein as expected. From statistical analysis on the percentage of positive cells sorted for each sample in two independent experiments performed by Tukey's multiple comparisons test, it was found that the difference between the percentage of positive GFP cells in the sample transfected with the pCX-EGFP vector compared to those transfected with multicistronic vectors was statistically significant. The difference between the percentage of GFP positive cells transfected with dicistronic

plasmids and those electroporated with tri-cistronic and quadri-cistronic plasmids was also statistically significant. Also, the difference between the percentage of GFP positive cells transfected with the tri-cistronic vectors and those transfected with the tetra-cistronic was also statistically significant. Moreover, the single cell sorting results showed that the percentage of GFP positive cells sorted decreased in the samples as the length of the vector with which the cells were electroporated increases. We will therefore have to improve and optimize the electroporation parameters as the reaction is less efficient when using large plasmids (greater than 10kb) as in the case of our multicistronics. On the other hand, from the translation point of view, the ribosomal apparatus takes less time to translate a shorter mRNA molecule (such as the CDS of APO or EGFP in monocistronic plasmids) rather than multicistronic mRNAs as in the case of plasmids based on the F2A system ¹³⁰.

From the results obtained we were also able to deduce that by reversing the order of the EGFP with respect to the F2A sequence in plasmids, the same result was produced at the level of expression of EGFP in the transfected cells and that therefore F2A sequence position does not impact on the level of the protein.

From the analysis of the ICC results with antibody against human APOA-I protein, positive signals were detected in all cell samples transfected with the plasmids carrying the APOA1 / AIM CDS. This is further support about the functionality of the F2A sequence with these combinations of CDSs. Further analyses are needed to accurately quantify the positive signals for each field on each well.

As expected, the positive signal detected is coherent with a plasma membrane and cytoplasmic localization. The potential secretion of the APOA-I protein, assembled or not in HDL-like particles, needs the application of different assays to be demonstrated.

Further investigation should be performed to evaluate by stable cellular transfection with next assays in WB regarding the expression of APO/AIM. The *in vitro* Reverse cholesterol transport assay should also

be performed to assess the impact expression of APO and AIM of the monocistronic and multigenic plasmids carrying multiple protein copies on cholesterol efflux at cellular level in transfected cells.

Further investigations on the functionality level of the plasmids will still have to be carried out when they are used as source of AIM sequence to carry out site-specific CRISPR in the new rice plant.

5 Future perspectives

In the light of the above results, further investigations are under way or must be carried out to better understand the mechanisms by which the therapeutic power of the conveyed AIM is exercised and to complete the new AIM rice superfood. For this purpose, intestinal absorption studies should be carried out either by static *in vitro* simulation of gastrointestinal food digestion or by much more precise techniques such as mass spectrometry and lipidomic studies. These investigations should be accompanied by kinetics studies to define the biodistribution of the AIM by analysing the organs of mice, at defined time points after the treatment, in the treated and control group on which to carry out single cell analyses and lipidomic studies. In parallel, dose-response studies on an atherosclerotic mouse model should also be carried out to better understand the impact and effects of the AIM oral delivery system.

Further investigations at both liver and intestine level should be conducted through IHC to better understand which cell types exhibited a positive signal in the assay conducted. The delivery system will have to be further improved enhancing the formulation from the point of view of the quantity of AIM supplied. Another important objective is to improve the formulation from the point of view of quality, in fact, a dissolution protocol (study in progress) of the starch contained in rice seeds is being perfected with the aim of making the formulation dissoluble and more concentrate in water once the downstream lyophilization process is in completion. The protocol, which consists only

of the hydrolysis and removal of starch by amylase enzyme, will be the aim to improve the APO rice administration preserving the organoleptic characteristics of the rice grain and is part of a partnership established with USZ Zurich for the IBD study.

Among future perspectives there are also studies at the molecular level to better understand the pathways and the interactors in which APOA-I is involved; the study of molecular mechanisms in different cell models and in organoids of liver and intestines could make understand better the pathways in which the APO is involved mainly as a result of its increased expression caused by the APO rice treatment. We will therefore rely on genetic analysis tools to support the correlation between the impact of APO rice and CVDs incidence.

6 Conclusions

The use of food as a source of food is well known; recently there has also been considerable interest in the scientific community towards nutraceutical or about the beneficial effects that different components of certain foods have on health, regardless of their nutritional value. this has led to interesting results, although not always clinically confirmed. With this project we propose to go further and consider food, in addition to nutritional value and nutraceutical potential, also as an efficient vehicle for the synthesis and release by the enteric pathway of real peptide-based drugs. The studies are still ongoing and in the process of improvement, but the results obtained to present day are hopeful for the extension in the future to humans of this innovative method of delivery.

7 Bibliography

1. Drucker, D. J. Advances in oral peptide therapeutics. *Nat Rev Drug Discov* **19**, 277–289 (2020).
2. Hamman, J. H., Enslin, G. M. & Kotzé, A. F. Oral delivery of peptide drugs: barriers and developments. *BioDrugs* **19**, 165–77 (2005).
3. Kiela, P. R. & Ghishan, F. K. Physiology of Intestinal Absorption and Secretion. *Best Practice & Research Clinical Gastroenterology* **30**, 145–159 (2016).
4. Goodman, B. E. Insights into digestion and absorption of major nutrients in humans. *Adv Physiol Educ* **34**, 44–53 (2010).
5. Lundquist, P. & Artursson, P. Oral absorption of peptides and nanoparticles across the human intestine: Opportunities, limitations and studies in human tissues. *Adv Drug Deliv Rev* **106**, 256–276 (2016).
6. Johansson, M. E. v, Sjövall, H. & Hansson, G. C. The gastrointestinal mucus system in health and disease. *Nat Rev Gastroenterol Hepatol* **10**, 352–61 (2013).
7. Groschwitz, K. R. & Hogan, S. P. Intestinal barrier function: molecular regulation and disease pathogenesis. *J Allergy Clin Immunol* **124**, 3–20; quiz 21–2 (2009).
8. Hua, S. Advances in Oral Drug Delivery for Regional Targeting in the Gastrointestinal Tract - Influence of Physiological, Pathophysiological and Pharmaceutical Factors. *Front Pharmacol* **11**, 524 (2020).
9. Maher, S., Mrsny, R. J. & Brayden, D. J. Intestinal permeation enhancers for oral peptide delivery. *Adv Drug Deliv Rev* **106**, 277–319 (2016).
10. Smart, A. L., Gaisford, S. & Basit, A. W. Oral peptide and protein delivery: intestinal obstacles and commercial prospects. *Expert Opin Drug Deliv* **11**, 1323–35 (2014).

11. Sturmer, A. *et al.* Pharmacokinetics of oral recombinant human parathyroid hormone [rhPTH(1-31)NH₂] in postmenopausal women with osteoporosis. *Clin Pharmacokinet* **52**, 995–1004 (2013).
12. Rubattu, S. & Volpe, M. Natriuretic Peptides in the Cardiovascular System: Multifaceted Roles in Physiology, Pathology and Therapeutics. *Int J Mol Sci* **20**, (2019).
13. Geho, W. B., Rosenberg, L. N., Schwartz, S. L., Lau, J. R. & Gana, T. J. A single-blind, placebo-controlled, dose-ranging trial of oral hepatic-directed vesicle insulin add-on to oral antidiabetic treatment in patients with type 2 diabetes mellitus. *J Diabetes Sci Technol* **8**, 551–9 (2014).
14. Pantzar, N., Lundin, S. & Weström, B. R. Different properties of the paracellular pathway account for the regional small intestinal permeability to the peptide desmopressin. *J Pharm Sci* **84**, 1245–8 (1995).
15. Gordon Still, J. Development of oral insulin: progress and current status. *Diabetes Metab Res Rev* **18 Suppl 1**, S29-37.
16. Desai, T. & Shea, L. D. Advances in islet encapsulation technologies. *Nat Rev Drug Discov* **16**, 367 (2017).
17. Anselmo, A. C., Gokarn, Y. & Mitragotri, S. Non-invasive delivery strategies for biologics. *Nat Rev Drug Discov* **18**, 19–40 (2019).
18. Geho, W. B., Rosenberg, L. N., Schwartz, S. L., Lau, J. R. & Gana, T. J. A single-blind, placebo-controlled, dose-ranging trial of oral hepatic-directed vesicle insulin add-on to oral antidiabetic treatment in patients with type 2 diabetes mellitus. *J Diabetes Sci Technol* **8**, 551–9 (2014).
19. Leman, L. J., Maryanoff, B. E. & Ghadiri, M. R. Molecules That Mimic Apolipoprotein A-I: Potential Agents for Treating Atherosclerosis. *Journal of Medicinal Chemistry* **57**, 2169–2196 (2014).

20. Cochran, B. J., Ong, K.-L., Manandhar, B. & Rye, K.-A. APOA1: a Protein with Multiple Therapeutic Functions. *Curr Atheroscler Rep* **23**, 11 (2021).
21. Chiesa, G. & Sirtori, C. R. Use of recombinant apolipoproteins in vascular diseases: the case of apoA-I. *Curr Opin Investig Drugs* **3**, 420–6 (2002).
22. van der Vorst, E. P. C. High-Density Lipoproteins and Apolipoprotein A1. in 399–420 (2020). doi:10.1007/978-3-030-41769-7_16.
23. Roma, P. *et al.* In vivo metabolism of a mutant form of apolipoprotein A-I, apo A-I_{Milano}, associated with familial hypoalphalipoproteinemia. *Journal of Clinical Investigation* **91**, 1445–1452 (1993).
24. Chiesa, G. & Sirtori, C. R. Apolipoprotein A-I(Milano): current perspectives. *Curr Opin Lipidol* **14**, 159–63 (2003).
25. Ducroux, C. *et al.* Protective Effect of ApoA1 (Apolipoprotein A1)-Milano in a Rat Model of Large Vessel Occlusion Stroke. *Stroke* **51**, 1886–1890 (2020).
26. Parolini, C. A Compendium of the Biological Effects of Apolipoprotein A-I_{Milano}. *Journal of Pharmacology and Experimental Therapeutics* **372**, 54–62 (2020).
27. Zanoni, P. & von Eckardstein, A. Inborn errors of apolipoprotein A-I metabolism: implications for disease, research and development. *Curr Opin Lipidol* **31**, 62–70 (2020).
28. Bielicki, J. K. & Oda, M. N. Apolipoprotein A-I_{Milano} and Apolipoprotein A-I_{Paris} Exhibit an Antioxidant Activity Distinct from That of Wild-Type Apolipoprotein A-I. *Biochemistry* **41**, 2089–2096 (2002).
29. Roma, P. *et al.* In vivo metabolism of a mutant form of apolipoprotein A-I, apo A-I_{Milano}, associated with familial hypoalphalipoproteinemia. *J Clin Invest* **91**, 1445–52 (1993).

30. Funke, H. *et al.* A frameshift mutation in the human apolipoprotein A-I gene causes high density lipoprotein deficiency, partial lecithin: cholesterol-acyltransferase deficiency, and corneal opacities. *J Clin Invest* **87**, 371–6 (1991).
31. Ng, D. S., Leiter, L. A., Vezina, C., Connelly, P. W. & Hegele, R. A. Apolipoprotein A-I Q[-2]X causing isolated apolipoprotein A-I deficiency in a family with analphalipoproteinemia. *J Clin Invest* **93**, 223–9 (1994).
32. Matsunaga, T. *et al.* Apolipoprotein A-I deficiency due to a codon 84 nonsense mutation of the apolipoprotein A-I gene. *Proc Natl Acad Sci U S A* **88**, 2793–7 (1991).
33. Nichols, W. C., Dwulet, F. E., Liepnieks, J. & Benson, M. D. Variant apolipoprotein AI as a major constituent of a human hereditary amyloid. *Biochem Biophys Res Commun* **156**, 762–8 (1988).
34. Vigushin, D. M. *et al.* Familial nephropathic systemic amyloidosis caused by apolipoprotein AI variant Arg26. *Q J Med* **87**, 149–54 (1994).
35. Nichols, W. C., Gregg, R. E., Brewer, H. B. & Benson, M. D. A mutation in apolipoprotein A-I in the Iowa type of familial amyloidotic polyneuropathy. *Genomics* **8**, 318–23 (1990).
36. Obici, L. *et al.* The new apolipoprotein A-I variant leu(174) --> Ser causes hereditary cardiac amyloidosis, and the amyloid fibrils are constituted by the 93-residue N-terminal polypeptide. *Am J Pathol* **155**, 695–702 (1999).
37. Hamidi Asl, K., Liepnieks, J. J., Nakamura, M., Parker, F. & Benson, M. D. A novel apolipoprotein A-1 variant, Arg173Pro, associated with cardiac and cutaneous amyloidosis. *Biochem Biophys Res Commun* **257**, 584–8 (1999).
38. Lachmann, H. J. *et al.* Misdiagnosis of hereditary amyloidosis as AL (primary) amyloidosis. *N Engl J Med* **346**, 1786–91 (2002).

39. van Camp, G. Cardiovascular disease prevention. *Acta Clin Belg* **69**, 407–11 (2014).
40. van Camp, G. Cardiovascular disease prevention. *Acta Clin Belg* **69**, 407–11 (2014).
41. Peng, J., Xiao, X., Hu, M. & Zhang, X. Interaction between gut microbiome and cardiovascular disease. *Life Sci* **214**, 153–157 (2018).
42. Cannon, B. Cardiovascular disease: Biochemistry to behaviour. *Nature* **493**, S2–S3 (2013).
43. Shore, B. & Shore, V. Heterogeneity in protein subunits of human serum high-density lipoproteins. *Biochemistry* **7**, 2773–7 (1968).
44. Flaim, E., Ferreri, L. F., Thye, F. W., Hill, J. E. & Ritchey, S. J. Plasma lipid and lipoprotein cholesterol concentrations in adult males consuming normal and high cholesterol diets under controlled conditions. *Am J Clin Nutr* **34**, 1103–8 (1981).
45. de LALLA, O. F. & GOFMAN, J. W. Ultracentrifugal analysis of serum lipoproteins. *Methods Biochem Anal* **1**, 459–78 (1954).
46. Ben-Aicha, S., Badimon, L. & Vilahur, G. Advances in HDL: Much More than Lipid Transporters. *Int J Mol Sci* **21**, (2020).
47. Kuai, R., Li, D., Chen, Y. E., Moon, J. J. & Schwendeman, A. High-Density Lipoproteins: Nature’s Multifunctional Nanoparticles. *ACS Nano* **10**, 3015–41 (2016).
48. Rothblat, G. H. & Phillips, M. C. High-density lipoprotein heterogeneity and function in reverse cholesterol transport. *Current Opinion in Lipidology* **21**, 229–238 (2010).
49. Ben-Aicha, S., Badimon, L. & Vilahur, G. Advances in HDL: Much More than Lipid Transporters. *International Journal of Molecular Sciences* **21**, 732 (2020).
50. Kontush, A. *et al.* Structure of HDL: particle subclasses and molecular components. *Handb Exp Pharmacol* **224**, 3–51 (2015).

51. Márquez, A. B., Nazir, S. & van der Vorst, E. P. C. High-Density Lipoprotein Modifications: A Pathological Consequence or Cause of Disease Progression? *Biomedicines* **8**, (2020).
52. Hennessy, L. K., Kunitake, S. T. & Kane, J. P. Apolipoprotein A-I-containing lipoproteins, with or without apolipoprotein A-II, as progenitors of pre- β . high-density lipoprotein particles. *Biochemistry* **32**, 5759–5765 (1993).
53. Ertek, S. High-density Lipoprotein (HDL) Dysfunction and the Future of HDL. *Curr Vasc Pharmacol* **16**, 490–498 (2018).
54. Márquez, A. B., Nazir, S. & van der Vorst, E. P. C. High-Density Lipoprotein Modifications: A Pathological Consequence or Cause of Disease Progression? *Biomedicines* **8**, (2020).
55. Ouimet, M., Barrett, T. J. & Fisher, E. A. HDL and Reverse Cholesterol Transport. *Circulation Research* **124**, 1505–1518 (2019).
56. Arnold von Eckardstein, D. K. High Density Lipoproteins. *Springer Open*.
57. Rousset, X., Vaisman, B., Amar, M., Sethi, A. A. & Remaley, A. T. Lecithin: cholesterol acyltransferase--from biochemistry to role in cardiovascular disease. *Curr Opin Endocrinol Diabetes Obes* **16**, 163–71 (2009).
58. Kowalska, K., Socha, E. & Milnerowicz, H. Review: The role of paraoxonase in cardiovascular diseases. *Ann Clin Lab Sci* **45**, 226–33 (2015).
59. Karasawa, K., Harada, A., Satoh, N., Inoue, K. & Setaka, M. Plasma platelet activating factor-acetylhydrolase (PAF-AH). *Prog Lipid Res* **42**, 93–114 (2003).
60. Ertek, S. High-density Lipoprotein (HDL) Dysfunction and the Future of HDL. *Curr Vasc Pharmacol* **16**, 490–498 (2018).

61. Kontush, A., Lhomme, M. & Chapman, M. J. Unraveling the complexities of the HDL lipidome. *J Lipid Res* **54**, 2950–63 (2013).
62. Hoofnagle, A. N., Vaisar, T., Mitra, P. & Chait, A. HDL lipids and insulin resistance. *Curr Diab Rep* **10**, 78–86 (2010).
63. Grundler, F. *et al.* Long-term fasting improves lipoprotein-associated atherogenic risk in humans. *Eur J Nutr* **60**, 4031–4044 (2021).
64. Tiziana Sampietro, F. B. B. D. P. M. P. A. B.-*Laboratorio D. e A. I. di F. C. del C. D. di M. I. U. degli S. P. Lipoproteine ad alta densità: il “nuovo” target della medicina cardiovascolare. *G Ital Cardiol* 2005;6(6):341-353 (2005).
65. Koenig, W. & Khuseyinova, N. Biomarkers of atherosclerotic plaque instability and rupture. *Arterioscler Thromb Vasc Biol* **27**, 15–26 (2007).
66. Hansson, G. K., Robertson, A.-K. L. & Söderberg-Nauclér, C. Inflammation and atherosclerosis. *Annu Rev Pathol* **1**, 297–329 (2006).
67. Hansson, G. K. & Libby, P. The immune response in atherosclerosis: a double-edged sword. *Nat Rev Immunol* **6**, 508–19 (2006).
68. Hafiane, A. & Genest, J. HDL, Atherosclerosis, and Emerging Therapies. *Cholesterol* **2013**, 891403 (2013).
69. van der Vorst, E. P. C. High-Density Lipoproteins and Apolipoprotein A1. in 399–420 (2020). doi:10.1007/978-3-030-41769-7_16.
70. van der Vorst, E. P. C. High-Density Lipoproteins and Apolipoprotein A1. in 399–420 (2020). doi:10.1007/978-3-030-41769-7_16.
71. Curtiss, L. K., Valenta, D. T., Hime, N. J. & Rye, K.-A. What Is So Special About Apolipoprotein AI in Reverse Cholesterol Transport? *Arteriosclerosis, Thrombosis, and Vascular Biology* **26**, 12–19 (2006).

72. Rosenson, R. S. *et al.* Cholesterol efflux and atheroprotection: advancing the concept of reverse cholesterol transport. *Circulation* **125**, 1905–19 (2012).
73. Zhang, Y. *et al.* Overexpression of Apolipoprotein A-I Promotes Reverse Transport of Cholesterol From Macrophages to Feces In Vivo. *Circulation* **108**, 661–663 (2003).
74. Curtiss, L. K., Valenta, D. T., Hime, N. J. & Rye, K.-A. What Is So Special About Apolipoprotein AI in Reverse Cholesterol Transport? *Arteriosclerosis, Thrombosis, and Vascular Biology* **26**, 12–19 (2006).
75. Zhao, G.-J., Yin, K., Fu, Y. & Tang, C.-K. The Interaction of ApoA-I and ABCA1 Triggers Signal Transduction Pathways to Mediate Efflux of Cellular Lipids. *Molecular Medicine* **18**, 149–158 (2012).
76. Curtiss, L. K., Valenta, D. T., Hime, N. J. & Rye, K.-A. What Is So Special About Apolipoprotein AI in Reverse Cholesterol Transport? *Arteriosclerosis, Thrombosis, and Vascular Biology* **26**, 12–19 (2006).
77. Rousset, X., Shamburek, R., Vaisman, B., Amar, M. & Remaley, A. T. Lecithin Cholesterol Acyltransferase: An Anti- or Pro-atherogenic Factor? *Current Atherosclerosis Reports* **13**, 249–256 (2011).
78. Nong, Z. *et al.* Hepatic lipase expression in macrophages contributes to atherosclerosis in apoE-deficient and LCAT-transgenic mice. *Journal of Clinical Investigation* **112**, 367–378 (2003).
79. Chapman, M. J., le Goff, W., Guerin, M. & Kontush, A. Cholesteryl ester transfer protein: at the heart of the action of lipid-modulating therapy with statins, fibrates, niacin, and cholesteryl ester transfer protein inhibitors. *European Heart Journal* **31**, 149–164 (2010).

80. Zhang, M. *et al.* Structural basis of the lipid transfer mechanism of phospholipid transfer protein (PLTP). *Biochimica et Biophysica Acta (BBA) - Molecular and Cell Biology of Lipids* **1863**, 1082–1094 (2018).
81. Leman, L. J., Maryanoff, B. E. & Ghadiri, M. R. Molecules that mimic apolipoprotein A-I: potential agents for treating atherosclerosis. *J Med Chem* **57**, 2169–96 (2014).
82. Cao, P. *et al.* Advances in the Study of the Antiatherogenic Function and Novel Therapies for HDL. *Int J Mol Sci* **16**, 17245–72 (2015).
83. Kontush, A. & Chapman, M. J. Antiatherogenic function of HDL particle subpopulations: focus on antioxidative activities. *Current Opinion in Lipidology* **21**, 312–318 (2010).
84. Cao, P. *et al.* Advances in the Study of the Antiatherogenic Function and Novel Therapies for HDL. *International Journal of Molecular Sciences* **16**, 17245–17272 (2015).
85. Kontush, A., Chantepie, S. & Chapman, M. J. Small, Dense HDL Particles Exert Potent Protection of Atherogenic LDL Against Oxidative Stress. *Arteriosclerosis, Thrombosis, and Vascular Biology* **23**, 1881–1888 (2003).
86. Georgila, Vyrla & Drakos. Apolipoprotein A-I (ApoA-I), Immunity, Inflammation and Cancer. *Cancers (Basel)* **11**, 1097 (2019).
87. Levine, D. M., Parker, T. S., Donnelly, T. M., Walsh, A. & Rubin, A. L. In vivo protection against endotoxin by plasma high density lipoprotein. *Proceedings of the National Academy of Sciences* **90**, 12040–12044 (1993).
88. Ansell, B. J. *et al.* Inflammatory/antiinflammatory properties of high-density lipoprotein distinguish patients from control subjects better than high-density lipoprotein cholesterol levels and are favorably affected by simvastatin treatment. *Circulation* **108**, 2751–6 (2003).

89. Fogelman, A. M. Further evidence that high-density lipoprotein is a chameleon-like lipoprotein. *Eur Heart J* **36**, 3017–9 (2015).
90. Rosenson, R. S. *et al.* Dysfunctional HDL and atherosclerotic cardiovascular disease. *Nature Reviews Cardiology* **13**, 48–60 (2016).
91. Sirtori, C. R. *et al.* HDL therapy today: from atherosclerosis, to stent compatibility to heart failure. *Annals of Medicine* **51**, 345–359 (2019).
92. Nicholls, S. J. *et al.* Effect of Serial Infusions of CER-001, a Pre- β High-Density Lipoprotein Mimetic, on Coronary Atherosclerosis in Patients Following Acute Coronary Syndromes in the CER-001 Atherosclerosis Regression Acute Coronary Syndrome Trial. *JAMA Cardiology* **3**, 815 (2018).
93. B. Uribe, K., Benito-Vicente, A., Martin, C., Blanco-Vaca, F. & Rotllan, N. (r)HDL in theranostics: how do we apply HDL's biology for precision medicine in atherosclerosis management? *Biomaterials Science* **9**, 3185–3208 (2021).
94. Ghoshhajra, B. B. *et al.* Coronary Atheroma Regression From Infusions of Autologous Selectively Delipidated Pre β -HDL-Enriched Plasma in Homozygous Familial Hypercholesterolemia. *J Am Coll Cardiol* **76**, 3062–3064 (2020).
95. Guo, Y. *et al.* Synthetic High-Density Lipoprotein-Mediated Targeted Delivery of Liver X Receptors Agonist Promotes Atherosclerosis Regression. *EBioMedicine* **28**, 225–233 (2018).
96. Kaul, S. *et al.* Intramural Delivery of Recombinant Apolipoprotein A-I_{Milano} /Phospholipid Complex (ETC-216) Inhibits In-Stent Stenosis in Porcine Coronary Arteries. *Circulation* **107**, 2551–2554 (2003).
97. Aboumsallem, J. P., Muthuramu, I., Mishra, M., Kempen, H. & de Geest, B. Effective treatment of diabetic cardiomyopathy


- and heart failure with reconstituted HDL (Milano) in mice. *International Journal of Molecular Sciences* **20**, (2019).
98. Gibson, C. M. *et al.* The CSL112-2001 trial: Safety and tolerability of multiple doses of CSL112 (apolipoprotein A-I [human]), an intravenous formulation of plasma-derived apolipoprotein A-I, among subjects with moderate renal impairment after acute myocardial infarction. *American Heart Journal* **208**, 81–90 (2019).
99. El-Eshmawi, A. *et al.* Surgical Cryoablation of Papillary Muscle PVCs During Mitral Valve Surgery: Therapeutic Consideration for Malignant MVP. *Journal of the American College of Cardiology* vol. 76 3061–3062 (2020).
100. Nasr, H. *et al.* Investigating the Effect of a Single Infusion of Reconstituted High-Density Lipoprotein in Patients with Symptomatic Carotid Plaques. *Annals of Vascular Surgery* **29**, 1380–1391 (2015).
101. Chattopadhyay, A. *et al.* A novel approach to oral apoA-I mimetic therapy. *Journal of Lipid Research* **54**, 995–1010 (2013).
102. Chattopadhyay, A. *et al.* A novel approach to oral apoA-I mimetic therapy. *Journal of Lipid Research* **54**, 995–1010 (2013).
103. Navab, M. *et al.* Oral D-4F Causes Formation of Pre- β High-Density Lipoprotein and Improves High-Density Lipoprotein-Mediated Cholesterol Efflux and Reverse Cholesterol Transport From Macrophages in Apolipoprotein E-Null Mice. *Circulation* **109**, 3215–3220 (2004).
104. Bloedon, L. T. *et al.* Safety, pharmacokinetics, and pharmacodynamics of oral apoA-I mimetic peptide D-4F in high-risk cardiovascular patients. *Journal of Lipid Research* **49**, 1344–1352 (2008).
105. Edmunds, S. J., Liébana-García, R., Stenkula, K. G. & Lagerstedt, J. O. A short peptide of the C-terminal class Y

- helices of apolipoprotein A-I has preserved functions in cholesterol efflux and in vivo metabolic control. *Scientific Reports* **10**, 18070 (2020).
106. Edmunds, S. J. *et al.* ApoAI-derived peptide increases glucose tolerance and prevents formation of atherosclerosis in mice. *Diabetologia* **62**, 1257–1267 (2019).
 107. Juarez, P., Viridi, V., Depicker, A. & Orzaez, D. Biomanufacturing of protective antibodies and other therapeutics in edible plant tissues for oral applications. *Plant Biotechnology Journal* **14**, 1791–1799 (2016).
 108. Chan, H.-T. & Daniell, H. Plant-made oral vaccines against human infectious diseases-Are we there yet? *Plant Biotechnology Journal* **13**, 1056–1070 (2015).
 109. Tokuhara, D. *et al.* Rice-based oral antibody fragment prophylaxis and therapy against rotavirus infection. *Journal of Clinical Investigation* **123**, 3829–3838 (2013).
 110. Azegami, T., Yuki, Y. & Kiyono, H. Challenges in mucosal vaccines for the control of infectious diseases. *International Immunology* **26**, 517–528 (2014).
 111. Anantharamaiah, G. M. *et al.* Structural requirements for antioxidative and anti-inflammatory properties of apolipoprotein A-I mimetic peptides. *Journal of Lipid Research* **48**, 1915–1923 (2007).
 112. Romano, G. *et al.* APOA-1Milano muteins, orally delivered via genetically modified rice, show anti-atherogenic and anti-inflammatory properties in vitro and in Apoe atherosclerotic mice. *International Journal of Cardiology* **271**, 233–239 (2018).
 113. Sirtori, C. R. *et al.* Cardiovascular Status of Carriers of the Apolipoprotein A-I_{Milano} Mutant. *Circulation* **103**, 1949–1954 (2001).

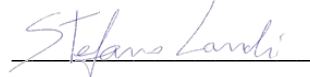
114. Chiesa, G. *et al.* Human Apolipoproteins A-I and A-II in Cell Cholesterol Efflux. *Arteriosclerosis, Thrombosis, and Vascular Biology* **18**, 1417–1423 (1998).
115. Calabresi, L., Sirtori, C. R., Paoletti, R. & Franceschini, G. Recombinant apolipoprotein A-IMilano for the treatment of cardiovascular diseases. *Curr Atheroscler Rep* **8**, 163–7 (2006).
116. LANG, G., KAGIYA, Y., OHNISHI-KAMEYAMA, M. & KITTA, K. Evaluation of Extraction Solutions for Biochemical Analyses of the Proteins in Rice Grains. *Bioscience, Biotechnology, and Biochemistry* **77**, 126–131 (2013).
117. Bradford, M. M. A rapid and sensitive method for the quantitation of microgram quantities of protein utilizing the principle of protein-dye binding. *Anal Biochem* **72**, 248–54 (1976).
118. Compton, S. J. & Jones, C. G. Mechanism of dye response and interference in the Bradford protein assay. *Anal Biochem* **151**, 369–74 (1985).
119. Sedmak, J. J. & Grossberg, S. E. A rapid, sensitive, and versatile assay for protein using Coomassie brilliant blue G250. *Anal Biochem* **79**, 544–52 (1977).
120. Chisci, E. *et al.* Simultaneous overexpression of human E5NT and ENTPD1 protects porcine endothelial cells against H₂O₂-induced oxidative stress and cytotoxicity in vitro. *Free Radic Biol Med* **108**, 320–333 (2017).
121. Liu, Z. *et al.* Systematic comparison of 2A peptides for cloning multi-genes in a polycistronic vector. *Sci Rep* **7**, 2193 (2017).
122. Donnelly, M. L. L. *et al.* Analysis of the aphthovirus 2A/2B polyprotein “cleavage” mechanism indicates not a proteolytic reaction, but a novel translational effect: a putative ribosomal “skip”. *J Gen Virol* **82**, 1013–1025 (2001).

123. Sharma, P. *et al.* 2A peptides provide distinct solutions to driving stop-carry on translational recoding. *Nucleic Acids Res* **40**, 3143–51 (2012).
124. Cinti, A. *et al.* Simultaneous Overexpression of Functional Human HO-1, E5NT and ENTPD1 Protects Murine Fibroblasts against TNF- α -Induced Injury In Vitro. *PLoS One* **10**, e0141933 (2015).
125. Khan, M. S., Joyia, F. A. & Mustafa, G. Seeds as Economical Production Platform for Recombinant Proteins. *Protein Pept Lett* **27**, 89–104 (2020).
126. Takaiwa, F., Wakasa, Y., Hayashi, S. & Kawakatsu, T. An overview on the strategies to exploit rice endosperm as production platform for biopharmaceuticals. *Plant Science* **263**, 201–209 (2017).
127. Watson, C. E. *et al.* Treatment of patients with cardiovascular disease with L-4F, an apo-A1 mimetic, did not improve select biomarkers of HDL function. *Journal of Lipid Research* **52**, 361–373 (2011).
128. Han, Y.-H. *et al.* Enterically derived high-density lipoprotein restrains liver injury through the portal vein. *Science* (1979) **373**, (2021).
129. Brodkorb, A. *et al.* INFOGEST static in vitro simulation of gastrointestinal food digestion. *Nature Protocols* **14**, 991–1014 (2019).
130. Roulston, C. *et al.* "2A-Like" Signal Sequences Mediating Translational Recoding: A Novel Form of Dual Protein Targeting. *Traffic* **17**, 923–39 (2016).

Firma Dottorando



Firma Tutor



8 Thanks

At the end of this PhD program, also crossed by the Covid 19 pandemic, I would like to thank my Tutors, Prof. Federica Gemignani and Prof. Stefano Landi who have always supported me and who have always been available for help and valuable advice.

Secondly, but not least, thanks to Prof. Roberto Giovannoni, my co-tutor and owner of the project. Working with him has been a privilege for me and an opportunity for enormous professional growth and I hope there will continue to be opportunities.

Thanks to my research group with whom I share the long days in the laboratory: each of them has given me something that has allowed me to improve over the years.

Thanks to the research staff of the CNR of Pisa and the FPScience of Pisa with whom I had a pleasure of collaborating.

Last but most important I would like to thank my family, my friends and my Mom who have always supported me during these years and they continue to do so every day.

Because, in the end, the most important things in life aren't things!